Siberian Branch of Russian Academy of Science

BUDKER INSTITUTE OF NUCLEAR PHYSICS

N. Angert, K. Blasche, O. Boine-Frankenheim, N. Dikansky,
Yu. Eidelman, I. Hofmann, B. Grishanov, V. Parkhomchuck,
D. Pestrikov, V. Petrov, V. Shevelko, A. Skrinsky,
B. Sukhina

STUDY FOR A HIGH-INTENSITY HEAVY ION SYNCHROTRON WITH STRONG BUNCH COMPRESSION

(Part I)

Budker INP 2000-93

NOVOSIBIRSK
2000

Study for a high-intensity heavy ion synchrotron with strong bunch compression (Part I)

N. Angert [†], *K. Blasche* [†], *O. Boine-Frankenheim* [†], *N. Dikansky* [‡], *Yu. Eidelman* [‡], *I. Hofmann* [†], *B. Grishanov* [‡], *V. Parkhomchuck* [‡], *D. Pestrikov* [‡], *V. Petrov* [‡], *V. Shevelko* [*], *A. Skrinsky* [‡], *B. Sukhina* [‡]

[†]Gesellschaft für Schwerionenforschung mbH (GSI),
Planckstrasse 1, 62491 Darmstadt, Germany
[‡]Budker Institute of Nuclear Physics (BINP),
630090, Novosibirsk, Russia
[*]P.N. Lebedev Physical Institute,
Leninskii prospect 53, 117924 Moscow, Russia

Summary

We report a conceptual design study for a high intensity heavy ion synchrotron which should enable accelerations of U^{4+} ions up to 125 MeV/u with subsequent compression of the accelerated beam in a single bunch with the length of 10 ns (or, shorter) so that this bunch could be exposed at a pellet to study the heavy ion driven fusion. The intensity of the compressed bunch should be 10^{13}, or 10^{12} of U^{4+} ions. The bunch diameter at the target should be 1 mm for 10^{13} U^{4+} ions and 0.2 mm for 10^{12} U^{4+} ions. The primary ion beam for these operations should be provided by a linear accelerator same as new UNILAC at GSI.

Most important features of such a machine are determined by low charges of accelerated ions. The lifetime of the ion beam in the synchrotron is mainly determined by the charge changing ion collisions with atoms of the residual gas and typically is very short. For example, for the gas mixture in the vacuum chamber of 77%H_2+20%N_2+3%Ar and for the gas pressure of 0.01 nTorr this lifetime ranges from 2 s for the ion energy 10 MeV/u (injection) to 5 s for the ion energy 125 MeV/u.

So short lifetimes strongly determine basic design concepts of the machine. For reasonable amplitudes of the accelerating RF voltages the acceleration time of ions can be about 0.2–0.3 s. It means that all the post-acceleration operations with ion beam should be done as short as possible (practically, within several hundred of turns in the synchrotron). That requirement can be satisfied due to extremely low longitudinal bunch emittances, which are expected from new UNILAC (in a single injected bunch 3 [keV/u]·ns). In line with a requirement of the suppression of the space charge instability of ion bunches it implies the operations with the bunches having extraordinary small momentum spreads (range in 10^{-5}–3×10^{-6}). On the other hand, the compression of such bunches can be done as a direct $\pi/2$ bunch rotation in the longitudinal phase space. During this rotation the space charge forces may result in the instability of ion oscillations in the compressing bunch. However, the lattice of the synchrotron can be designed in such a way that significant transverse and longitudinal blowups of the bunch will occur during the turn, which is the next to the compression event.

The most significant limitations on the beam intensity in the discussed synchrotron are due to longitudinal and transverse space charge instabilities during injections and then, during the bunch compression. Conventional multibunch and single bunch instabilities are rather weak and can be suppressed by Landau damping. However, due to low beam momentum spread required for fast bunch compression the longitudinal feedback system can be useful to suppress coherent oscillations during debunching.

Geometrically, the ring consists of two 50 FODO-cells arcs each providing the total bending angle π, connected by two 200 m long straight sections. One of the long straight section is designed as a three-beamline bypass. One beamline providing the acceleration of ions, another providing the energy modulation required for the bunch compression and the last is the RF-free beam line for the final bunch compression. The opposite straight section contains a two beamline bypass.

Contents

Chapter 1

Introduction

Our objective in writing of this Report was an investigation of accelerator concepts for the future extension of the GSI accelerator facilities. The main topic of these researches was a design study for a heavy ion synchrotron including schemes for bunch compression, which could enable subsequent plasma and controlled nuclear fusion studies using heavy ion beam of U^{4+}_{238} with an intensity up to 10^{13} ions.

Starting these studies we assumed as an injector the new linear heavy ion accelerator at GSI (new UNILAC) and that it will provide, e.g. for U^{4+} ions the following parameters:

ion energy	E	MeV/u	5 to 10
beam current	I	emA	15
bunch repetition frequency	f_b	MHz	36
beam pulse duration		ms	up to 1
transverse beam emittances (normalized)	$\epsilon_{x,z}$	mmmrad	1
longitudinal bunch emittance	ϵ_s	(keV/u)·ns	3

The starting design parameters for the synchrotron were adopted to be the following

- a top magnetic rigidity BR=100 Tm, corresponding to 125 MeV/u for U^{4+};
- ion beam intensities per cycle of about 10^{13} of U^{4+} ions with multiturn injection and about 10^{12} of U^{4+} ions with single turn injection;
- the bunch compression scheme for the compression of all ions in the synchrotron into a single short bunch with a duration of about 10 ns or less at the target; the bunch diameter at the target should be $d \simeq 1$ mm for 10^{13} U^{4+} ions and $d \simeq 0.2$ mm for 10^{12} U^{4+} ions;
- synchrotron operations at high energies and at a repetition rate of 3 Hz, e.g. the acceleration of 10^{12} U^{12+} ions up to 800 MeV/u, or the acceleration of 10^9 U^{92+} ions from SIS up to 10 GeV/u.

It means that desired synchrotron should be a multi-functional machine, which in line with the beam fusion studies could enable possible high energy extensions of the GSI accelerator complex. In particular, that could be a first step for an already discussed electron nucleon collider (see, e.g. in Ref.[1]).

There are several specific features of the discussed synchrotron, which make the designing of this machine more challenging compared to the bunch compressors discussed previously (see, e.g. in Ref.[2]). First, low charges of the uranium ions imply that ions still have many of electron shells. In these conditions, the cross sections of the charge changing collisions of the ions with atoms of the residual gas are large. For example, according to data calculated in Ref.[3] these cross sections range from 2×10^{-15} [cm^2] for the ion energy 1 MeV/u to 5×10^{-17} [cm^2] for the ion energy 100 MeV/u. Correspondingly, the lifetimes of the beam in the discussed synchrotron are rather short. As we shall see in the next Chapter, relevant lifetimes ranges from 2 s for the ion energy of 10 MeV/u to approximately 5 s for the ion energy of 125 MeV/u. In order to keep the ion losses within, say, 10%, both the acceleration of ions and post-acceleration operations should be done rather fast. Although the accuracy of these calculations is given by a factor of about 2, short lifetimes of ions can strongly limit the operational performance of the discussed synchrotron.

Second, for given ion energy in units of MeV/u low charges make the ion motion less sensitive to effects of electro-magnetic fields on the closed orbit. In particular, in equivalent conditions that demands higher accelerating voltages. As we shall see in Chapter 6, the amplitude of this voltage which can be achieved using, e.g. ferrite loaded cavities is limited by the value of $\approx$ 12 keV per a single RF cavity. So that an increase in the required RF amplitudes demands to increase the number of cavities on the closed orbit. In the high current operational modes that can limit the beam performance in the synchrotron. The longitudinal beam emittance from new UNILAC is expected to be very low (ϵ_s =3 [keV/u]·ns).

Finally, if we inject 1000 bunches without significant increase in ϵ_s, the total longitudinal emittance of the bunch before its compression will be 0.003 eV·s. This number is at least one order of magnitude lower than that discussed for the bunch compressors previously. For realistic values of the RF voltages, low longitudinal emittances of injected bunches and their matching in the longitudinal phase space of the synchrotron imply that the momentum spread of injected bunches ($\Delta p/p$) should be unusually low (of the order of 10^{-5}). On one hand, low momentum spreads of the bunches enables to reduce the time required for the bunch compression. On the other hand, the motion of ion in the bunches becomes more sensitive to collective perturbations and to the noises on the closed orbit (noises in RF systems and others).

The report consists of two parts. The Part I describes the conceptual design study of the synchrotron bunch-compressing. The Part II describes the RF systems for acceleration of ions and for the bunch compression of ion beam at the energy 125 MeV/u.

Chapter 2

Design Concepts

In this Chapter, we discuss the desired parameter set of the synchrotron when it will work in the U^{4+} bunch compression mode. Our main objective will be to figure out the requirements to the parameters of the injected beam which could enable its preparation for the compression. One of the most important issue is providing the possible longer lifetime of the beam. Another scope of problems occurs due to the requirement of the matching the phase space volumes of injected bunches to the ring acceptances. Assuming that deeper analysis of the beam intensity limitations will be done in the subsequent chapters, we shall take here into account only crude space charge effects. However, since some limitations on the beam performance due to space charge fields may have a transient character while theoretical predictions in this field are not very sure, it can be more beneficial to prepare the bunches with safe parameters prior their injection in the synchrotron.

2.1 General parameters

Similar to the ENC-ring [1], we adopt that the closed orbit perimeter in the synchrotron is $\Pi = 1200$ m. Then, taking $B = 1.4$ T, we find that with $BR = 100$ Tm the curvature radius in the bending magnets is $R = 71.4$ m. As we shall see in Chapter 5, the lattice design enabling better longitudinal compression without significant transverse blowup of the beam demands an employment of the arc lattice cells, which are 10 m long. The total number of the arc cells is 100. So that the length of the closed orbit in the arc regions of the ring is 1000 m. Remaining 200 m of the orbit perimeter can be equally divided between 2 straight sections, each of 100 m long, subsequently for injection/extraction and for RF–systems. The revolution period of ions ($T_0 = \Pi/v$, v is the ion velocity) in the ring with such a perimeter ranges from $T_0 = 38.9$ μs (for kinetic energy $W_{in} = 5$ MeV/u) and $T_0 = 27.6$ μs ($W_{in} = 10$ MeV/u) till $T_0 = 8.5$ μs at the extraction energy $W_f = 125$ MeV/u. The number of U^{4+} ions which can be injected in the synchrotron during one turn is

$$\Delta N_{in} = \frac{T_0 I}{Ze}, \tag{2.1}$$

where Ze is the ion charge. For U^{4+} ions this yields

W_{in} [MeV/u]	5	10
$\Delta N_{in}/10^{11}$	9.1	6.47

The number of ions which can be injected with the kinetic energy 5 MeV/u is close to the required value to operate the synchrotron in the low intensity mode ($N_t = 10^{12}$ U^{4+}ions in the beam) and is about a half of this value for $W_{in} = 10$ MeV/u. So that the operations starting from 10 MeV/u demands the two-turn injection. The filling of the synchrotron in the high intensity mode ($N_t = 10^{13}$ U^{4+} ions in the beam) demands correspondingly 10-turn injection for $W_{in} = 5$ MeV/u and 20-turn injection for $W_{in} = 10$ MeV/u. These multiturn injections last during $10T_0 \simeq 0.4$ ms for injection at 5 MeV/u and during $20T_0 \simeq 0.55$ ms for $W_{in} = 10$ MeV/u. Both numbers do not exceed the beam pulse duration from the linac and therefore do not limit the possibilities of the high intensity operations of the synchrotron. In the case of the multiturn injection, the normalized transverse bunch emittance increase at least in the number of injection turn times.

The cross section geometry of the beam obtained after the multiturn injection depends on the injection scenario. For example, if new bunches are injected in the betatron phase space in the horizontal plane, resulting beam will have a flat geometry with the vertical rms width equal to $\sqrt{\beta\epsilon}$ and with the horizontal width exceeding, or equal to $\sqrt{n_{inj}\beta\epsilon}$, where n_{inj} is the number of the injections and ϵ is the emittance of an injected bunch. After 20-turn injection the aspect ratio in such a beam will vary along the ring according to

$$\frac{\sigma_y}{\sigma_x} \simeq 0.223 \times \sqrt{\frac{\beta_y(s)}{\beta_x(s)}}. \tag{2.2}$$

An advantage of this injection mode is the smaller required vertical aperture in the arc regions of the synchrotron.

Another possibility occurs when equal number of injections fill the beam in the vertical and in the horizontal betatron phase space. In this case and provided that β-functions of the vertical and of the horizontal betatron oscillations do not differ very strongly, the cross section of the resulting beam can be close to a round one. The radius of such a beam is

$$r = \sqrt{\frac{n_{inj}}{2}\left[\beta_y + \beta_x\right]\epsilon} \simeq \sqrt{n_{inj}\beta_\perp\epsilon}, \quad \beta_\perp = \frac{\beta_y + \beta_x}{2}. \tag{2.3}$$

After 20-turn injection the beam radius will be $r \simeq 4.5\sqrt{\beta_\perp\epsilon}$. Employment of this injection mode, generally, demands larger vertical aperture in the ring. However, this injection mode enables one to decrease the modulations of the beam size along the ring (at least in the arc sections of the synchrotron).

In order to avoid the problems with the crossing of the transition energy of the ring during the high energy operation modes, the horizontal betatron tune should exceed 10. If the tunes of the vertical and horizontal betatron oscillations have close values, the average value of the β-function of the ring ($\beta_{av} = R_0/\nu$, $R_0 = \Pi/2\pi$ =191 m is the average radius of the closed orbit) should be about 18 m. However, if we assume the

single-bunch normalized emittance ϵ_0 =1 mmmrad and that the beam containing 10^{13} U^{4+} ions is obtained after 20-turn injection without additional emittance losses, the transverse emittance of the injected bunch

$$\epsilon = \frac{\epsilon_0}{\gamma(v/c)} \tag{2.4}$$

will be at least $\epsilon_{inj} = 0.1$ mm for injection energy $W_{inj} = 5$ MeV/u and $\epsilon_{inj} = 0.067$ mm for $W_{inj} = 10$ MeV/u. With $\beta_{av} = 18$ m corresponding beam radii ($r_b = \sqrt{\epsilon\beta_{av}}$) are 4.2 cm and 3.5 cm. Since the pipe radius should 2–3 times exceed the beam radius, it can be reasonable to decrease β_{av} a few times to avoid too large geometrical aperture in the ring.

2.2 Lifetime

One of the most important features of the discussed synchrotron is a rather short lifetime of the beam due to charge changing collisions of the U^{4+} ions with the particles (atoms, or molecules) of the residual gas. Since the charge of U^{4+} ions is small these collisions result in the particle losses reducing the lifetime of the beam. Apart from severe limitations on the vacuum conditions in the synchrotron, that fact makes as more preferable the shortest beam manipulation modes.

In our analysis we use as the data for the total cross sections for such processes those calculated in Ref.[3]. According to these data, within the energy range of W =10–120 MeV/u the total cross section of the charge changing collisions of U^{4+} ions per a particle of the gas can be fitted using (see also Fig.2.1)

$$\sigma_{tot}(W) = 10^{-16} \left(\frac{W_0}{W}\right)^{0.83} [\mathrm{cm}^2], \tag{2.5}$$

where $W_0 = 40$ MeV/u is the fitting parameter. Corresponding ion loss rate from the beam is defined as

$$\frac{d\ln N}{dt} = -n_{at} v \sigma_{tot}, \tag{2.6}$$

where n_{at} is the density of the residual gas particles. Since the loss cross section data are given in units of [cm^2/particle], the density n_{at} should be recalculated from e.g. gas pressure in the vacuum chamber as the density of the one-atomic gas. In this case, n_{at} reads:

$$n_{at}[\mathrm{cm}^{-3}] \simeq 3.5 \times 10^{16} P\,[\mathrm{Torr}], \tag{2.7}$$

For a given ion energy the beam intensity decays exponentially with the e-folding lifetime

$$\tau(W) = \frac{1}{n_{at} v \sigma_{tot}}. \tag{2.8}$$

Fig.2.2 shows that in the energy range 10–125 MeV/u and for the gas pressure of 0.01 nTorr, the beam lifetime ranges between 2.1 s at the injection energy 10 MeV/u till 5.2 s at W =125 MeV/u. Since during the lifetime the beam loses about 63% of its particles, all time-consuming operations with the beam should be done with the accelerated beam. The particle losses during acceleration are estimated integrating Eq.(2.6) over the acceleration

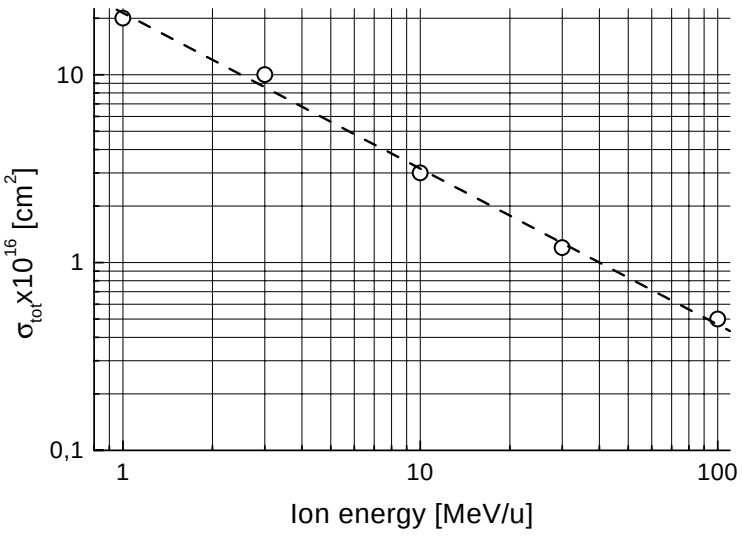

Figure 2.1: Dependence of the total charge changing cross section (on a single particle in the gas mixture) on the ion energy. Open circles are redrawn from Ref.[3], dashed line – result of the fitting using Eq.(2.5); U^{4+} ions, residual gas is assumed to be the mixture of 77%H_2+20%N_2+3%Ar; .

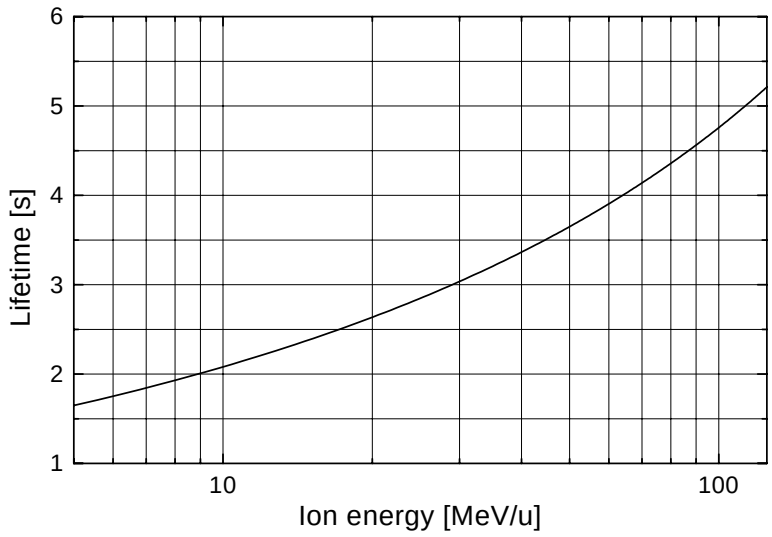

Figure 2.2: Dependence of the lifetime on the U^{4+} ion energy. P=0.01 nTorr, the gas mixture is assumed to be 77%H_2+20%N_2+3%Ar.

time interval (Δt). Assuming that ion momentum linearly increases during the time interval Δt

$$p(t) = p_{in} + \frac{p_f - p_{in}}{\Delta t} t,$$

we find the number of the lost ions

$$\frac{\Delta N}{N_{in}} = 1 - \exp\left(-\frac{\Delta t}{\tau_1}\right), \tag{2.9}$$

where

$$\frac{1}{\tau_1} = \frac{n_{at} c \sigma_0}{(v_f/c)^{0.66}} \frac{1-\chi^{0.33}}{1-\chi}, \quad \chi = \frac{(BR)_{in}}{(BR)_f}, \tag{2.10}$$

and

$$\sigma_0 = \frac{10^{-16}}{0.34} \left(\frac{2W_0}{m_p c^2}\right)^{0.83} \simeq 3.812 \times 10^{-17}\,[\mathrm{cm}^2].$$

For the same gas mixture and for the gas pressure of 0.01 nTorr we find $\tau_1 = 3.173$ s. As is seen from Fig.2.3, the number of the lost ions ranges from 3% to 14%, if the acceleration time changes between 0.1 and 0.5 seconds.

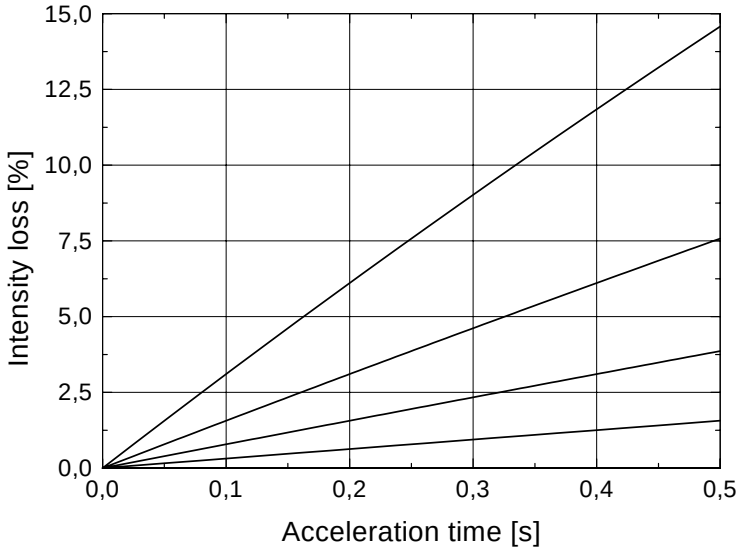

Figure 2.3: Dependence of the particle losses from the beam on the acceleration time. The gas mixture is assumed to be 77%H_2+20%N_2+3%Ar, from top to bottom P=10, 5, 2.5 and 1 pTorr.

If we take as the acceleration time $\Delta t = 0.3$ s and P=0.01 nTorr, then during the acceleration the beam loses about 9% of its intensity. Provided that subsequent beam transformations can be made during the lifetime, the integral particle losses due to charge

changing collisions with the atoms of the residual gas will be about 72% of the beam intensity. To keep the total ion losses within, say, 10 % of the beam intensity, all the post-acceleration operations should be done within the time interval of about 0.01 of the lifetime. As is seen from Fig.2.3 for the acceleration time $\Delta t = 0.3$ s the beam particle losses during this period do not exceed 1% for the residual gas pressure P =1 pTorr. Scaling the data in Fig.2.2 we find, that for this residual gas pressure the beam lifetime ranges from 20 s for the ion energy 10 MeV/u to 52 s or the ion energy 125 MeV/u. Correspondingly, the time intervals available for the post-acceleration beam transformations became 10 times longer.

Another channel for the charge-changing processes provides inelastic intrabeam scatterings (IBS) of ions in the bunch. According to results given in Section 3.1, the lifetime due to these collisions decreases with an increase in the ion energy and with a decrease in the average β-function of the ring. If the average value of β-function in the ring exceeds 10 m, the contribution of inelastic IBS in the lifetime approaches 100 s for the ion energy 125 MeV/u. So that the contribution of the charge changing IBS in the particle loss for the discussed synchrotron is negligible small.

Lower ion losses demand a reduction of the cycle duration of the synchrotron. As we shall see in Section 2.6, in the high intensity mode ($N_t = 10^{13}$ of the U^{4+} ions) the required accelerating voltage is already high. Therefore, for realistic parameter sets of the RF-system of the synchrotron the duration of the acceleration cycle cannot be reduced very strongly. In particular, it means that in order to reduce the particle loss-rate during the cycle, we have to choose among different compression scenario those, which demand the bunch compression time being substantially shorter than the lifetime of the beam. These calculations also show that operation with U^{4+} ion beam will be more reliable, if the pressure of the residual gas in the vacuum chamber is reduced to, say, 1 pTorr. For a given pressure of the residual gas in the vacuum chamber, a significant increase in the lifetime can be achieved, if the populations of heavy atoms in the gas mixture are reduced. According to the paper [4], the weight of the population in the mixture in the particle losses rate is determined by the factor $Y^{(k)}(Z_T^2 + Z_T)^{(k)}$, where $Y^{(k)}$ is the partial concentration of the atoms of a sort k in the mixture and $(Z_T)^{(k)}$ is the atomic number of atoms of the sort k. So that the total ion loss rate is proportional to the value

$$\mathcal{R} = \sum_{k=1} Y^{(k)}(Z_T^2 + Z_T)^{(k)}.$$

For the mixture 77%H_2+20%N_2+3%Ar the value of $\mathcal{R}$ is equal to

$$\mathcal{R} = 3.08 + 22.4 + 10.26 = 35.74.$$

It is about of same value ($\mathcal{R}$ =37.8) for the mixture 90%H_2+10%Ar, but will be about 2.5 times smaller ($\mathcal{R}$ =14.8) for the mixture 90%H_2+10%N_2. Correspondingly, for same gas pressure ($P = 0.01$ nTorr) the lifetime in the last case, will be 2.5 times larger (5 s for W= 10 MeV/u and 12.5 s for $W = 125$ MeV/u) than for the mixture of 77%H_2+20%N_2+3%Ar.

2.3 Transverse space charge instability

One of the most important and most known limitation on the beam intensity occurs due to transverse space charge fields of the beam. For betatron oscillations the strength of perturbations from the bunch space charge fields is evaluated calculating the so-called Laslett tune shift of betatron oscillations ($\Delta\nu_L$). For the beam with a radius $r_b = \sqrt{\epsilon\beta_{av}}$ the value of $\Delta\nu_L$ reads

$$\Delta\nu_L \simeq \frac{Z^2}{A}\frac{Nr_p}{2\pi\gamma^2(v/c)\epsilon_0}\left(\frac{\Pi}{2\sigma_s}\right), \quad r_p = \frac{e^2}{m_p c^2}, \tag{2.11}$$

where N is the number of ions in the bunch, Ze is the charge of the ion, A is its atomic number. For the multibunch mode, when $\Pi = h\lambda_{RF}$, where h is RF-harmonic number (number of bunches in the beam), Eq.(2.11) can also be rewritten in the form

$$\Delta\nu_L \simeq \frac{Z^2}{A}\frac{N_t r_p}{2\pi\gamma^2(v/c)\epsilon_0 B}, \quad N_t = hN, \tag{2.12}$$

where $B \simeq 2\sigma_s/\lambda_{RF}$ is the bunching factor.

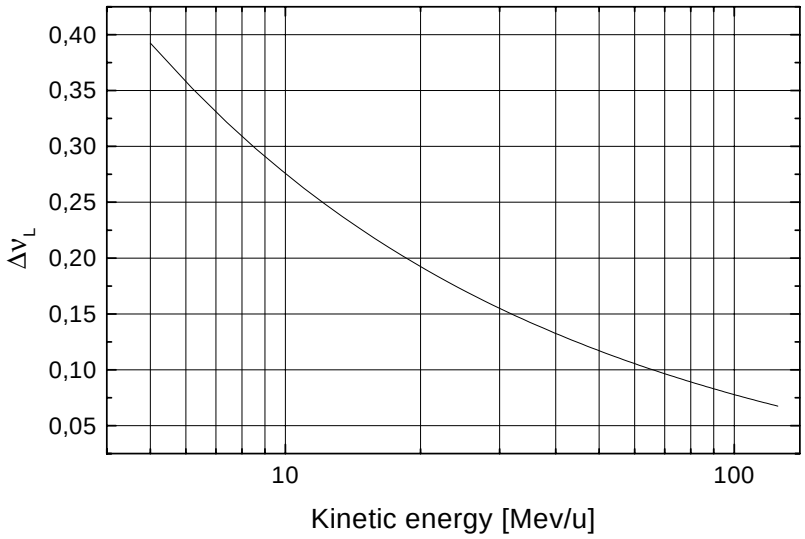

Figure 2.4: Dependence of the Laslett tune shift on the ion kinetic energy; 10^{13} of U^{4+} ions in the beam, $B = 0.4$, $\epsilon_0 = 10$ mmmrad.

As is seen from Fig.2.4 and even if the bunching factor in the beam is not very small ($B = 0.4$), for 10^{13} of U^{4+} ions in the beam the Laslett tune shift at energies W =5–10 MeV/u ranges between 0.4 and 0.27. So high values of $\Delta\nu_L$ imply that in order to avoid strong betatron emittance blowups just after injection the beam should be quickly accelerated (at least to energies with safer values of $\Delta\nu_L$).

After acceleration the beam space charge can strongly limit the beam performance during the bunch compression. During this process the bunch length decreases approxi-

mately by the factor of 1000. Even if the initial value of the Laslett tune shift is about 0.01, after compression it reaches the value 10. So that the working point in the betatron oscillations tune diagram may cross many resonances. If this process can be completed during a small amount of turns in the ring, only lower order resonances (parametric and, probably, integer-type resonances) can limit the beam performance. This problem can be eliminated decreasing the strengths of the dangerous harmonics in the perturbing fields, as well as increasing the speed of the resonance crossing.

Apart from the limitations due to perturbations in the single particle oscillations the Coulomb interactions of the bunches in the multiple injection mode can result in the resonant instability of their coherent oscillations. This limitation occurs during the time intervals which are shorter than the debunching periods in the betatron phase space. For a given value of the bunch intensity in the betatron phase space ($N/[\epsilon_0 B]$) the instability limits the position of the working point in the tune diagram. In particular, this instability is weaker for the rings with higher number of the superperiods in the lattice.

2.4 Bunch compression

The ultimate goal of the synchrotron operation in the U^{4+}–mode is the longitudinal bunch compression at the target to a length corresponding to $2\tau_b$ =10 ns, or less. It implies that before compression the beam is accelerated in the synchrotron from, say, W= 10 MeV/u till W= 125 MeV/u, then it is transformed in a single bunch. Generally, the beam transformation may occur in the following steps:

1. Debunching by slow switching-off of the accelerating RF-voltage.

2. Precompression using slow switching-on of the voltage of the RF-system compression. The precompression occurs until the Laslett tune shift of the compressed beam reaches its threshold value. We take as the threshold the value $\Delta\nu_L \simeq 0.25$.

3. Final bunch compression due to $\pi/2$-bunch rotation in the longitudinal phase space.

Such a compression scenario implies that the beam lifetime is not limited very strongly and that the beam momentum spread after debunching is high enough.

If the beam is obtained using the multiturn injections in the betatron phase space and provided that the longitudinal beam emittance is not increased during the steps preceding its transformation in the single bunch, the momentum spread in this bunch cannot be less than

$$\delta_c = \frac{\epsilon_s h}{2(2\tau_b)pv}.$$

Taking ϵ_s = 3 (keV/u)·ns, and $pv \simeq 2W = 2 \times 125$ MeV/u, we find δ_c = 0.06 % for W_{in} = 10 MeV/u and δ_c = 0.08 % for W_{in} = 5 MeV/u. These values do not pose any strong limitations on the lattice performance of the required beam transport lines.

In the simplest case, the length of the ejected bunch can be decreased, if prior to (or, just after) ejection particle momenta are modulated along the bunch to decelerate

the head-on ions and to accelerate the tail-on ions. If the (rms) length of the bunch before such a modulation is σ_{s0} and if the amplitude of the momentum modulation is $[\Delta p/p]_A = -\kappa\sigma_{s0}$, then after drifting the path L the bunch length decreases by $2L[\Delta p/p]_A$. These two transformations produce the $\pi/2-$rotation in the bunch longitudinal phase space. We shall call such a compression process an inertial one.

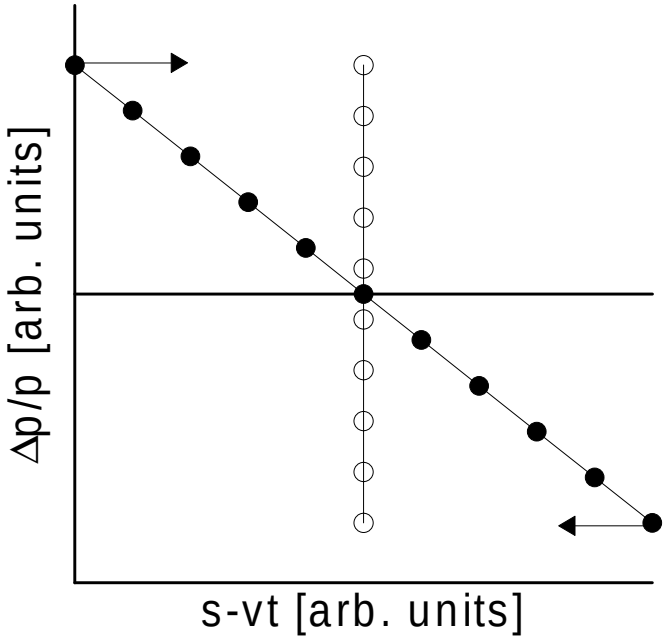

Figure 2.5: To the inertial bunch compression. Solid line without symbols shows initial bunch; solid line with full circles shows initial bunch after energy modulation, with open circles – compressed bunch.

One of the most important limitation on the compressed bunch parameters poses the transverse space charge field of the bunch. Reduction of the bunch factor during compression results in an increase in the bunch Laslett tune shift which may exceed the threshold value. As is seen from Fig.2.6, at the energy of 125 MeV/u the Laslett tune shift of a single bunch containing 10^{13} ions of U^{4+} exceeds 0.3, when the bunch length approaches 50 m.

The description of the compression of so intense beam demands to find out particular threshold value of $\Delta\nu_L$, which is specific for a particular lattice of the ring as well as for a particular compression duration. As we shall see in Chapter 4, substantial reduction in the compression time becomes possible only in the case, when the bunch momentum spread is very small. An increase in the momentum spread of the compressed bunch both increases the time required for the compression and limits a possible value of the bunch length reduction. If before the momentum modulation the rms momentum spread of the bunch is σ_δ, the (rms) bunch length due to inertial compression reaches its minimum

$$\sigma^2_{\min} = \sigma^2_{s0}\frac{\sigma^2_\delta}{\sigma^2_\delta + \kappa^2\sigma^2_{s0}}, \tag{2.13}$$

when the bunch passes the length (see, e.g. in Appendix A.3)

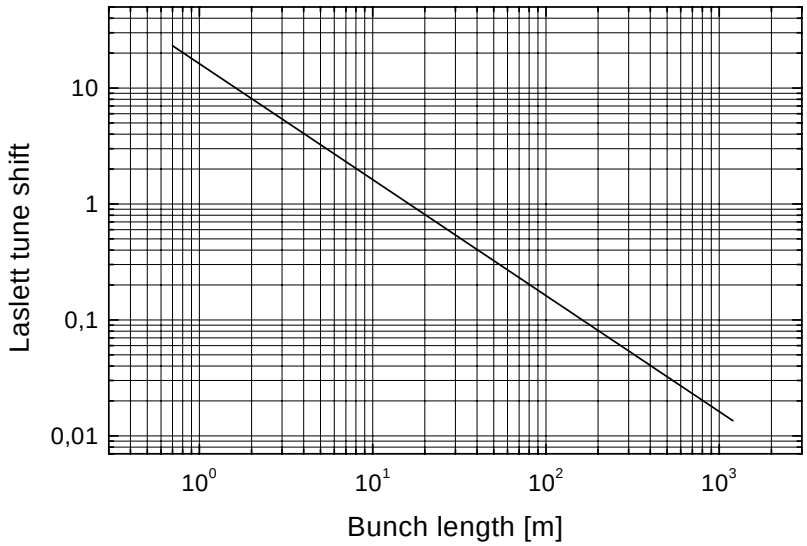

Figure 2.6: Dependence of the Laslett tune shift on the bunch length; $W = 125$ MeV/u, $\epsilon_0 = 10$ mmmrad, $N_t = 10^{13}$ of U^{4+} ions in the beam.

$$L = L_{\min} = \frac{1}{\eta\kappa} \times \frac{1}{1 + (\sigma_\delta/\kappa\sigma_{s0})^2}, \quad \kappa = \frac{d\delta}{ds}. \tag{2.14}$$

During subsequent drifting the bunch length increases again. These expressions show that without other limitations, the compressed bunch will be shorter, if its momentum spread before modulation is smaller. Defining the compression factor as

$$X = \frac{\sigma_{s0}}{\sigma_s}, \tag{2.15}$$

we find that a required (inertial) compression will be feasible, if the momentum spread in the precompressed bunch is

$$\sigma_\delta = \frac{\kappa\sigma_{s0}}{\sqrt{X^2 - 1}}. \tag{2.16}$$

Taking as an example $\kappa\sigma_{s0} = 0.04$ and $\sigma_{s0} = 50$ m ($2\tau_{s0} \simeq 700$ ns),

$$X = \frac{700}{10} = 70,$$

we find that the momentum spread in the bunch before compression should not exceed $\sigma_\delta = 5.8 \times 10^{-4}$. Higher values of σ_δ will result in longer bunches. The value of $L_{\min}$ in this example is a little bit longer than the closed orbit perimeter

$$L_{\min} \simeq 1/\kappa = 1250\,[\mathrm{m}].$$

Smaller momentum spreads are necessary to reach same desired compression factors using smaller momentum modulation amplitudes ($\kappa\sigma_{s0}$). For example, if $\kappa\sigma_{s0}$ is set 4 times

smaller, which is much more realistic, the obtaining of the same compression factor demands 4 times more monochromatic precompressed bunch.

Additional limitations on the final length of the bunch occur due to electrostatic repulsion of ions. For a monochromatic beam ($\sigma_\delta = 0$) and after inertial compression, the bunch length cannot become shorter than

$$\tau_f = \frac{\tau_{in}}{1 + \frac{\tau_{in} v\gamma (v/c)^2 (\Delta p/p)^2_{in}}{6Z^2 N r_p \Lambda}}, \tag{2.17}$$

where $(\Delta p/p)_{in}$ is the amplitude of the momentum modulation before compression, τ_{in} is initial bunch length.

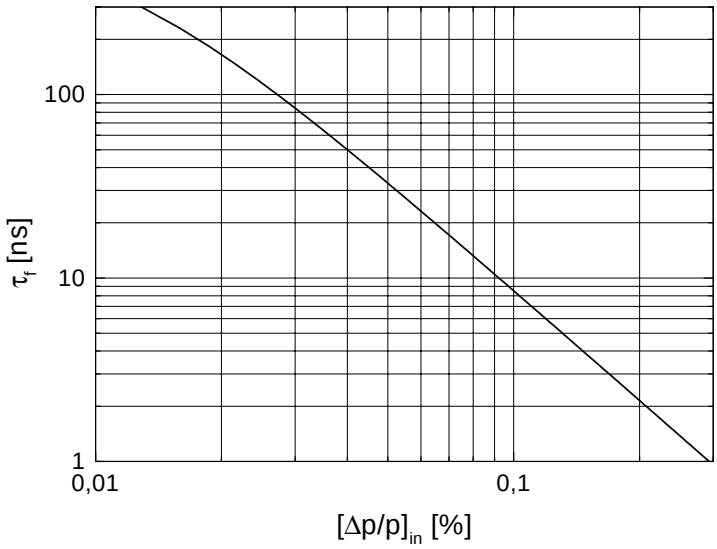

Figure 2.7: Dependence of the minimum bunch duration on the amplitude of the momentum modulation; $W = 125$ MeV/u, 10^{13} of U^{4+} ions in the bunch, $\tau_{in} = 708$ ns.

Due to finite momentum spread in the beam the compressed bunch length should exceed τ_f. As is seen from Fig. 2.7, the bunch length at the target can correspond to 10 ns, if $(\Delta p/p)_{in}$ exceeds 0.2 %.

2.5 Longitudinal acceptance and emittance

In order to avoid the longitudinal phase space dilution it can be reasonable to choose RF-frequency at injection energy (f^{in}_{RF}) equal to the bunch frequency in the injected beam (f^{in}_{RF} =36 MHz). In this case, the bunch to bunch distance ($\lambda_{RF} = v/f^{in}_{RF}$) and RF-harmonic number ($h = T_0 f^{in}_{RF}$) are correspondingly $\lambda_{RF} = 0.86$ m, $h = 1400$ for W_{in} =5 MeV/u and $\lambda_{RF} = 1.21$ m, $h = 994$ for $W_{in} = 10$ MeV/u.

The phase space volumes of the injected bunches should match the lattice acceptances. The matching of the longitudinal acceptance of the synchrotron with the longitudinal

phase space volumes of injected bunches poses some limitations on the parameters of the RF-system of the ring. The phase space trajectories of small synchrotron oscillations read (see, e.g. in Appendix A.1)

$$\frac{\Delta p^2}{2\mu\omega_s J_s} + \frac{\mu\omega_s z^2}{2J_s} = 1, \tag{2.18}$$

where $\mu = p/(\eta v)$,

$$\eta = \frac{1}{\gamma^2} - \frac{1}{\gamma_{tr}^2} \tag{2.19}$$

is the slip factor of the ring, $\omega_s = \omega_0\nu_s$ is the frequency of the synchrotron oscillations and ν_s is the tune of the synchrotron oscillations

$$\nu_s = \sqrt{\frac{ZeV\sin(\phi_s)h\eta}{A2\pi pv}}, \tag{2.20}$$

A is the atomic number of the ion. The action variable J_s in Eq.(2.18) determines the area (S_J) of the phase space encircled by the ellipse ($S_J = 2\pi J_s$). The ellipse with $S_J = \epsilon_s$ encircles the longitudinal bunch emittance. The main half-axes of such an ellipse read ($\delta = \Delta p/p$ and $\tau = z/v$)

$$\sigma_\delta = \delta_b = \sqrt{\frac{2\nu_s\epsilon_s}{pv\eta T_0}}, \quad \tau_b = \sqrt{\frac{\eta\epsilon_s T_0}{2\pi^2\nu_s pv}}. \tag{2.21}$$

If effects of the longitudinal space charge of the beam are small, these two formulae define the required phase space parameters of the bunches, which should be prepared before injecting in the synchrotron. Provided that the values σ_δ and τ_b are given for some reason, Eqs.(2.21) define the value of the synchrotron tune, which matches the longitudinal acceptance of the synchrotron and the longitudinal emittance of the injected bunches.

Inspecting Fig.2.8 we find out that if σ_δ is within the interval 0.1–0.01 o/oo, the acceptable values of the synchrotron tune should be large enough. In particular, it reaches the stability threshold ($\nu_s = 1/\pi$, a single RF-station per turn), if $\sigma_\delta = 0.06$ o/oo for the injection energy $W = 10$ MeV/u and if $\sigma_\delta = 0.07$ o/oo for the injection energy $W = 5$ MeV/u. In order to avoid too high values of the synchrotron tunes at injection energy the momentum spread in the injected bunches should not exceed 0.02–0.03 o/oo. The required values of the RF-amplitude (indeed, $V\sin(\phi_s)$, where ϕ_s is the synchronous phase) within the stability region range till 300 kV for $W = 5$ MeV/u and till 800 kV for $W = 10$ MeV/u (Fig.2.9)

Calculations of the bunch length (bunching factor) and of the Laslett tune shifts for the cases, corresponding to the matching of the longitudinal ring acceptance and of the injected bunch emittance also indicate that the reasonable region for the momentum spreads of injected bunches lies below 0.03 o/oo (see in Fig.2.10).

If the linear charge density of the bunch is not small, its longitudinal electric field can substantially decrease the gradient of the accelerating field within the bunch changing the matching conditions. If $\rho(z)$ is the linear particle density in the bunch and provided that

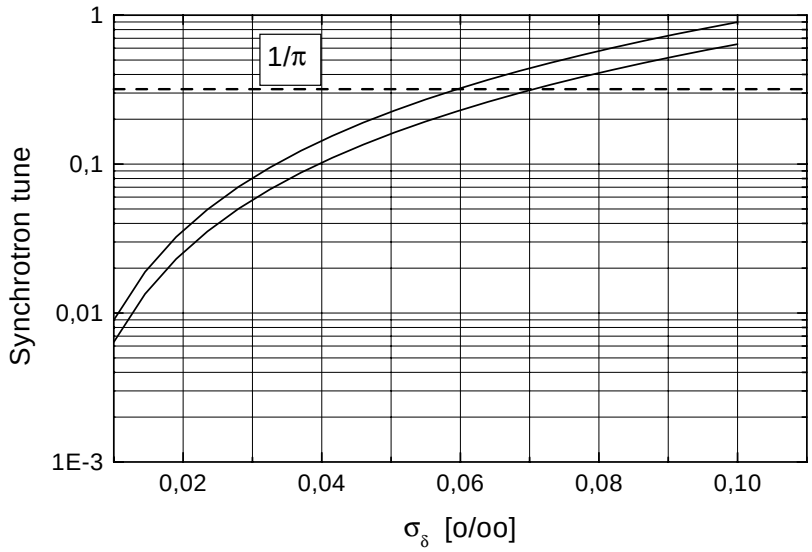

Figure 2.8: Dependence of the synchrotron tune matching the phase space ellipse ($\epsilon_s = 3$ (keV/u)·ns) on the injected bunch momentum spread. Upper solid line – W =10 MeV/u, lower – W =5 MeV/u, dashed line shows the stability limit $\nu_s = 1/\pi$.

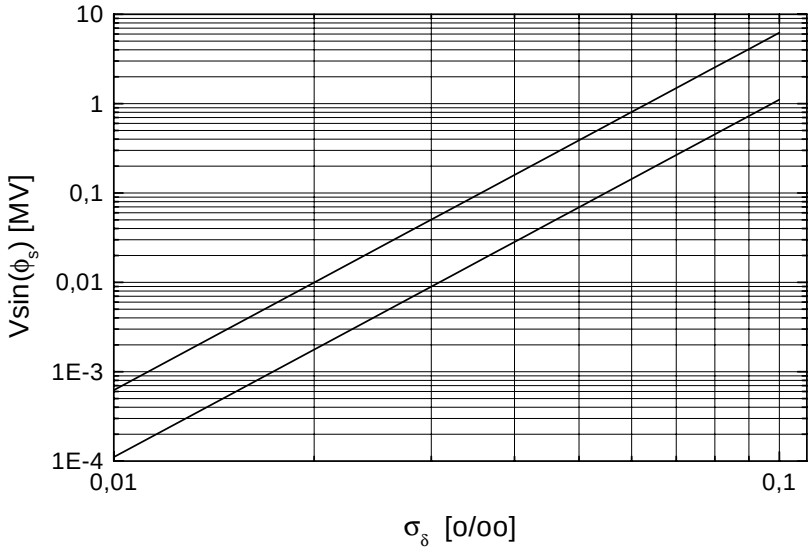

Figure 2.9: Dependence of the RF-amplitude ($V\sin(\phi_s)$) corresponding to the tunes in Fig.2.8 on the injected bunch momentum spread. Upper line – W =10 MeV/u, $h = 994$, lower line – W =5 MeV/u, $h = 1400$.

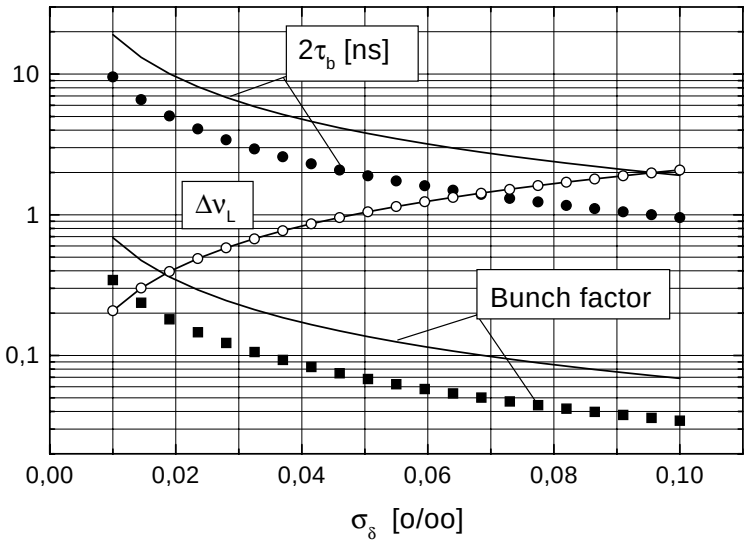

Figure 2.10: Dependencies of the bunch length ($2\tau_b$), bunching factor ($B = 2h\tau_b/T_0$) and of the Laslett tune shift in cases of longitudinal phase space matching on the momentum spread of injected bunches. Solid lines –W =5 MeV/u, h = 1400, symbols – W =10 MeV/u, $h = 994$.

the bunch length (σ_s) substantially exceeds the pipe radius ($l_\perp$), the longitudinal electric space charge field inside the bunch reads [1]

$$\mathcal{E} = \frac{ZNe\Lambda}{\gamma^2}\frac{d\rho}{dz}, \quad \Lambda = 1 + 2\ln\left(\frac{l_\perp}{a}\right). \tag{2.22}$$

Here, a is the beam radius. For given acceleration voltage $U = V\cos(\phi_s)$ [ϕ_s is the RF-phase of the synchronous particle] and number of particles in the bunch (N) the synchrotron oscillations of ions become unstable, if the bunch length is shorter than its threshold value. Assuming e.g. a parabolic linear density in the bunch

$$\rho(z) = \frac{3}{4\sigma_s}\left(1 - \frac{z^2}{\sigma_s^2}\right),$$

we find (see, for instance, in Appendix A.2):

[1] In the alternating focusing channels the beam cross section presents an ellipse

$$\frac{x^2}{\sigma_x^2} + \frac{y^2}{\sigma_y^2} \le 1.$$

In this case, the factor Λ in Eq(2.22) will read

$$\Lambda = 1 + 2\ln\left(\frac{2l_\perp}{\sigma_x + \sigma_y}\right).$$

However, in, for example, FODO channels the modulation of the sum $\sigma_x + \sigma_y$ is usually very weak. So that we can use the simplified expression for Λ from Eq.(2.22).

$$\sigma_{th} = \left(\frac{3}{2} m_p c^2 \frac{ZNr_p \Lambda R_0 \lambda_{RF}}{\gamma^2 eV \sin(\phi_s)} \right)^{1/3}. \tag{2.23}$$

Note, that for non relativistic particles ($W \ll m_p c^2$) this threshold bunch length very weakly depends on the ion kinetic energy. It means that for a given ratio of $N/(V \sin \phi_s)$, after acceleration of ions till the energy of W_f=125 MeV/u the value of σ_{th} will be approximately same as that for injected bunches. Correspondingly, if the longitudinal emittances of the bunches are not increased during this acceleration and provided that their lengths were set close to σ_{th}, the bunch momentum spread ($p\sigma_\delta$) after acceleration will have the safe values as that at the injection energy, while the values of σ_δ will decrease (p_{in}/p_f) times.

Note also that after the multiturn injection in the same bucket, the number of particles in a bunch will increase proportional to number of injections $N \to N n_{inj}$. Correspondingly, for a given amplitude of RF-voltage (V) the value of σ_{th} will increase proportionally to $n_{inj}^{1/3}$. For example, for the bunch obtained after 20-turn injection ($n_{inj} = 20$) the value of σ_{th} will increase by the factor of about 2.71. To keep during injection the value of σ_{th} unaltered, the amplitude of the RF-voltage should increase proportional to the number of particles in the bunch.

For the stable synchrotron oscillations ($\sigma_s > \sigma_{th}$) the effect of the space charge field modifies the second equation in (2.21) in the following way

$$\sigma_s^2 \sqrt{1 - \frac{\sigma_{th}^3}{\sigma_s^3}} = \sigma_0^2 = \frac{\eta \epsilon_s \Pi}{2\pi^2 \nu_s p}. \tag{2.24}$$

It has the root $\sigma_s \simeq \sigma_{th}$, if the bunch length calculated neglecting the space charge fields (σ_0) is much smaller than σ_{th}. Due to the conservation of the phase space volume the bunch momentum spread in such a case is evaluated using

$$\sigma_\delta \simeq \frac{\epsilon_s}{\pi p \sigma_{th}}. \tag{2.25}$$

For the discussed synchrotron we have $f_{RF}^{in} = 36$ MHz so that the number of ions in a single injected bunch is $N = I/(Zef_{RF}^{in}) \simeq 6.51 \times 10^8$. Taking $l_\perp = 3\sqrt{\epsilon_\perp \beta_{av}}$ and as ϕ_s, for example, $\phi_s = \pi/6$, we obtain [2]

W_{in}	λ_{RF}^{in}	σ_{th}	σ_δ	$B = 2\sigma_{th}/\lambda_{RF}^{in}$	σ_0	$\sigma_{\delta 0}$	V	ν_s
MeV/u	cm	cm	o/oo		cm	o/oo	MV	
5	86	17.35	0.017	0.4	3.5	0.084	1.2	0.018
10	121	20	0.01	0.33	3.9	0.053	1	0.0096

In order to avoid uncontrollable transformations of the longitudinal phase space volume in the synchrotron, it seems to be reasonable to prepare bunches with such longitudinal and momentum widths prior to injection.

[2] The value ν_s in this table was calculated accounting its reduction due to the bunch space charge.

2.6 Acceleration

In order to suppress intensity limitations which will be discussed below, it is reasonable to accelerate the beam as fast as possible. If we assume a linear increase in time of the guiding magnetic field of the synchrotron

$$B(t) = B_{in} + \frac{B_f - B_{in}}{\Delta t} t, \tag{2.26}$$

the required acceleration voltage $U = V\cos(\phi_s)$ reads (see, e.g. in Appendix A.1)

$$U = 300\left([BR]_f - [BR]_{in}\right)\frac{\Pi}{c\Delta t}. \tag{2.27}$$

Here, Δt is the acceleration time, B_{in} is the value of the magnetic field at the injected energy and B_f is its final value. For the U^{4+}ions accelerated to the kinetic energy $W_f =$ 125 MeV/u during, for instance, $\Delta t = 0.1$ s, we find

W_{in}	$(BR)_{in}$	U	$(f_{RF})_f$
MeV/u	Tm	MV	MHz
5	19.23	0.97	164.69
10	27.23	0.873	116.9

The last column in this table defines the RF-frequencies at the extraction energy ($W = 125$ MeV/u) assuming that at injection energies this frequency is 36 MHz.

During the acceleration the azimuthal length of the bucket depends on the value of the synchronous phase and, generally is shorter than λ_{RF} (see, e.g. in Fig.2.11).

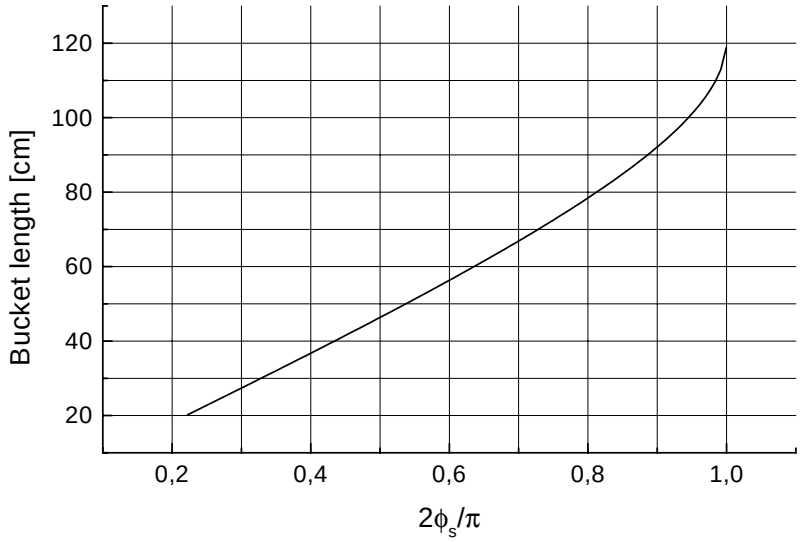

Figure 2.11: Dependence of the bucket length on the synchronous phase. W =10 MeV/u, $\lambda_{RF} = 121$ cm.

Correspondingly, during acceleration the linear densities of the bunches increase. That may pose additional limitations on the parameters of the accelerating RF-system. If we define as ϕ_1 the phase corresponding to the right end of the bucket, then the azimuthal length of the bucket reads

$$\Delta l = \lambda_{RF}\frac{\phi_1 + \phi_s}{2\pi}. \tag{2.28}$$

For a given value of the bunching factor

$$B = \frac{2\sigma_s}{\Delta l} = \frac{2\sigma_s}{\lambda_{RF}}\frac{2\pi}{\phi_1 + \phi_s}$$

Eq.(2.23) defines the minimum amplitude RF-voltage, which overcomes the ion repulsions for a given value of the synchronous phase

$$V(\phi_s) = \frac{3}{2}m_p c^2 \frac{ZNr_p\Lambda R_0\lambda_{RF}}{\gamma^2 e\sigma_s^3(\phi_s)\sin(\phi_s)} \tag{2.29}$$

On the other hand, if the acceleration is made using a single RF-station in the ring, this value should not exceed the threshold value corresponding to the stability criterion of the synchrotron oscillations

$$\nu_s^2 = \frac{ZeV\sin(\phi_s)h\eta}{A2\pi pv} < \frac{1}{\pi^2}. \tag{2.30}$$

For a high intensity beam, the value ν_s for incoherent synchrotron oscillations is small due to compensation of the RF-voltage by the space charge fields of bunches. However, the stability criterion in Eq.(2.30) should also be held for coherent synchrotron oscillations of bunches. Since the space charge fields do not perturb the dipole coherent oscillations, the stability criterion of these oscillations ($\pi\nu_s < 1$, one RF-station on the closed orbit) limit the number of particles in a bunch. Assuming a uniform filling pattern of bunches in the beam and defining the total number of ions in the beam as $N_t = Nh$, we find the following expression for the threshold number of ions in the beam

$$N_t \leq \frac{8}{3}\frac{A\gamma^3(v/c)^2\sigma_s^3(\phi_s)}{Z^2 r_p\eta\Lambda\Pi\lambda_{RF}}. \tag{2.31}$$

As is seen from Fig.2.12, the operations with the beams containing more than 10^{12} of U^{4+} ions are possible only in the case, when the bunch factor exceeds $B = 0.5$. The threshold number of particles in the beam can exceed 10^{13}, if the bunch factor is larger than B =0.7. However, the acceleration rate in this case is very low. For example, as is seen from Fig.2.13, for the bunch factor $B = 0.9$ the threshold number of particles exceeds 10^{13}, if $\phi_s = 0.45\pi$. Relevant threshold amplitude of accelerating voltage is approximately $V\cos(\phi_s) = 110$ kV. So that the required acceleration time till the energy $W = 125$ MeV/u is rather large $\Delta t = 0.9$ s.

The acceleration times can be decreased increasing the number of RF-stations in the ring. For example, if ions are accelerated using two identical RF-stations placed in the opposite straight sections of the ring, the threshold number of particles in Eq.(2.31) increases twice. As is seen from Fig.2.14, it well exceeds 10^{13} starting from $\phi_s = 0.4\pi$.

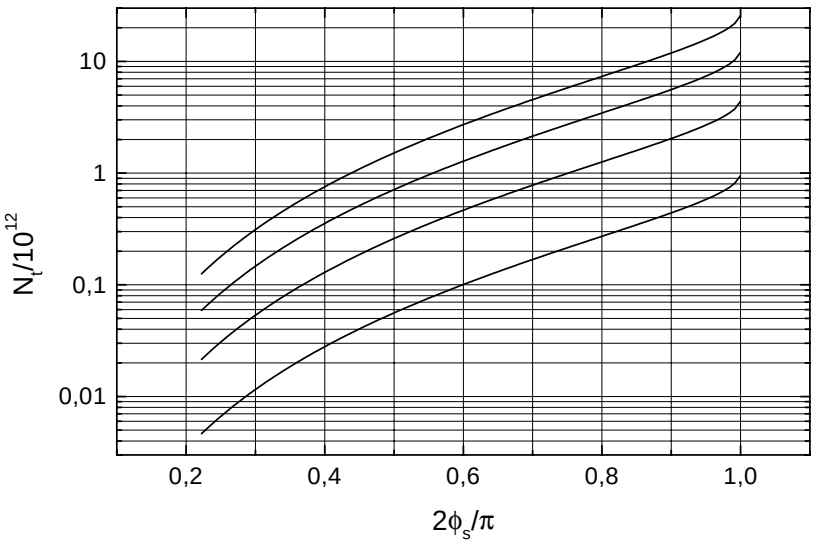

Figure 2.12: Dependencies of the threshold number of particles in the beam (Nh) on the synchronous phase. From top to bottom B = 0.9, 0.7, 0.5 and 0.3; U^{4+}−ions, W =10 MeV/u, λ_{RF} = 121 cm, one RF-station.

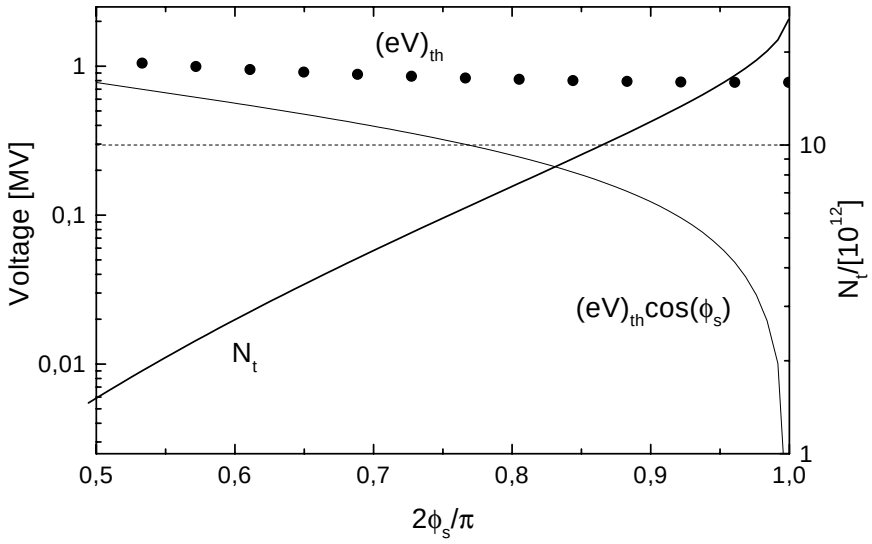

Figure 2.13: Dependencies of the threshold RF-amplitude (full circles) and of the accelerating voltage on the synchronous phase. U^{4+}−ions, B = 0.9, W =10 MeV/u, λ_{RF} = 121 cm, one RF-station.

The required accelerating voltage in this case is $V\cos(\phi_s) \simeq 500$ kV. So that ions will be accelerated till the energy 125 MeV/u during $\Delta t = 0.17$ s, which is quite acceptable.

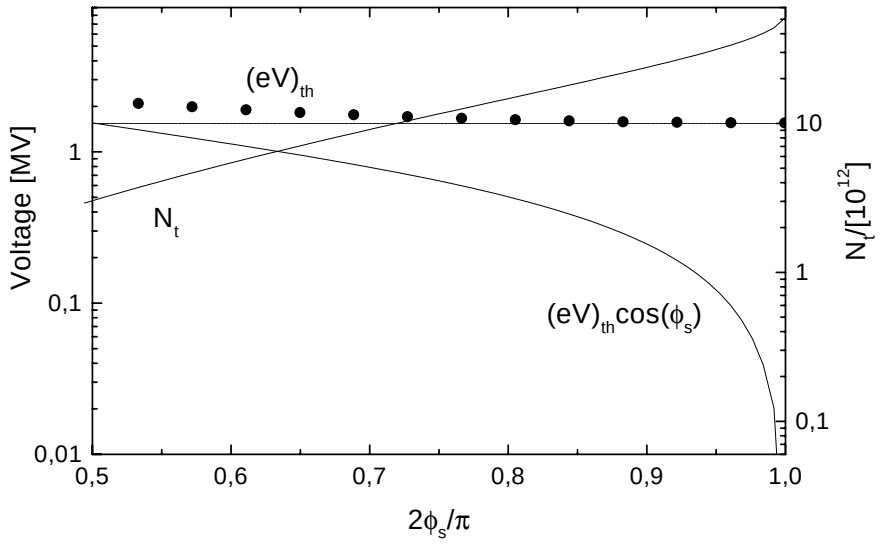

Figure 2.14: Same as in Fig.2.13, but the beam is accelerated using two identical RF-stations.

As is seen from Fig.2.14, the stability condition for the dipole synchrotron coherent oscillations for the low-intensity beam ($N_t = 10^{12}$ of U^{4+} ions) holds well in a wide region of the synchronous phases. For this beam intensity, the value $\phi_s = 0.4\pi$ and $B = 0.5$ seem to be reasonable(Fig.2.15). In this region the required amplitude of the RF-voltage is about 600 kV, while the accelerating voltage is 300 kV. The threshold bunch length for this value of the synchronous phase is 20 cm. With this accelerating voltage the acceleration time between the energies $W_{in} = 10$ MeV/u and $W_f = 125$ MeV/u is about 0.3 s.

For the beam containing 10^{13} of U^{4+} ions about same acceleration rate (380 kV/turn, the acceleration time $\Delta t = 0.22$ s) will be achieved, if the synchronous phase is set $\phi_s = 0.46\pi$ and the bunching factor $B = 0.7$. The required amplitude of the RF-voltage of a single station is about 1.56 MV (see in Fig.2.16). The threshold bunch length for this value of the synchronous phase is about 33.5 cm.

2.7 Preliminary parameter set in the bunch compression mode

In our calculations below we shall take as a bases the case, when the injection energy of the U^{4+} ions is 10 MeV/u. In this case, the requirements of the simultaneous stability of coherent and incoherent synchrotron oscillations of injected ions do not limit a possibility of operations with the beam containing 10^{13} of U^{4+} ions.

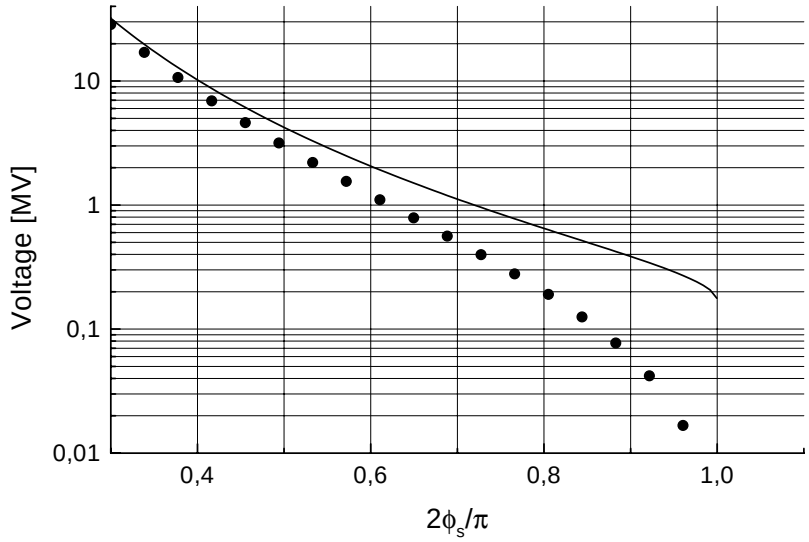

Figure 2.15: Dependencies of the amplitude of the RF-voltage (solid line) and of the accelerating voltage ($V\cos[\phi_s]$; symbols) on the synchronous phase. Number of ions in the beam 10^{12} of $U^{4+}-$ions, W =10 MeV/u, $\lambda_{RF} = 121$ cm, $B = 0.5$.

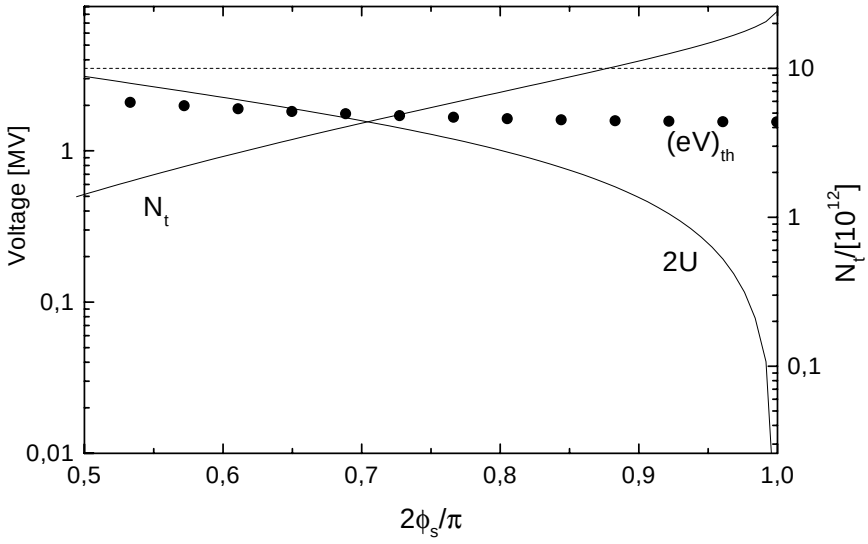

Figure 2.16: Same as in Fig.2.13, but the beam is accelerated using two identical RF-stations and $B = 0.7$.

Prior to the discussion of the parameter sets, we note that in the beam compression operation mode at least two RF systems are necessary. The acceleration RF system should enable the injection in the multiple bunches and their subsequent acceleration from injection energy to the final energy. To enable high intensity operations this system should contain at least two RF-stations. Another RF system should enable the energy modulation of the ions in the single bunch prior its compression. These RF systems have very different functions so that an optimization of the system design may require contradictional properties, if these functions will be realized in one system. As we already saw, the beam intensity in the synchrotron is high for about all steps of the operation cycle. Apart from the limitations due to space charge forces, we expect strong effects due to the fields, which the beam induced in surrounding electrodes. More close inspection shows, that one of the main contributions in these limitations occur due to interactions of bunches with the RF system of the synchrotron. These problems are eliminated, if in one of the straight sections of the ring the beam can go through different beam lines, so that it can see only one RF system. Another problem arises during the bunch compression operation. The bunch length decreases during its compression by a factor of about 1000. Correspondingly, the local bunch current increases from about 1 A at the beginning of the compression till about 1 kA after compression. So high values of the local bunch current may result in strong limitations on the bunch performance due to the bunch wake fields in the energy modulation RF system. On the other hand and as we shall see in Chapter 4, almost all necessary energy modulation occurs during the period, when the bunch length reduces less than twice. In order to avoid additional perturbations of the ion motions due their interactions with the fields induced in the energy modulation RF system, it is reasonable to pass the beam in the RF free space. As we shall see, the remaining reduction of the bunch length may take several tens turns in the synchrotron.

If we summarize all three options, we come to the necessity to have in the synchrotron at least two long straight sections. One of these straight sections contains three beam lines. One for the accelerating RF system, a second containing the energy modulation RF system, and a third is the RF-free straight section (Fig.2.17). The opposite straight section has two beam lines: one for the second accelerating RF-station and the injection system, while the second is the RF-free beam line for the extraction of the compressed ion bunch. The switching of the beam trajectory between these bypasses must be done after acceleration of ions during a single turn in the ring and hence pulsed dipoles must be used for this purpose. Required parameters of these dipoles will be discussed in Section 5.3. Here we note that switching of the beam between the lines demands certain time intervals, when no bunches should pass these magnets. Adopting that switching can be done during 0.8 μs (10 % of the closed orbit perimeter), we conclude that the beam filling pattern should contain the empty of bunches gap with the length of 10% of the closed orbit perimeter.. In the high intensity operational mode the required number of particles in the beam is obtained using the 20-turn injection. It takes about 0.5 ms. New bunches are deposited in the horizontal betatron phase space. In the longitudinal phase space new bunches are accepted in the same buckets as those already collected. To compensate the longitudinal space charge repulsion of ions the amplitude of RF voltage should rise during this period linearly from 150 kV till 3 MV. For the designed accelerating RF system the required modulation of the RF voltage does not limit the ring performance.

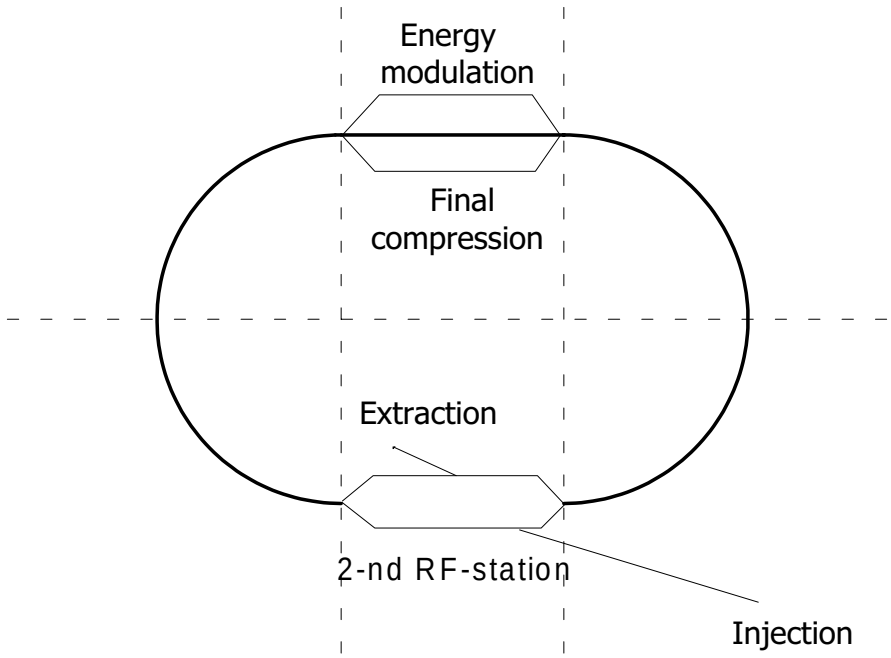

Figure 2.17: Schematic layout of the synchrotron with the separated energy modulation and final bunch compression.

Results of the calculations described in the previous Sections of this Chapter can be summarized in the following Tables 2.1 and 2.2 listing the synchrotron parameters, when it is operated in the bunch compression mode. However, it is necessary to note that these parameters or some of them can be changed, if necessary, during a subsequent design study.

Table 2.1: Preliminary general parameter set for the U^{4+}-synchrotron operating in the bunch compression mode.

Circumference	m	1200
Injection energy	MeV/u	10
Extraction energy	MeV/u	125
Injected ions/bunch	$1/10^8$	6.51
Injected ions/turn	$1/10^{11}$	6.41
BR_{in}	Tm	27.23
BR_f	Tm	100
Acceleration time	s	0.3
Revolution period (injection energy)	μs	27.6
Revolution period (final energy)	μs	8.5
Harmonic number		994
Acceleration rate	keV/turn	300
Average β-function	m	15
Accepted momentum spread	%	± 1.4
Betatron acceptance	mmmrad	420
$(\Delta\nu_L)_{inj}$		0.215
$(\Delta\nu_L)_f$		0.06
Vacuum	nTorr	below 0.01
Beam lifetime (injection)	s	2.1
Beam lifetime (extraction)	s	5.2
Beam intensity loss factor	%	10

Table 2.2: Preliminary parameter set for the U^{4+}-synchrotron operating in the low and high intensity bunch compression modes.

Number of ions		10^{12}	10^{13}
Number of injections/bunch		2	20
RF-amplitude	MV	0.6	1.56
Synchronous phase		0.4π	0.46π
Transverse emittance (inv.)	mmmrad	2	20
Transverse emittance (non-inv.)	mmmrad	13.8	138
Bunch length (σ_s; injection)	m	0.2	0.335
Momentum spread	o/oo	0.01	0.008
Bunching factor ($2\sigma_s/\lambda_{RF}$)		0.5	0.7

Chapter 3

Intensity Limitations Due to Intrabeam Scatterings

In this Chapter we discuss possible limitations on the beam performance due to scatterings of ions in the bunch. For the case, when the ions have electron shells both inelastic and elastic processes may limit the beam intensity. The inelastic scatterings due to ion charge exchange may result in the particle losses from the beam and in the corresponding reduction of the beam lifetime. Elastic scatterings may cause undesirable redistributions of particles in their phase space. In particular, for the discussed ring it can result in a blowup of the longitudinal phase space of the bunches.

3.1 Lifetime due to charge exchange and ionization

Since we want to operate the ring with U^{4+} ions, their collisions may result in the charge transfer reactions:

$$U^{4+} + U^{4+} \rightarrow U^{3+} + U^{5+},$$

and in the ionization reactions

$$U^{4+} + U^{4+} \rightarrow U^{5+} + U^{4+} + e.$$

Due to small charges of ions the relative variations of the curvature radius of the closed orbits for the produced ions are large ($\Delta R^{\pm 1}/R = 1/(Z \pm 1)$), so that these ions will be lost from the beam resulting in the reductions of the lifetimes of bunches .

The rate of the ion losses from the bunch due to charge changing collisions of ions can be estimated using

$$\frac{dN}{dt} = -N\rho_b v\sqrt{\frac{\epsilon}{\beta_{av}}}\sigma_{tot}(W_{col}), \tag{3.1}$$

Here, N is the number of ions in the bunch, v is the ion velocity, ϵ is the bunch emittance, $\beta_{av} \simeq R_0/\nu_\perp$ is the average value of the $\beta-$function of the ring, σ_{tot} is the total cross section of the charge exchange processes due to collisions of ions, ρ_b is the bunch density

$$\rho_b = \frac{Nh}{\pi\epsilon\beta_{av}B\Pi} = \frac{Nh(v/c)}{\pi\epsilon_0\beta_{av}B\Pi}. \tag{3.2}$$

The total cross section (σ_{tot}) describing the particle losses from the beam due to charge changing collisions of ions are expressed in terms of the cross section for the charge transfer (σ_{CT}) and for ionization (σ_I) in the following way. Since colliding ions are identical particles the values σ_{CT} and σ_I should be doubled. Next, due to a charge transfer collision the beam loses two ions. Resulting expression for σ_{tot} reads

$$\sigma_{tot} = 2[2\sigma_{CT} + \sigma_I]. \tag{3.3}$$

Particular behavior of the functions $\sigma_{CT}(W_{col})$ and $\sigma_I(W_{col})$ is discussed in the Appendix B. Using Eqs.(3.1) and (3.2), we find

$$\frac{dN}{dt} = -N^2 \frac{hc\sigma_{tot}}{\pi B\Pi} \sqrt{\frac{(v/c)^3}{\epsilon_0 \beta_{av}^3}}, \tag{3.4}$$

or

$$N(t) = \frac{N_{in}}{1 + t/\tau}\ , \tag{3.5}$$

where N_{in} is the initial number of particles in a bunch, and

$$\tau = \frac{\pi B\Pi}{N_t \sigma_{tot}(W_{col}) c} \sqrt{\frac{\epsilon_0 \beta_{av}^3}{(v/c)^3}}, \quad N_t = N_{in} h \tag{3.6}$$

is the lifetime of the beam. The cross section σ_{tot} in these equations depends on the collision energy, which was calculated according to

$$W_{col} \simeq 4.62 \times 10^5 \frac{(v/c)\epsilon_0}{\beta_{av}}\ [\mathrm{keV/u}]. \tag{3.7}$$

Using these equations and the data from Fig.B.1 or, from the Table B.2 (Appendix B), we can estimate dependence of the lifetime on the beam parameters. One of the most important is the dependence of the lifetime on the strength of the lattice focusing assuming the beam emittances and initial beam intensities be given. As is seen from Fig.3.1, the lifetime generally increases with an increase in β_{av} (lower collision frequencies and collision energies). For a given β_{av} the lifetime decreases with an increase in the ion energy. For given N_t/ϵ_0 and β_{av}, the lifetime of the low intensity beam (e.g. $N_t = 10^{12}$ ions) is higher than that of the high intensity beam.

We already saw in Section 2.2 that even with a vacuum in the chamber of 0.01 nTorr, the lifetime of the U^{4+} ion beam due to charge changing collisions of ions with the atoms of the residual gas is limited to several seconds. A comparison of these numbers with data in Fig.3.1 shows that in the discussed ring charge changing collisions of U^{4+} ions in the beam give negligible small contributions to the beam ion loss rate for all discussed here conditions [1].

[1] Indeed, the common ion loss rate due to inelastic IBS and due to ion charge changing collisions with the residual gas atoms reads

$$\frac{dN}{dt} = -aN^2 - \frac{N}{\tau_0},$$

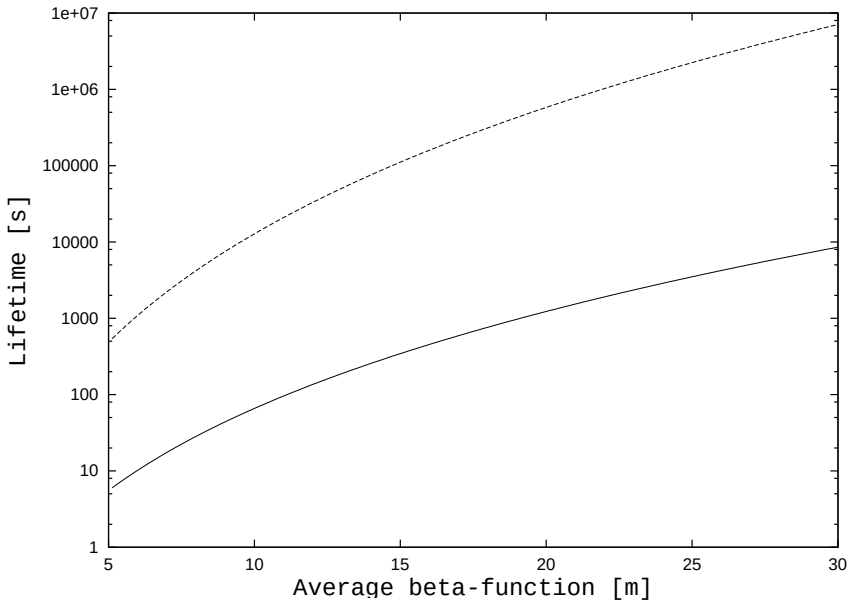

Figure 3.1: Dependence of the beam lifetime due to IBS charge exchange on β_{av}. Upper curve – 10 MeV/u, bottom – 125 MeV/u, $\epsilon_0 = 20$ mmmrad (20-turn injection), $N_t = 10^{13}$

3.2 Elastic intrabeam scattering

Elastic collisions of ions redistribute the partial phase space volumes in the bunches. Such a redistribution can be undesirable, if we want to avoid, for example, the blow-up of the ion momentum spread, or the longitudinal bunch emittances.

For the sake of simplicity we estimate the growth-rates of ion bunches due to intrabeam scattering (IBS) assuming the smoothed focusing approximation. For same reason, we shall also assume $\beta_x = \beta_z = \beta \simeq R_0/\nu$ and $D \simeq R_0/\nu^2$, where $R_0 = \Pi/2\pi$ is the average radius of the closed orbit, D is the average value of the ring dispersion function and $\nu_x = \nu_z = \nu$ denotes the tune of betatron oscillations. With these assumptions the partial

where τ_0 is the lifetime due to charge changing collisions with the gas atoms. Integrating this equation, we obtain

$$N = \frac{N_0 e^{-t/\tau_0}}{1 + \frac{\tau_0}{\tau}\left(1 - e^{-t/\tau_0}\right)},$$

Initial behavior of this function ($t \ll \tau_0$) coincides with that predicted in Eq.(3.5)

$$N = \frac{N_0}{1 + \frac{t}{\tau}}, \quad t \ll \tau_0.$$

The last equation may describe a real decrease in the beam intensity only in the case, when $\tau \leq \tau_0$. In the inverse region of the beam parameters ($\tau_0 \ll \tau$), the inelastic IBS give small contributions to the ion loss rate

$$N = N_0 e^{-t/\tau_0}\left[1 - \frac{\tau_0}{\tau}\left(1 - e^{-t/\tau_0}\right)\right], \quad \tau_0 \ll \tau.$$

growth-rates can be written in the following form (see, e.g. in Ref.[1], or in Appendix C):

$$\frac{1}{\tau_z} = \frac{d\ln\epsilon_z}{dt} \simeq -\frac{N(Z^2/A)^2 r_p^2 c L_{IBS}}{4\pi\gamma^2\epsilon_0^2\sigma_s\delta}F(q), \tag{3.8}$$

$$\frac{1}{\tau_x} = \frac{N(Z^2/A)^2 r_p^2 c L_{IBS}}{2\pi\gamma^2\epsilon_0^2\sigma_s\delta}\left[\frac{\gamma^2 D^2}{\beta^2} - \frac{1}{2}\right]F(q), \tag{3.9}$$

$$\frac{1}{\tau_s} = \frac{d\ln(\delta^2)}{dt} = \frac{N(Z^2/A)^2 r_p^2 c L_{IBS}}{2\pi\gamma^2\epsilon_0^2\sigma_s\delta}\left(\frac{\gamma^2\epsilon}{\delta^2\beta}\right)F(q) \tag{3.10}$$

Another important value describing IBS relaxation in the bunch is the sum of the growth-rates

$$\begin{aligned}\Sigma &= \frac{1}{\tau_z} + \frac{1}{\tau_x} + \frac{1}{\tau_s} \\ &= \frac{N(Z^2/A)^2 r_p^2 c L_{IBS}}{2\pi\gamma^2\epsilon_0^2\sigma_s\delta} q F(q).\end{aligned} \tag{3.11}$$

Here, $F(q)$ is a universal function:

$$F(q) = \int_0^1 \frac{1-3z^2}{1+qz^2}dz = \begin{cases} \dfrac{[3+q]\arctan\sqrt{q} - 3\sqrt{q}}{\left(\sqrt{q}\right)^3}, & q > 0, \\ \dfrac{3}{p} + \dfrac{p-3}{2p^{3/2}}\ln\left(\dfrac{\sqrt{p}+1}{1-\sqrt{p}}\right), & p = -q > 0, \end{cases} \tag{3.12}$$

$$q = \frac{\gamma^2\epsilon}{\delta^2\beta} + \frac{\gamma^2 D^2}{\beta^2} - 1, \tag{3.13}$$

N is the number of particles in the bunch, $r_p = e^2/(m_p c^2)$ is the classical radius of the proton, $\epsilon_0 = \gamma(v/c)\epsilon_{x,z}$ denotes either the horizontal, or vertical invariant bunch emittances, $L_{IBS} \simeq 5$ is the so-called Coulomb logarithm, σ_s and δ are the rms bunch length and the rms (relative) bunch momentum spread. The last values are related to the longitudinal bunch emittance

$$\epsilon_s = \gamma m_p v \sigma_s \delta. \tag{3.14}$$

In particular, IBS relaxation may reach an equilibrium, if $\Sigma = 0$. According to Eqs.(3.12) and (3.13) it occurs, when $q = 0$, or when

$$\frac{\gamma^2\epsilon}{\delta^2\beta} = 1 - \frac{\gamma^2 D^2}{\beta^2} \simeq 1 - \frac{\gamma^2}{\gamma_{tr}^2}, \quad \gamma_{tr} \simeq \frac{\beta}{D} \simeq \nu \tag{3.15}$$

For our estimations we take $\epsilon_0 = 10 \times 10^{-4}$ cm, $\Pi = 1200$ m and $\beta = 20$ m, which corresponds to $\nu \simeq 9.55$ and $D \simeq 2$ m. We also assume that the ions equally populate $h = 994$ bunches of the beam, so that, if N_t is the total number of ions in the beam, the number of ions in the bunch is $N = N_t/h$. Taking $N_t = 10^{13}$, we find that $N \simeq$

1.1×10^{10}. For ion kinetic energies within the range $W = 10$ MeV/u (injection) till $W = 125$ MeV/u (extraction energy) we have $\gamma \simeq 1.01 \div 1.13$, $\epsilon \simeq (6.1 \div 1.87) \times 10^{-3}$ cm. It means that during acceleration and preceding/subsequent transformations of the beam in its longitudinal phase space the value $\sqrt{\epsilon/\beta}$ varies within the range $\sqrt{\epsilon/\beta} \simeq 1.74 \div 1$mrad. An equilibrium may occur only in the case, when the momentum spread in a bunch is relatively high ($\delta \simeq 10^{-3}$). For lower values of δ the parameter q is positive (see in Fig.3.2 and 3.4 left). According to Eqs.(3.8) – (3.10) calculations of the partial

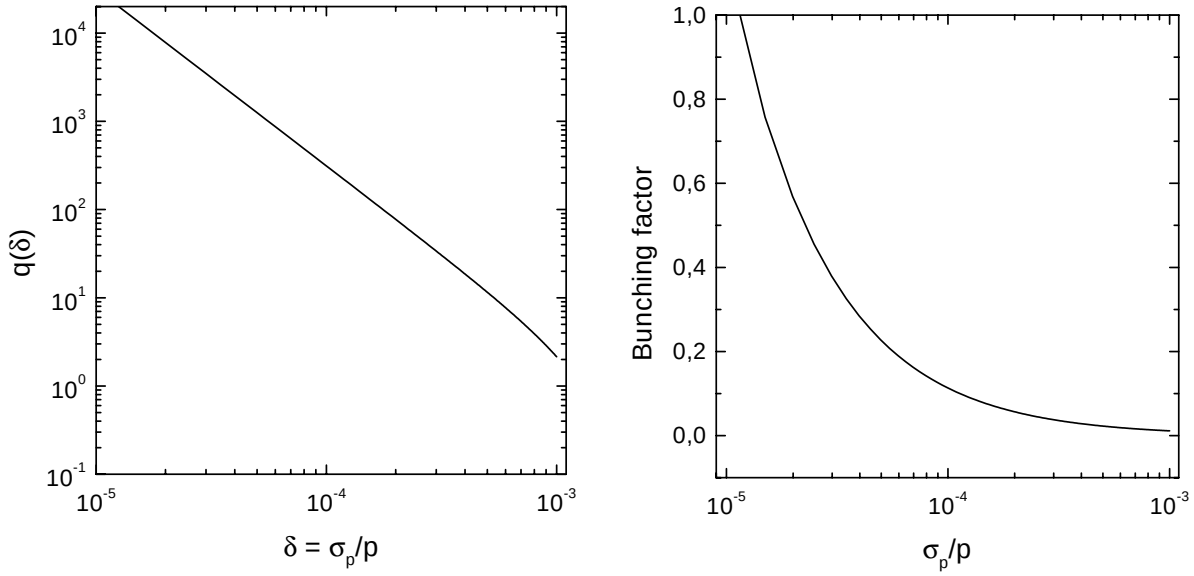

Figure 3.2: Dependences of the factor q (left) and of the bunching factor $B = \sigma_s\sqrt{2\pi}/\lambda_{RF}$ on δ. The rms bunch length was calculated assuming $\epsilon_s = const = 3$ [(keV/u)·ns]; W =10 MeV/u.

growth-rates due to IBS also demands the knowledge of the bunch rms length (σ_s). For our estimations we adopted that acceleration and required beam transformations do not increase the longitudinal bunch emittance. So that $\sigma_s(W, \delta)$ can be calculated using Eq.(3.14). Resulting dependencies of the bunching factors $B = \sigma_s\sqrt{2\pi}/\lambda_{RF}$ are shown in Figs.3.2 and 3.4 (right figures).

If we neglect the effects of the bunch space charge on IBS, these assumptions enable the calculations of the partial growth-rates of ion bunches due to IBS (Fig. 3.3 and 3.5). According to these data, during acceleration and preliminary beam transformations IBS most strongly affects the longitudinal phase space of bunches. However, even in this case and for the worst case, when $\delta = 10^{-5}$, the growth-time (τ_s) is about 80 s at injection energy (Fig.3.3) and is about 40 s at the extraction energy (Fig.3.5). These calculations show that IBS does not limit the beam performance in the discussed synchrotron.

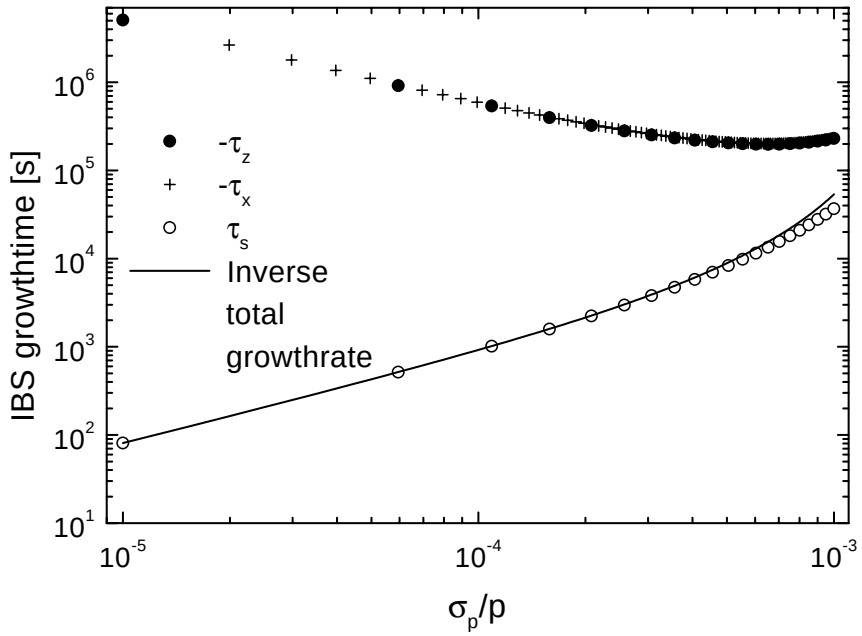

Figure 3.3: Dependences of the partial growth-times and of $1/\Sigma$ on δ. Ion kinetic energy is 10 MeV/u.

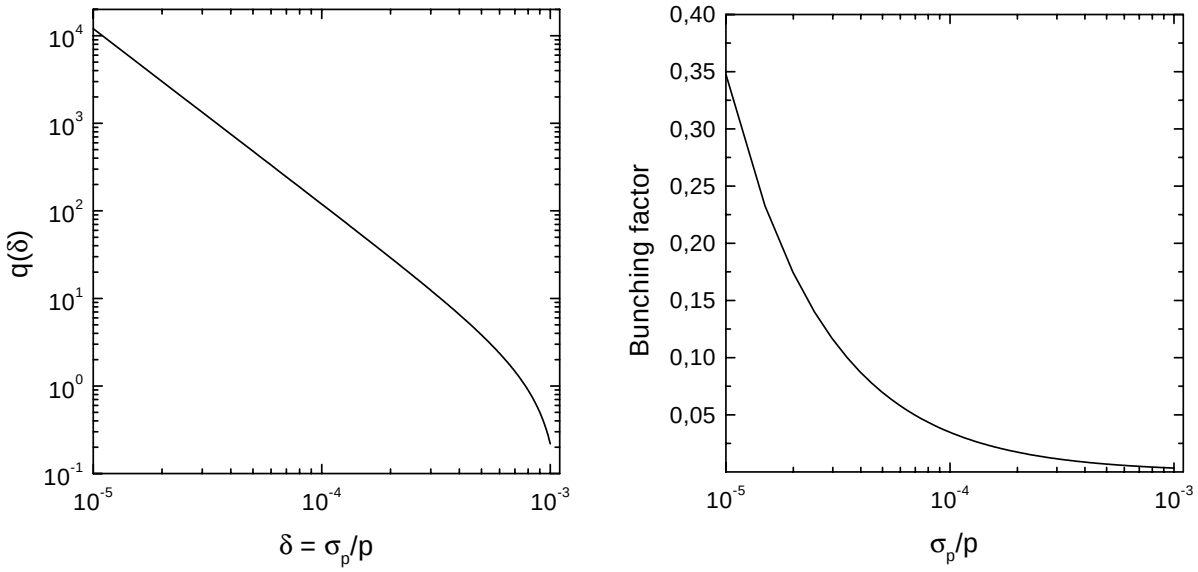

Figure 3.4: Same as in Fig.3.2, but W =125 MeV/u.

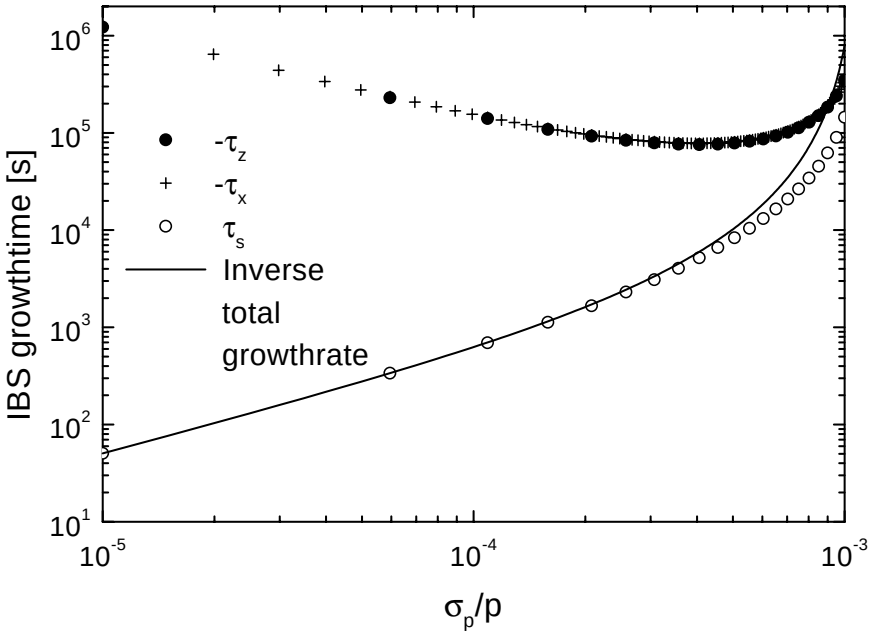

Figure 3.5: Same as in Fig.3.3 but W=125 MeV/u.

Chapter 4

Bunch Compression

In this Chapter we discuss the transformations of the multi-bunched beam in a single short bunch. As we saw, even in the case when the pressure of the residual gas is about 0.01 nTorr, the lifetime of the U^{4+} ion beam due to charge-changing scatterings is very short. It ranges between 2 s for $W = 10$ MeV/u and about 5 s for $W = 125$ MeV/u. We adopt that in order to decrease the particle losses during the transformation and in order to reduce effects of the beam intensity limitations, the re-bunching should be performed at the top energy of the synchrotron ($W = 125$ MeV/u). In order to reduce the blow-up of the longitudinal beam emittance the debunching should be done using adiabatically slow variations of the RF-voltage. Due to very small values of the longitudinal emittances of injected and accelerated bunches as well as due to very short lifetime of U^{4+} ions we cannot use the bunch compression scenario as it was described in the beginning of Section 2.4. Instead, due to small values of the bunch momentum spread after debunching we can use the following scenario:

1. Debunching by slow decreasing of the accelerating RF-voltage.

2. The bunch precompression/compression due to $\pi/2$-bunch rotation in the longitudinal phase space using the RF-voltage with high amplitudes.

The time scales for these transformations are determined by the values of relevant frequencies of small synchrotron oscillations

$$\omega_s = \omega_0 \nu_s, \quad \nu_s = \sqrt{\frac{hZeV\eta}{2\pi Apv}}, \quad \phi_s = \frac{\pi}{2}. \tag{4.1}$$

The first step in the list is performed decreasing the amplitude of the RF-voltage in the accelerating RF-system. As we shall see, due to high harmonic number used in this system the required time intervals for debunching can be rather short. During the second step the bunching is performed under conditions, where the longitudinal phase space of the beam is strongly mismatched to the longitudinal ring acceptance. That can be done using high amplitudes (of the order 1 MV) of the RF-voltages of the compression RF-system. Such voltages are necessary to overcome the longitudinal space charge repulsion of ions as well as other perturbations due to electromagnetic fields induced by the bunch in the

surrounding electrodes (or, cavities), when the bunch length decreases. Provided that the RF-voltage can be set high enough, the bunch compression may take several hundred turns in the ring (corresponding time intervals are in the millisecond range).

Although some steps during re-bunching may occur under conditions where the synchrotron oscillations of particles are nonlinear, we shall use a heuristic model, where the bunching, or initial stage of debunching occur due to orthogonal transformations of small synchrotron oscillations. If we take as an independent variable the azimuth along the closed orbit θ and if $f_0(z_0, z_0')$ is initial distribution function in the longitudinal phase space, while the oscillations are described using a symplectic transformation

$$z_0 = z_0(z, z', \theta), \quad z_0' = z_0'(z, z', \theta), \quad \left| \begin{array}{cc} \frac{\partial z_0}{\partial z} & \frac{\partial z_0}{\partial z'} \\ \frac{\partial z_0'}{\partial z} & \frac{\partial z_0'}{\partial z'} \end{array} \right| = 1, \tag{4.2}$$

the instantaneous distribution function reads

$$f(z, z', \theta) = f_0(z_0[z, z', \theta], z_0'[z, z', \theta]). \tag{4.3}$$

In our heuristic model we assume that the instantaneous position of a particle is defined by a linear transformation

$$\begin{pmatrix} z \\ z' \end{pmatrix}_0 = \begin{pmatrix} a(\theta) & b(\theta) \\ c(\theta) & d(\theta) \end{pmatrix} \begin{pmatrix} z \\ z' \end{pmatrix}, \quad ad - bc = 1. \tag{4.4}$$

In the case of the bunch compression, such transformations are realized provided that the RF-voltage linearly decreases with the ion synchrotron phase [1]

$$V(\phi) = -\frac{V_0}{\pi}(\phi - 2m\pi), \quad (2m-1)\pi < \phi < (2m+1)\pi, \quad m = 0, \pm 1, \ldots$$

If $f_0(z_0, z_0')$ is a Gaussian function [2]

$$f_0(z_0, z_0') = \frac{1}{2\pi\sigma\delta} \exp\left(-\frac{z_0^2}{2\sigma^2} - \frac{(z_0')^2}{2\delta^2}\right), \tag{4.5}$$

then the instantaneous rms bunch length and momentum spread can be calculated using (see in Appendix E.1 for more detail)

$$\sigma^2(\theta) = \sigma^2 d^2 + \delta^2 b^2, \quad \delta^2(\theta) = \delta^2 a^2 + \sigma^2 c^2. \tag{4.6}$$

[1] Note, that with such a sawtooth shaped RF-voltage the synchrotron tune reads

$$\nu_s^2 = \sqrt{\frac{ZeV_0\eta}{2\pi^2 Apv}}.$$

[2] Indeed, the following results will hold for any distribution function described by the equation

$$f_0 = f_0\left(\frac{z_0^2}{\sigma^2} + \frac{z_0'^2}{\delta^2}\right).$$

If the longitudinal displacements of particles inside the beam (z) are measured in the units of length, the rms width of z' (the value of δ) is measured in the same units. The relationship between δ and the rms bunch momentum spread (σ_δ) reads

$$\sigma_\delta = \frac{\delta}{R_0\eta},$$

so that

$$\sigma(\theta) = \sqrt{\sigma^2 d^2 + \left(R_0\eta\sigma_\delta\right)^2 b^2} \tag{4.7}$$

and

$$\sigma_\delta(\theta) = \sqrt{\sigma_\delta^2 a^2 + \frac{\sigma^2 c^2}{R_0^2\eta^2}}. \tag{4.8}$$

4.1 Debunching

The beam debunching occurs adiabatically slow, if e.g. the RF-voltage is turned-off according to an exponential law

$$V(\theta) = V_0 e^{-\theta/\theta_0}. \tag{4.9}$$

If the bunching factor before debunching is small, the initial period of the process in a low intensity beam is described by the following transformation (see e.g. in Appendix E.2)

$$\begin{pmatrix} z \\ z' \end{pmatrix}_0 = \pi\theta_0 \begin{pmatrix} J_0(k) & N_0(k) \\ \nu_s J_1(k) & \nu_s N_1(k) \end{pmatrix} \begin{pmatrix} -\nu_s u N_1(ku) & N_0(ku) \\ \nu_s u J_1(ku) & -J_0(ku) \end{pmatrix} \begin{pmatrix} z \\ z' \end{pmatrix} \tag{4.10}$$

Here, $k = 2\nu_s\theta_0$, $u = \exp(-\theta/[2\theta_0])$ and

$$\nu_s = \sqrt{\frac{hZeV_0\eta}{2\pi Apv}},$$

$J_n(x)$ and $N_n(x)$ are correspondingly the Bessel and Neumann functions [10]. For this case, the functions a, b, c and d which were defined in Eq.(4.4) read where

$$\begin{aligned}
a &= \pi\theta_0\nu_s u\left[J_1(ku)N_0(k) - N_1(ku)J_0(k)\right], \\
b &= \pi\theta_0\left[J_0(k)N_0(ku) - N_0(k)J_0(ku)\right], \\
c &= \pi\theta_0\nu_s^2 u\left[J_1(ku)N_1(k) - N_1(ku)J_1(k)\right], \\
d &= \pi\theta_0\nu_s\left[J_1(k)N_0(ku) - N_1(k)J_0(ku)\right],
\end{aligned}$$

while

$$\sigma(\theta) = \sqrt{\sigma^2 d^2 + \delta^2 b^2}, \quad \delta(\theta) = \sqrt{\delta^2 a^2 + \sigma^2 c^2}. \tag{4.11}$$

In this case, the debunching will be adiabatically slow, if $k \gg 1$. In the region, where ku also is large ($ku \gg 1$), we can use asymptotes

$$J_0(k) \simeq \sqrt{\frac{2}{\pi k}} \cos\left(k - \frac{\pi}{4}\right), \quad J_1(k) \simeq \sqrt{\frac{2}{\pi k}} \sin\left(k - \frac{\pi}{4}\right),$$
$$N_0(k) \simeq \sqrt{\frac{2}{\pi k}} \sin\left(k - \frac{\pi}{4}\right), \quad N_1(k) \simeq -\sqrt{\frac{2}{\pi k}} \cos\left(k - \frac{\pi}{4}\right),$$

and

$$J_0(ku) \simeq \sqrt{\frac{2}{\pi ku}} \cos\left(ku - \frac{\pi}{4}\right), \quad J_1(ku) \simeq \sqrt{\frac{2}{\pi ku}} \sin\left(ku - \frac{\pi}{4}\right),$$
$$N_0(k) \simeq \sqrt{\frac{2}{\pi ku}} \sin\left(ku - \frac{\pi}{4}\right), \quad N_1(ku) \simeq -\sqrt{\frac{2}{\pi ku}} \cos\left(ku - \frac{\pi}{4}\right).$$

Then, simple calculations result in ($\delta = \nu_s \sigma$)

$$\sigma(\theta) = \sigma \exp\left(\frac{\theta}{4\theta_0}\right), \quad \delta(\theta) = \delta \exp\left(-\frac{\theta}{4\theta_0}\right). \tag{4.12}$$

So that the bunch length exponentially increase, while the bunch momentum spread exponentially decrease in time.

We note also another interesting feature of solutions in Eq.(4.10). In a more deep asymptotic region, where $ku \ll 1$, we should use the following asymptotes of the Bessel functions

$$J_0(ku) \simeq 1, \quad N_0(ku) \simeq \frac{2}{\pi} J_0(ku) \left[\ln \frac{ku}{2} + C\right] + O(k^2 u^2) \simeq -\frac{2\theta}{\pi\theta_0}$$

and

$$J_1(ku) \simeq 0, \quad N_1(ku) \simeq \frac{2}{\pi} J_1(ku) \left[\ln \frac{ku}{2} + C\right] - \frac{2}{\pi ku} + O(ku) \simeq -\frac{2}{\pi ku}.$$

In this region the bunch length linearly increases in time

$$\sigma(\theta) \simeq 2\theta\sigma \sqrt{\frac{\nu_s}{\pi\theta_0}}, \tag{4.13}$$

while the bunch momentum spread tends to a constant value

$$\delta(\theta) \simeq \frac{\delta}{\sqrt{\pi \nu_s \theta_0}}. \tag{4.14}$$

These asymptotes correspond to the region, where the RF-voltage is actually turned off.

Both debunching and bunching were simulated using the multiparticle tracking code. After setting up initial conditions for particles, the codes tracked the particle synchrotron oscillations using the following equations for synchrotron coordinates of the particle:

$$\phi_{n+1} = \phi_n + 2\pi P_n, \quad P_{n+1} = P_n - \frac{ZeV_n\eta}{Apv} \sin(h\phi_{n+1}), \quad P = \eta \frac{\Delta p}{p}. \tag{4.15}$$

No space charge phenomena were taken into account in these simulations.

The adiabatic debunching was simulated assuming an exponential decay of the RF-voltage amplitude after acceleration

$$V_n = V_0 \exp(-n/n_0), \quad n_0 = 10\pi/\nu_s.$$

The particles were uniformly distributed to have 10 particles for each of 994 bunches. Within a bunch the initial conditions for particles were generated to have the uniform distribution in the synchrotron phases with the bunching factor $B = 0.3$, and the Gaussian distribution in P with the rms width $\sigma_\delta = 1 \times 10^{-4}$.

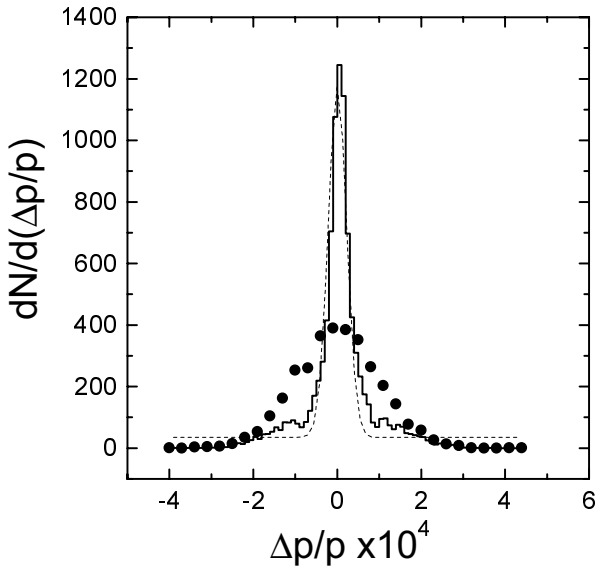

Figure 4.1: Momentum distributions in the initial bunches (full dots) and in the debunched beam (solid steps). $V_0 = 300$ kV; the dotted line shows a Gaussian fit of the final momentum distribution ($\sigma_f = 3.12 \times 10^{-5}$).

As seen from Fig. 4.1, due to debunching the beam momentum distribution shrinks till approximately 3.12×10^{-5}. Because of the high value of the harmonic number the debunching takes only 21 ms, so that it does not limit the repetition rate of the synchrotron.

A small value of the momentum spread in the beam after its debunching may pose limitations on the acceptable values of the synchrotron vacuum pipe impedance. In storage rings and particle accelerators working above the transition energy of the ring the threshold values of the longitudinal coupling impedance, or of the beam current are determined by the so-called Keil-Schnell criterion (see in Ref. [12]). In our case, the ring will work entirely below its transition energy, where the widths of the so-called stability diagram can substantially exceed that defined by the Keil-Schnell criterion.

Namely, for the coasting beam with a Gaussian momentum distribution

$$f_0(\Delta p) = \frac{N}{\sqrt{2\pi}\sigma_\delta} \exp\left(-\frac{[\Delta p/p]^2}{2\sigma_\delta^2}\right).$$

the equation defining the stability diagram of the longitudinal coherent oscillations reads [8]

$$\left(\frac{Z^2}{A}\right)\frac{Ne^2\omega_0}{2\pi pv\eta\sigma_\delta^2}\left[\frac{-iZ_n}{n}\right]=\frac{1}{F(z)}, \tag{4.16}$$

where

$$F(z)=\frac{1}{\sqrt{2\pi}}\int_{-\infty}^{\infty}\frac{dxxe^{-x^2/2}}{z-x}, \quad \mathrm{Im}(z)>0. \tag{4.17}$$

The stability diagram calculated for the coasting beam containing 10^{13} of U^{4+} ions with the kinetic energy 125 MeV/u is shown in Fig.4.2. Inspecting this plot we have to take into account that without other electromagnetic perturbation the perfectly conducting pipe of the radius $l_\perp$ and containing the beam with the radius a, has the capacitive impedance

$$\left(\frac{Z_n}{n}\right)=\frac{30}{\beta\gamma^2}\left[1+2\ln\left(\frac{l_\perp}{a}\right)\right]\ [\mathrm{Ohm}].$$

Taking e.g. $l_\perp = 5$cm (the average beam rms radius is about 1.4 cm), we find $(Z_n/n) \simeq$ 175 Ohm. If this is the only reactive part of the pipe impedance, the active part of

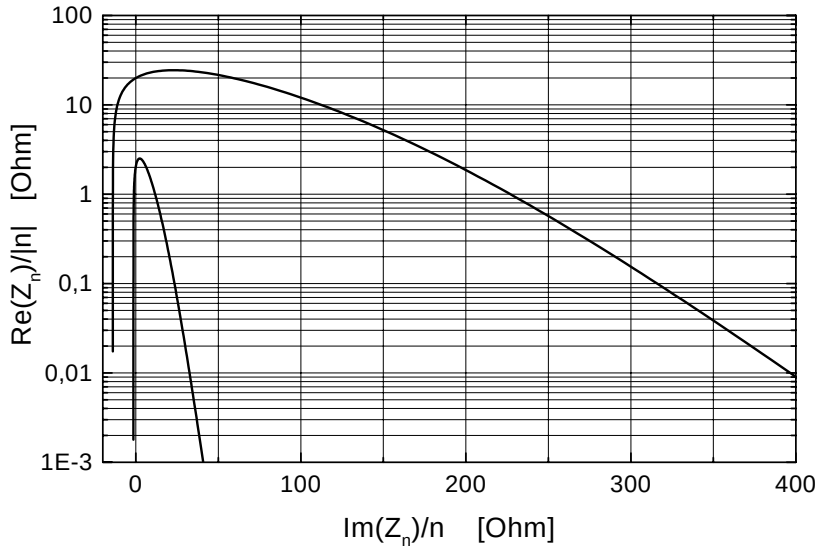

Figure 4.2: Stability diagram for coherent oscillations of the coasting beam after debunching. The beam contains 10^{13} of ions U^{4+}, kinetic energy 125 MeV/u, slip factor 0.77, outer curve – $\sigma_\delta = 3.5 \times 10^{-5}$, inner curve – $\sigma_\delta = 1 \times 10^{-5}$. Only upper half of the diagrams are shown in the graph.

Z_n/n is limited by the value of about 1 Ohm. This value is not high but it is typical for the coupling impedances of the modern synchrotrons and storage rings. Note also, that inductive impedance of about 150 Ohm shifts the working point to the region, where the width of the stability diagram is 10 times wider.

As we shall see, the bunch precompression time can be substantially decreased, if after debunching its momentum spread is decreased till the value of about $\sigma_\delta = 1 \times 10^{-5}$. This number also fits well the longitudinal phase space matching conditions of injected bunches. Due to a quadratic dependences of the widths of the stability diagram on the beam momentum spread, the limitations on the wall impedance will be much more severe (inner curve in Fig.4.2).

For a given closed orbit perimeter and number of particles in the beam, the width of the discussed stability diagram varies proportional to $p\sigma_\delta^2(p)$. Taking into account that Z_n/n also varies proportional to $1/v$, we conclude that effective width of the stability diagram of the coasting beam will be more strongly limited, if the debunching will be performed at the injection energy of particles. Say, at 10 MeV/u and $\sigma_\delta = 10^{-4}$, the vertical width of the diagram increase 3 times, but Z_n/n also increase 3 times and becomes about 500 Ohm. According to data shown in Fig.4.2, the acceptable value of the active part of the impedance is then limited by the region $\mathrm{Re}(Z_n)/n < 10^{-3}$ Ohm.

4.2 Prebunching

If after acceleration the bunches are uniformly distributed along the beam, then after debunching the bunch compression should begin with the prebunching. To form a single bunch that should start with the prebunching in the first harmonic of the revolution frequency rising the RF-voltage adiabatically slow to avoid the blow-up of the longitudinal beam emittance. A reasonable decrease in the bunch length during this period is determined by the threshold value of the Laslett tune shift of the ring. After initial prebunching, the RF-harmonic number can be increased to speed-up the bunch shortening. Prior discussion of particular results we note that a compression during a given time interval may contradict to the necessity of obtaining a given (short) bunch length. The problem is that prior to the bunching the beam already has some momentum spread. During RF compression this momentum spread increases, which can limit the minimum final bunch length from below. Although the compression of the beam with a long enough gap in its filling pattern does not need a special prebunching step, studying of this phenomenon helps to clarify some significant features of the longitudinal bunch compression. In this Section we study of the precompression using adiabatic prebunching due to the rise of the RF-voltage.

4.2.1 Prebunching due to exponentially increasing RF-voltage

Main features of the prebunching due to an increase in the RF-voltage can be studied using the simplified model described in the beginning of this Chapter. In the case, when a harmonic RF-voltage is used for the precompression, such an analysis may have a heuristic worth. However, prebunching may take place due to common effects of multiple harmonics forming a linear dependence of the compression voltage on the distance inside the beam. In such a case, the model will describe a real bunch compression.

Assuming an exponential increase in the amplitude of the RF-voltage

$$\nu_s(\theta) = \nu_s \exp\left(\frac{\theta}{\theta_0}\right),$$

we find that linear synchrotron oscillations are described using the following equations

$$\begin{pmatrix} z \\ z' \end{pmatrix}_0 = \pi\theta_0 \begin{pmatrix} J_0(k) & N_0(k) \\ -\nu_s J_1(k) & -\nu_s N_1(k) \end{pmatrix} \begin{pmatrix} -\nu_s u N_1(ku) & -N_0(ku) \\ \nu_s u J_1(ku) & J_0(ku) \end{pmatrix} \begin{pmatrix} z \\ z' \end{pmatrix}, \quad (4.18)$$

where $k = 2\nu_s\theta_0$ and $u = e^{\theta/(2\theta_0)}$, $J_m(x)$ and $N_m(x)$ are correspondingly the Bessel and Neumann functions of the order m. In this case, the functions a, b, c and d from Eq.(4.4) read

$$\begin{aligned} a &= \pi\nu_s\theta_0 u \left\{J_1(ku)N_0(k) - N_1(ku)J_0(k)\right\}, \\ b &= \pi\theta_0 \left\{J_0(ku)N_0(k) - N_0(ku)J_0(k)\right\}, \\ c &= -\pi\nu_s^2\theta_0 u \left\{J_1(ku)N_1(k) - N_1(ku)J_1(k)\right\}, \\ d &= \pi\nu_s\theta_0 \left\{N_1(k)J_0(ku) - N_0(ku)J_1(k)\right\}. \end{aligned}$$

The bunch length and the beam momentum spread are calculated using

$$\sigma(\theta) = \sqrt{\sigma^2 d^2 + \delta^2 b^2}, \quad \delta(\theta) = \sqrt{\delta^2 a^2 + \sigma^2 c^2}. \quad (4.19)$$

Simple calculations show that in the asymptotic region $k \gg 1$ and $ku \gg 1$ the bunch momentum spread exponentially increases while the bunch length exponentially decays (Fig.4.3).

More close inspection of data from Fig.4.3 shows the following features of such a precompression. The desired precompression factor due to a systematic decrease in the bunch length (about 1/12) is reached in about 0.07 s. However, due to strong mismatching of the longitudinal phase trajectories of the bunch and the ring acceptance both the bunch length and the bunch momentum spread are strongly modulated in time. Since effects of the space charge fields were ignored in our calculations, the calculations will give reliable results only during the time intervals, when the bunch length exceeds the value corresponding to the threshold values of the bunch space charge fields (the desired bunch length after precompression). According to data from Fig.4.3, for a beam with a momentum spread of $\sigma_\delta = 1 \times 10^{-5}$ it occurs when the bunch length reaches its first minimum (about 0.7 ms after beginning of the prebunching). However, due to mentioned mismatching of the longitudinal phase space of the bunch the bunch momentum spread at this time exceeds already about 1000 times its initial value (at Fig.4.3, $\sigma_\delta = 1 \times 10^{-5}$). Such a bunch cannot be used for the subsequent inertial compression.

More reliable parameters of the precompressed bunch can be obtained, if the initial amplitude of the compressing RF-voltage is decreased till e.g. 5 V (Fig.4.4). In this case, the bunch momentum spread initially blowups only twice so that the bunch can be used for a subsequent stronger compression. However, the precompression time becomes extraordinary long (the first minimum in the bunch length in Fig.4.4 is reached after about 0.3 s).

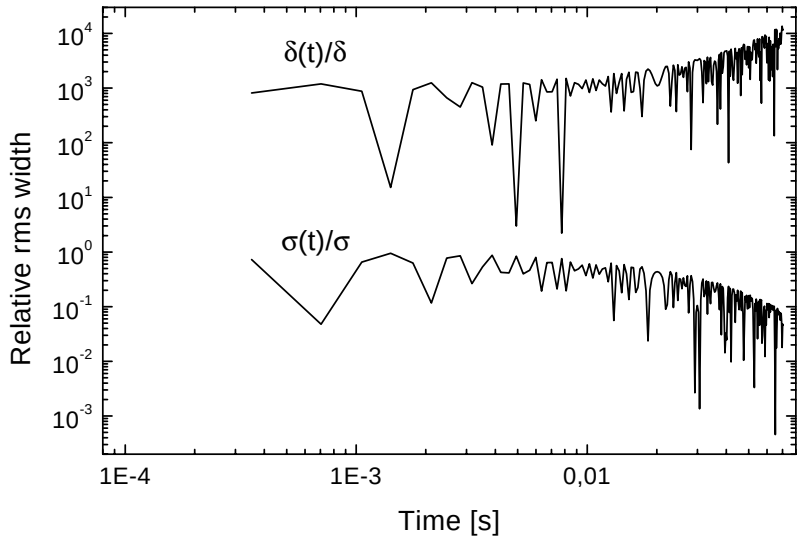

Figure 4.3: Dependences of the relative rms momentum spread (upper curve) and bunch length (lower curve) on time during an exponential increase in the compression voltage. U^{4+} ions, kinetic energy 125 MeV/u, slip factor 0.77, initial RF-voltage 1 MV, $\sigma = 600$ m, $\delta = 1 \times 10^{-5}$, $k = 30$, $\nu_s = 0.0029$.

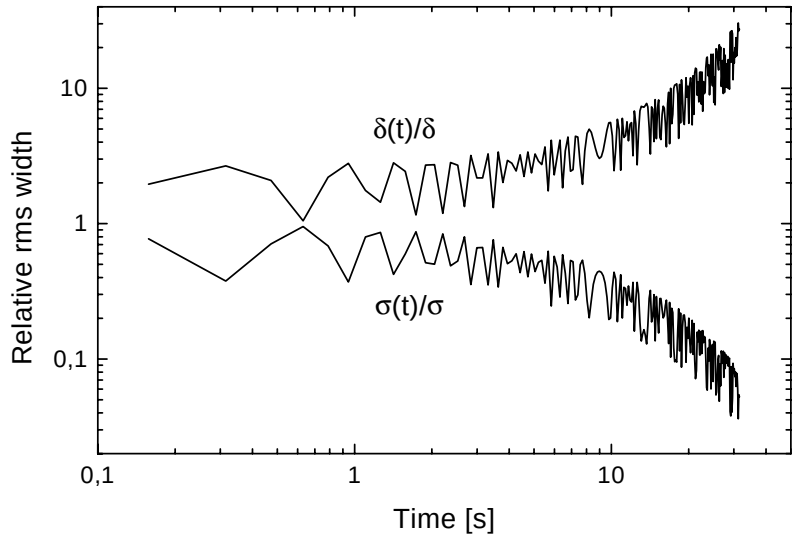

Figure 4.4: Same as in Fig.4.3, but $V_0 = 5$ V.

From these calculations we conclude that the realistic way of the bunch precompression during a reasonable short time providing reasonable values of the momentum spread in the precompressed bunch is a quarter-period longitudinal phase space rotation corresponding to initial parts in Figs.4.3 and 4.4. For example, if we take as initial amplitude of the RF-voltage 200 V, then the bunch length reaches the value $\sigma(\theta) = 50$ m after 0.05 s (solid line in Fig.4.5). If initial value of the beam momentum spread is 10^{-5}, the value of the momentum spread after such a precompression is $\sigma_\delta(\theta) \simeq 2 \times 10^{-4}$ (solid line in Fig.4.6). Open circles in Figs.4.5 and 4.6 show that prebunching of the beam with the initial momentum spread $\delta = 5 \times 10^{-5}$ will be accompanied by smaller modulations of $\delta(\theta)$ but will also take substantially longer time.

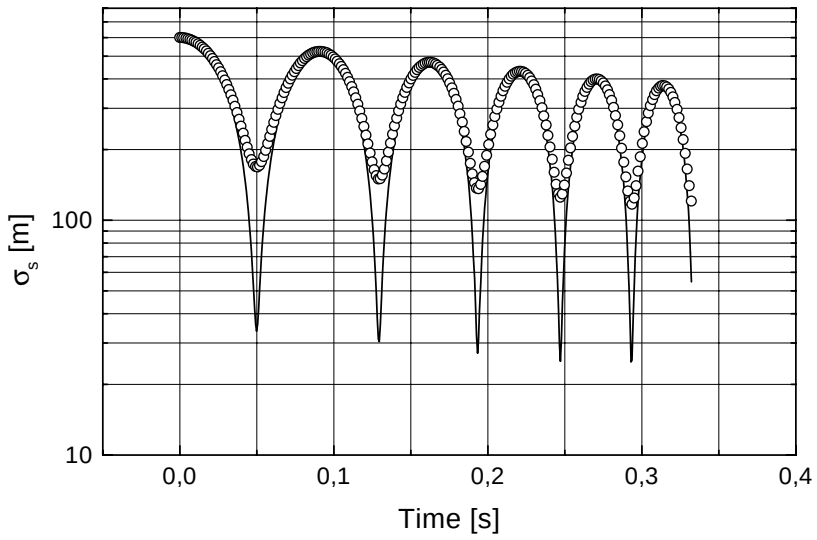

Figure 4.5: Dependences of the relative rms bunch length on time during an exponential increase in the compression voltage. U^{4+} ions, kinetic energy 125 MeV/u, slip factor 0.77, initial RF-voltage 200 V, $\sigma = 600$ m, $k = 30$, $\nu_s = 4 \times 10^{-5}$; solid line – $\delta = 1 \times 10^{-5}$, open circles – $\delta = 5 \times 10^{-5}$.

As we saw in Section 2.4, the final compression should provide the compression factor $X = 70$. If the inertial compression method will be used for the final bunch compression, that demands the following momentum modulation along the precompressed bunch

$$\kappa\sigma(\theta) = X\sigma_\delta = 0.014,$$

or $\delta W = pv\kappa\sigma(\theta) \simeq 3.5$ MeV/u. Such an energy modulation will be obtained when the ions pass the RF-voltage with the following amplitude

$$V = \frac{A\delta W}{Z} \simeq 208 \text{ [MV]}.$$

After this momentum modulation the final bunch compression demands the a drift length of $L \simeq 3.6$ km, or about 3 turns in the ring.

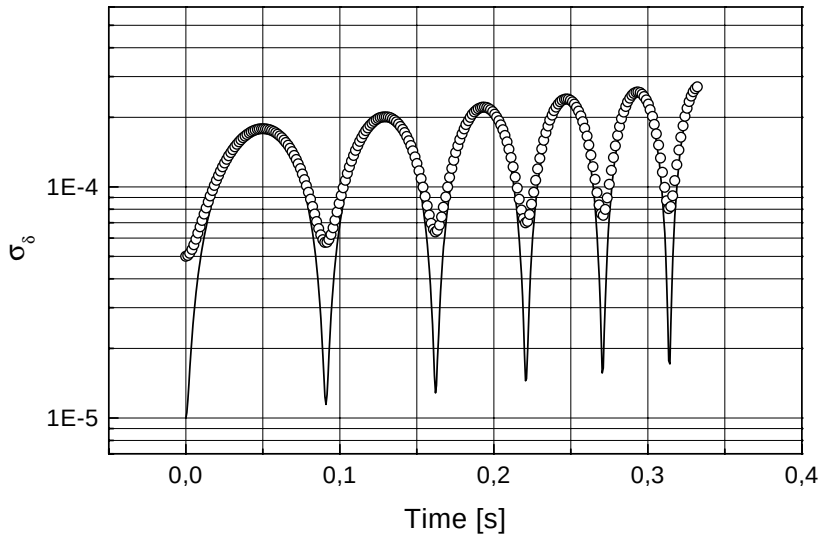

Figure 4.6: Dependences of the relative rms bunch momentum spread on time during an exponential increase in the compression voltage. U^{4+} ions, kinetic energy 125 MeV/u, slip factor 0.77, initial RF-voltage 200 V, $\sigma = 600$ m, $k = 30$, $\nu_s = 4 \times 10^{-5}$; solid line – $\delta = 1 \times 10^{-5}$, open circles – $\delta = 5 \times 10^{-5}$.

4.2.2 Effects of the longitudinal space charge fields on the pre-compression

In the previous subsection the calculations of the bunch length and of the momentum spread during the bunch compression were done neglecting effects of the transverse and longitudinal space charge forces on the motion of ions. For the longitudinal motion the strengths of these perturbations can be described in terms of a reduction of the synchrotron tune by the space charge forces of the bunch. If we assume for the sake of simplicity the parabolic linear density in the beam, the bunch length during compression should exceed its threshold value (Appendix A.2)

$$\sigma_{th}(\theta) = \left(\frac{3}{2} m_p c^2 \frac{ZN r_p \Lambda R_0 \lambda_{RF}}{\gamma^2 e V(\theta)} \right)^{1/3}.$$

If prebunching is performed in the first harmonic of the revolution frequency ($\lambda_{RF} = \Pi$), the amplitude of the RF-voltage should exceed the value

$$V(\theta) = \frac{3}{2e} m_p c^2 \frac{ZN r_p \Lambda R_0 \Pi}{\gamma^2 \sigma_{th}^3(\theta)}, \quad \Lambda = 1 + 2 \ln \frac{l_\perp}{a}. \tag{4.20}$$

According to data shown in Fig.4.7 for $V = 200$ V the space charge forces should be taken into account if the bunch length approaches 600 m.

Effects of the longitudinal space charge fields on the bunch compression were studied using numerical mapping of the following equations for the functions $a(\theta)$, $b(\theta)$, $c(\theta)$, $d(\theta)$,

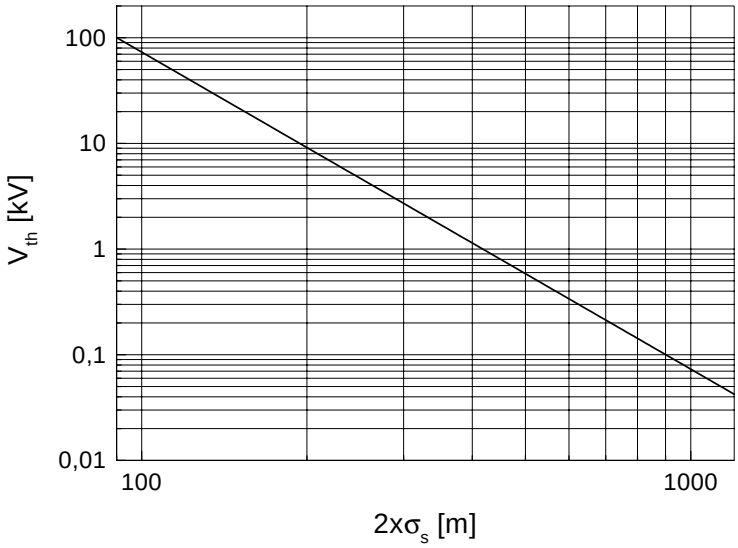

Figure 4.7: Dependences of the threshold RF-voltage ($\nu_s = 0$) on the bunch length ($2\times\sigma_s$). U^{4+} ions, kinetic energy 125 MeV/u, $\lambda_{RF} = \Pi$.

$\sigma(\theta)$ and $\delta(\theta)$:

$$\begin{pmatrix} d \\ c \end{pmatrix}_{n+1} = M_n \begin{pmatrix} d \\ c \end{pmatrix}_n, \quad \begin{pmatrix} d \\ c \end{pmatrix}_0 = \begin{pmatrix} 1 \\ 0 \end{pmatrix}, \tag{4.21}$$

$$\begin{pmatrix} b \\ a \end{pmatrix}_{n+1} = M_n \begin{pmatrix} b \\ a \end{pmatrix}_n, \quad \begin{pmatrix} b \\ a \end{pmatrix}_0 = \begin{pmatrix} 0 \\ 1 \end{pmatrix}, \tag{4.22}$$

$$\sigma_n = \sqrt{\sigma_0^2 d_n^2 + (\delta_0 R_0 \eta)^2 b_n^2}, \quad \delta(\theta) = \sqrt{\delta_0^2 a_n^2 + \left(\frac{\sigma_0}{R_0\eta}\right)^2 c_n^2}. \tag{4.23}$$

Here, n marks the mapping step,

$$M_n = \begin{pmatrix} \cos[\nu_{sn}\Delta\theta], & \dfrac{\sin[\nu_{sn}\Delta\theta]}{\nu_{sn}} \\ -\nu_{sn}\sin[\nu_{sn}\Delta\theta], & \cos[\nu_{sn}\Delta\theta] \end{pmatrix}, \tag{4.24}$$

and

$$\nu_{sn}^2 = \frac{ZeV_n\eta}{2\pi Apv}\left(1 - \frac{(\sigma_{th})_n^3}{\sigma_n^3}\right), \quad (\sigma_{th})_n = \left(\frac{3}{2} m_p c^2 \frac{ZNr_p\Lambda R_0\Pi}{\gamma^2 eV_n}\right)^{1/3}. \tag{4.25}$$

In the regions, where σ_n becomes smaller than $(\sigma_{th})_n$, the trigonometric functions in Eq.(4.24) are replaced for the hyperbolic ones. In order to test if Eqs.(4.21) – (4.23) simulate correctly the bunch compression, we compared the results of the mapping using these equations obtained for the low intensity beam and for the case, when the amplitude of the RF-voltage increases exponentially in time

$$V_n = V_0 \exp\left(\frac{n\Delta\theta}{\theta_0}\right), \quad n = 1, 2, \ldots n_{\max}$$

with results obtained using the analytic solutions (see in Eqs.(4.18) and (4.19)). Comparing

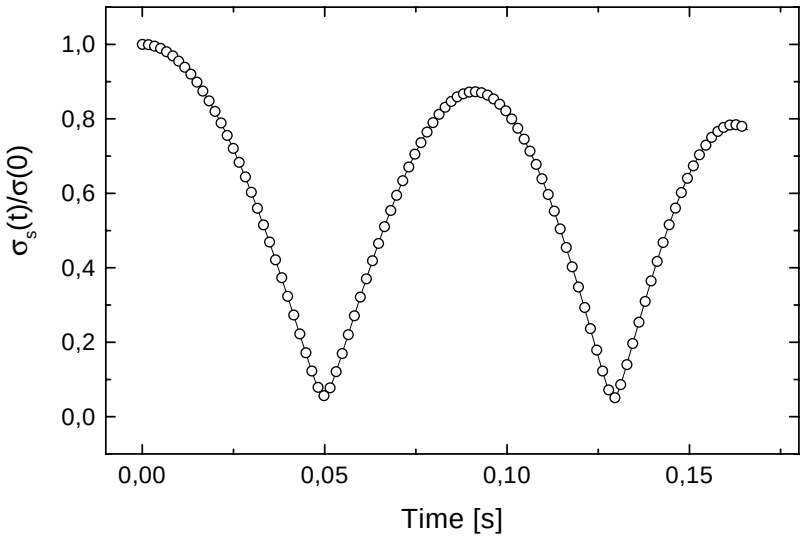

Figure 4.8: Dependences of the bunch length ($\sigma(t)/\sigma(0)$) on the time during exponential increase of the amplitude of RF-voltage. No space charge forces, solid line – exact solution using Eqs.(4.18) and (4.19), open circles – results of numerical mapping, $W = 125$ MeV/u, $V_0 = 200$ V, $k = 10$, $\sigma_0 = 600$ m, $\delta_0 = 1 \times 10^{-5}$.

in Figs.4.8 and 4.9 the curves depicted in the open circles (numerical solution) and in solid line (calculated using Eqs.(4.18) and (4.19)) we find a good agreement between the results of the mapping and of the analytic solution.

During the bunch compression in the low amplitude RF-field, the longitudinal space charge of the beam first of all limits the available compression ratio.

As is seen in Fig.4.10 for the chosen RF voltage the space charge fields hardly affect the compression of the beam containing $N = 10^{12}$ of U^{4+} ions. However, if the number of ions is increased till $N = 10^{13}$ the bunch cannot be compressed shorter than until $\sigma(t)/\sigma_0 \simeq 0.3$. In this case, the dependence of the bunch length on time becomes smoother, while the wave length of its beatings increase. Inspecting the data in Fig.4.11, we see that in the high intensity beam the bunch compression does not stop when the bunch length reaches its threshold value. In particular, in Fig.4.11 the first minimum in $\sigma(t)$ occurs, when it becomes about two times shorter than $\sigma_{th}(t)$. During the period, when $\sigma(t) \leq \sigma_{th}(t)$, the synchrotron oscillations of ions become unstable. For this reason, the time dependence of the bunch momentum spread has additional minima around the points, where the bunch length reaches its minimum value.

The required precompression depth ($\Pi/[2\sigma_s] \simeq 12$) of the high intensity beam ($N = 10^{13}$ of U^{4+} ions) demands higher initial voltages of the precompression RF-system. For

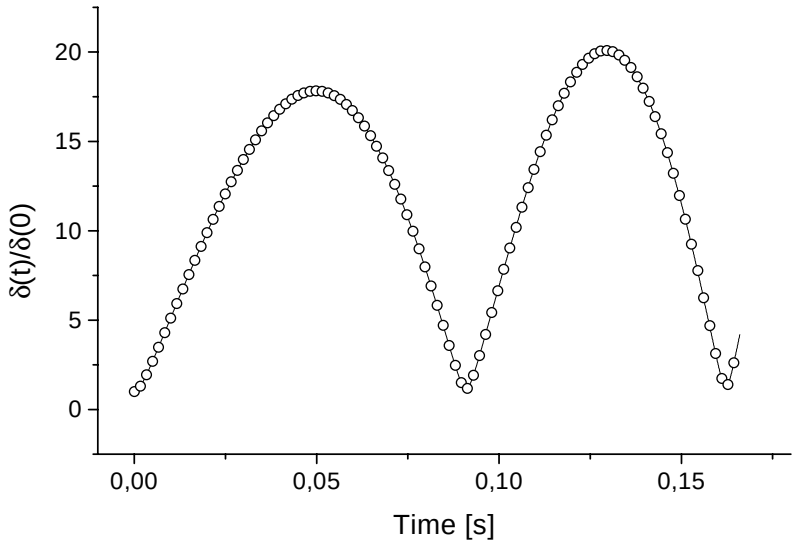

Figure 4.9: Same as in Fig.4.8, but for the beam momentum spread.

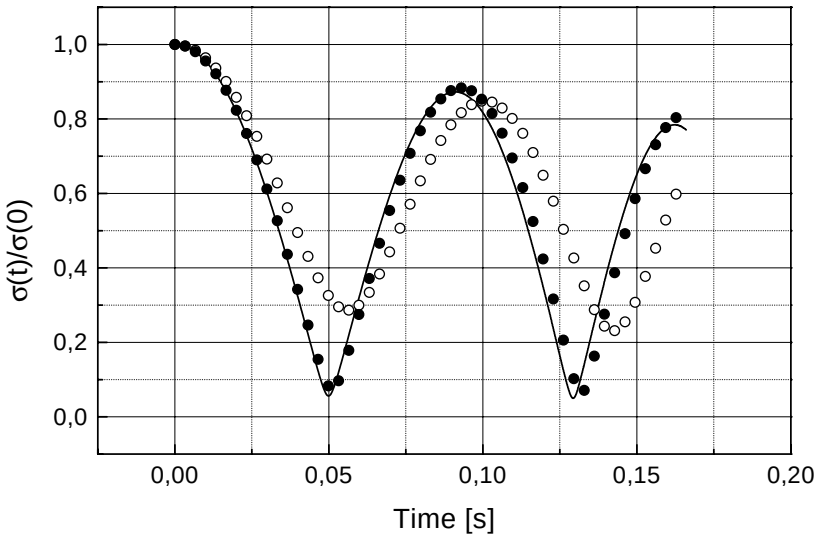

Figure 4.10: Dependences of the bunch length ($\sigma(t)/\sigma(0)$) on the time during exponential increase of the amplitude of RF-voltage. Solid line – neglecting the beam space charge, full circles – $N = 10^{12}$of U^{4+} ions, open circles – $N = 10^{13}$ of U^{4+} ions, $W = 125$ MeV/u, $V_0 = 200$ V, $k = 10$, $\sigma_0 = 600$ m, $\delta_0 = 1 \times 10^{-5}$.

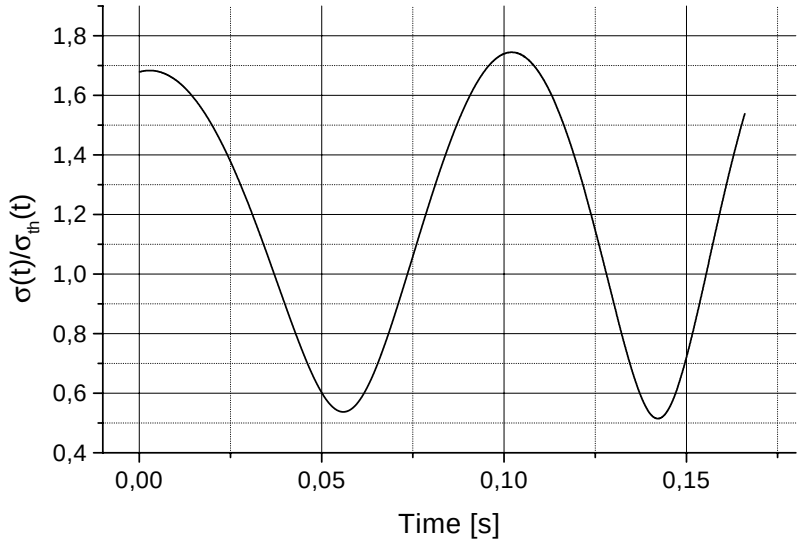

Figure 4.11: Dependences of the ratio $(\sigma(t)/\sigma_{th}(t))$ on time during exponential increase of the amplitude of RF-voltage. $N = 10^{13}$ of U^{4+} ions, $W = 125$ MeV/u, $V_0 = 200$ V, $k = 10$, $\sigma_0 = 600$ m, $\delta_0 = 1 \times 10^{-5}$.

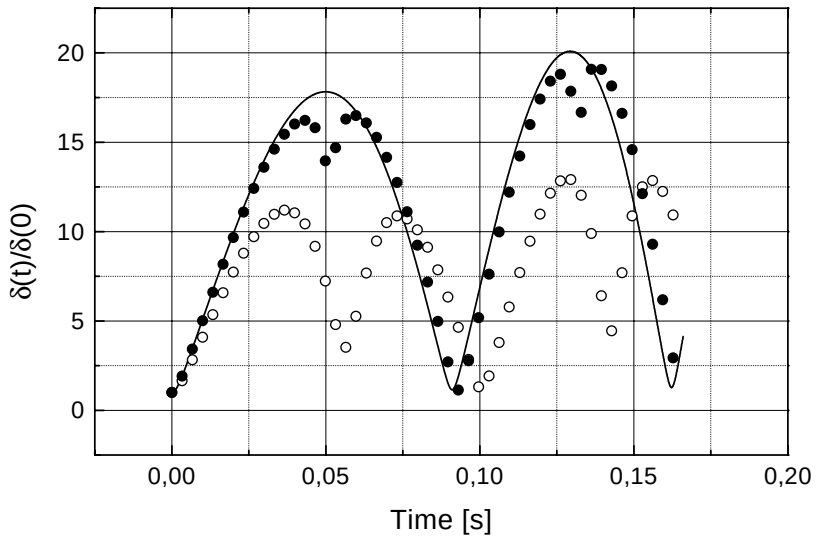

Figure 4.12: Same as in Fig.4.10, but for the beam momentum spread.

example, if we take $V_0 = 1$ kV, the time dependence of the precompressed bunch length ($2\sigma_s/v$) and of the rms bunch momentum spread will change as is shown in Figs.4.13 and 4.14.

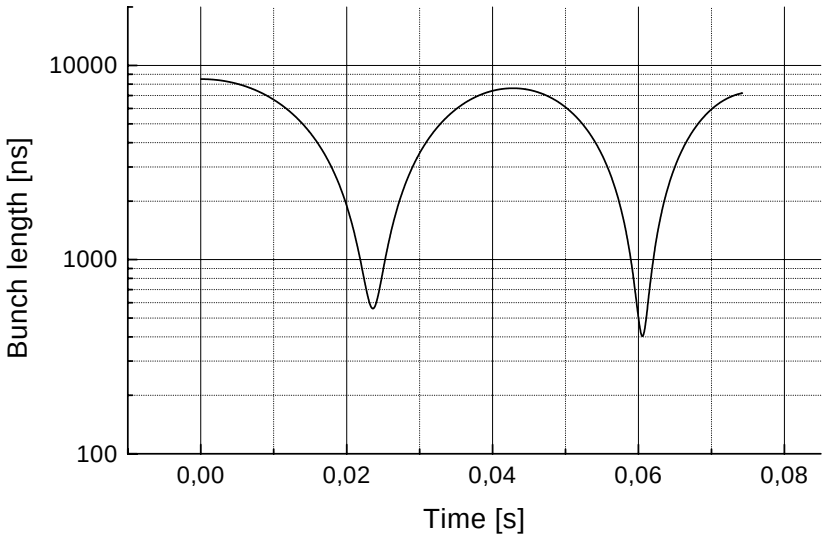

Figure 4.13: Dependences of the bunch length ($2\sigma_s/v$ [ns]) on time during exponential increase of the amplitude of RF-voltage. $N = 10^{13}$ of U^{4+} ions, $W = 125$ MeV/u, $V_0 = 1$ kV, $k = 10$, $\sigma_0 = 600$ m, $\delta_0 = 0.3 \times 10^{-5}$.

According to these data the required length of the precompressed bunch ($\tau_b \simeq 700$ ns) is reached in approximately 22 ms, the rms momentum spread of the bunch at this moment is about 2×10^{-4}. These numbers are quite acceptable for subsequent final bunch compression till $\tau_b = 10$ ns in a straight drift section, or in the ring.

4.3 Final compression

As we already mentioned, after precompression the bunch length can be decreased due to relevant modulation of the ion energy and subsequent inertial compression, or due to $\pi/2$-rotation in its longitudinal phase space. During this stage the space charge fields of the bunch are very strong, so that the Laslett tune shift of the compressed bunch subsequently exceeds the threshold values specific for circular accelerators. The length of the base required for the final compression depends on the amplitude of the energy modulation of the precompressed bunch. For example, as we saw at the end of Subsection 4.2.1 the desired final compression factor ($X = 70$) can be reached, if the beam passes about 3.6 km (three turns in the ring) after initial modulation of the ion energy along the bunch $\Delta p/p = \pm 1.4$ %. Corresponding amplitude of the ion energy modulation (3.5 MeV/u) is obtained if the bunch passes the RF-voltage about 205 MV. For technical reasons, so high RF-voltage cannot be created in a single RF-station. Hence, multiple turns

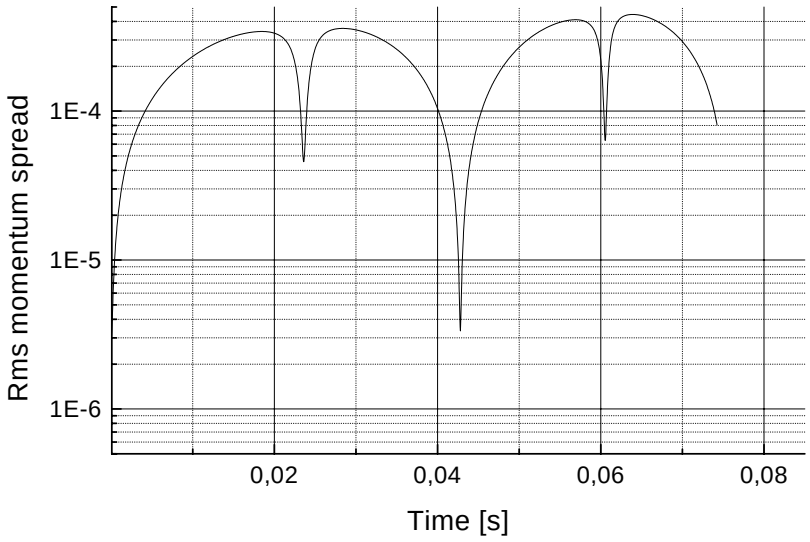

Figure 4.14: Same as in Fig.4.13, but for the bunch rms momentum spread.

become necessary to create required energy modulation in the bunch for its subsequent compression. In practice and depending on the advances in the technology of RF-station designs, the number of turns required to create desired energy modulation may range from 100 (2 MV/turn) till, say, about 7 (30 MV/turn).

In this Section we inspect possibilities of the final bunch compression due to its $\pi/2$-rotation in the longitudinal phase space. We note that in any case, the bunch is compressed due to its mismatching with the longitudinal acceptance of the ring. If the longitudinal beam emittance does not increased dramatically, the momentum spread in the beam after its acceleration till 125 MeV/u will be very low (approximately 3×10^{-6}). We also saw that except for cases, when the precompression starts from very low RF-voltages and therefore takes unacceptable long time, the first stage of the precompression is accompanied by strong blowup of the bunch momentum spread. For this reason, we may expect that, if we start the precompression using high enough initial RF-voltage, the energy modulation required for the final bunch compression can be created during the bunch precompression period. So that a special precompression circle becomes not necessary.

4.3.1 Turn by turn mapping

Since the final compression may take several tens of turns in the synchrotron. In such a case, more reliable results will give the calculations, when the turn by turn mapping is used to simulate the synchrotron oscillations of ions. In addition, these simulations give direct predictions concerning the stability of the synchrotron oscillations of ions during the compression.

For the sake of simplicity we again assume that the longitudinal space charge forces in the beam correspond to a parabolic linear density in the bunch. In this case, the one

turn map is described by the formulae analogous to Eqs.(4.21) – (4.23)

$$\begin{pmatrix} d \\ c \end{pmatrix}_{n+1} = M_n \begin{pmatrix} d \\ c \end{pmatrix}_n, \quad \begin{pmatrix} d \\ c \end{pmatrix}_0 = \begin{pmatrix} 1 \\ 0 \end{pmatrix}, \tag{4.26}$$

$$\begin{pmatrix} b \\ a \end{pmatrix}_{n+1} = M_n \begin{pmatrix} b \\ a \end{pmatrix}_n, \quad \begin{pmatrix} b \\ a \end{pmatrix}_0 = \begin{pmatrix} 0 \\ 1 \end{pmatrix}, \tag{4.27}$$

$$\sigma_n = \sqrt{\sigma_0^2 d_n^2 + (\delta_0 R_0 \eta)^2 b_n^2}, \quad \delta(\theta) = \sqrt{\delta_0^2 a_n^2 + \left(\frac{\sigma_0}{R_0 \eta}\right)^2 c_n^2}. \tag{4.28}$$

In the case, when the bunch is compressed by several (n_{RF}) RF-stations, we assumed that these stations are uniformly distributed along the closed orbit with an azimuthal period $\Delta\theta = 2\pi/n_{RF}$. Then, a single cell was constructed in such a way that it starts and ends at the middle of the arcs separated the RF-stations. The RF-station was described as a single longitudinal kick with the transport matrix

$$M_{RF} = \begin{bmatrix} 1 & 0 \\ -\dfrac{ZeV\eta}{A\pi pv} & 1 \end{bmatrix}. \tag{4.29}$$

The maps between the RF-kicks was constructed using the following matrixes

$$M_O(\theta) = \begin{bmatrix} \cosh(\kappa\theta) & \dfrac{\sinh(\kappa\theta)}{\kappa} \\ \kappa \sinh(\kappa\theta) & \cosh(\kappa\theta) \end{bmatrix}, \quad \kappa^2 = \frac{3}{2} \frac{Z^2 N r_p \Lambda \eta R_0^2}{A\gamma^3 (v/c)^2 \sigma^3}. \tag{4.30}$$

The path length (θ) in this equations was varied to enable an assumption that the bunch length is a constant within a single step. As is seen from Fig.4.15, results of the calculations of the bunch lengths using mappings are in a good agreement with the results of analytic calculations using Eq.(4.18).

The possibility to decrease the steps of numerical integrations in the one turn map enables more accurate accounting of the space charge effects especially in the cases, when the bunch length varies rapidly. These data also show that the amplitude of RF-voltage of 150 kV is not sufficient to reach the desired compression factor. Inspecting the dependence of the (first) minimum bunch length (τ_{bm}) on the initial amplitude of the compressing RF-voltage V_0 we find [Fig.4.16 (a)] that for a single RF-station on the orbit the minimum bunch length (τ_{bm}) decreases more or less regularly until $V_0 \leq 300$ kV. For higher RF-voltages this dependence indicates the oscillations with an increasing amplitude. For the first time it becomes smaller than 10 ns, when RF-voltage exceeds V_0 =900 kV [see in Fig.4.16 (a)]. On the contrary, the number of the turn, when the minimum is reached (the position of the minimum) indicates a smooth dependence on V_0 [Fig.4.16 (b)].

Let us consider in more detail the case, when V_0 =1.13 MV. In this region, the minimum bunch length varies periodically between 45 ns and about 8 ns (see in Fig.4.17). The period of these oscillations is about 15.7 kV. For the beam containing 10^{13} of U^{4+} ions the widths of the regions, where the final bunch length is smaller than 10 ns, is approximately 3 kV. It means that this compression method can be sensitive to the beam loading, which should be strongly suppressed. Comparing the data from Figs.4.17 and 4.18, we find out

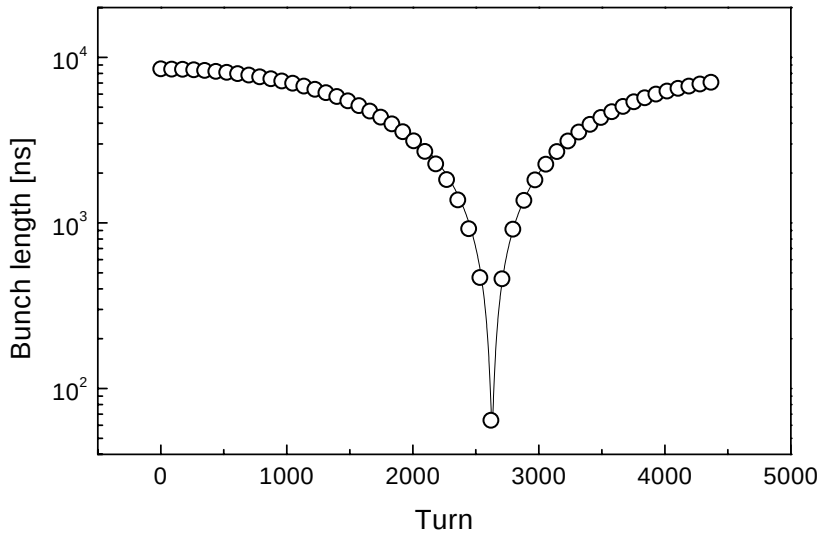

Figure 4.15: Dependence of the bunch length on the turn number for exponentially growing RF-amplitude. No space charge forces, W =125 MeV/u, V_0 =3 kV, $k = 10$, $\sigma_{in} = 600$ m, $\delta_{in} = 3 \times 10^{-6}$. Solid line – calculated using the turn by turn mapping, open circles – analytic solution.

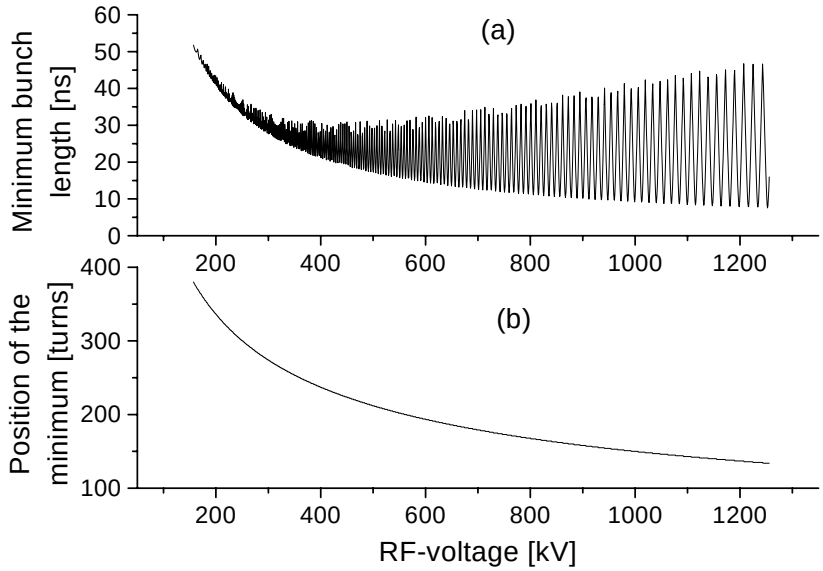

Figure 4.16: Dependence of the (first) minimum bunch length (a) and of the position of this minimum (b) on the amplitude of RF-voltage. $N = 10^{13}$ of U^{4+} ions, W =125 MeV/u, $k = 10$, $\sigma_{in} = 600$ m, $\delta_{in} = 3 \times 10^{-6}$, one RF-station/turn, a drift space between RF-stations is divided by 1200 steps.

that the period of the oscillations in the minimum bunch length is almost independent of the number of ions in the beam. Though, the beam with smaller number of ions can be compressed a bit stronger. The width of the region, where the length of the bunch containing 10^{12} of U^{4+} ions is shorter than 10 ns, is about 25% wider than that for the bunch containing 10^{13} of U^{4+} ions (Figs.4.18).

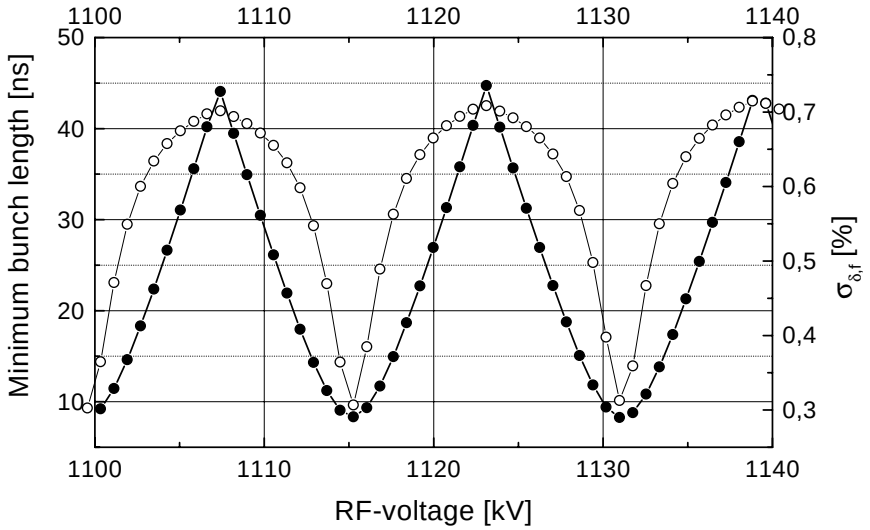

Figure 4.17: Fragment of Fig.4.16 (a) [full circles]. Open circles show the dependence of the compressed beam momentum spread on the amplitude of RF-voltage. Same conditions as in Fig.4.16.

The discussed variations of the minimum bunch length with V_0 occur due to effect of the space charge fields on the bunch compression. As is seen from Fig.4.19, during the turn, when the bunch length reaches its minimum value, the common effect of the RF-system and of the space charge forces may result in the over focusing of the synchrotron oscillations of ions. So that the bunch length reaches its minimum at the point which differs from the end point of the cell. The value of the minimum bunch length in all these points is approximately the same (Fig.4.19). No such phenomena occur during the preceding turn (compare solid and dashed curves in Fig.4.20).

If V_0 =1.131 MV, the final stage of the compression (the bunch length becomes shorter than 1 ms) takes 10 turns (Fig.4.21, full circles). The bunch momentum spread to this time reaches about ± 0.8 %. During the final compression the Laslett tune shift ranges from $\Delta\nu_L = 0.1$ till $\Delta\nu_L = 10$ (see in Fig.4.21, open diamonds). According to these data $\Delta\nu_L$ exceeds 0.3 during the last 5 turns before extraction and exceeds $\Delta\nu_L = 1$ during the very last turn (the turn number 141).

During the compression time the RF-amplitude increases by the factor of 1.85 exponentially varying from 1.131 MV till about 2.07 MV:

$$V_m = V_0 \exp\left(\frac{m}{230}\right), \quad m = 0, 1, \ldots 141 \tag{4.31}$$

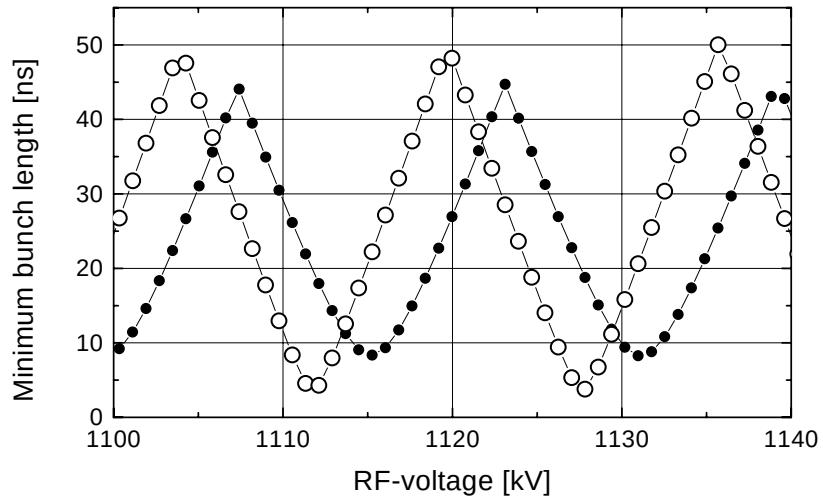

Figure 4.18: Dependence of the minimum bunch length on V_0. Full circles: 10^{13} of U^{4+} ions, open circles: 10^{12} ions. Other parameters are the same as in Fig.4.16.

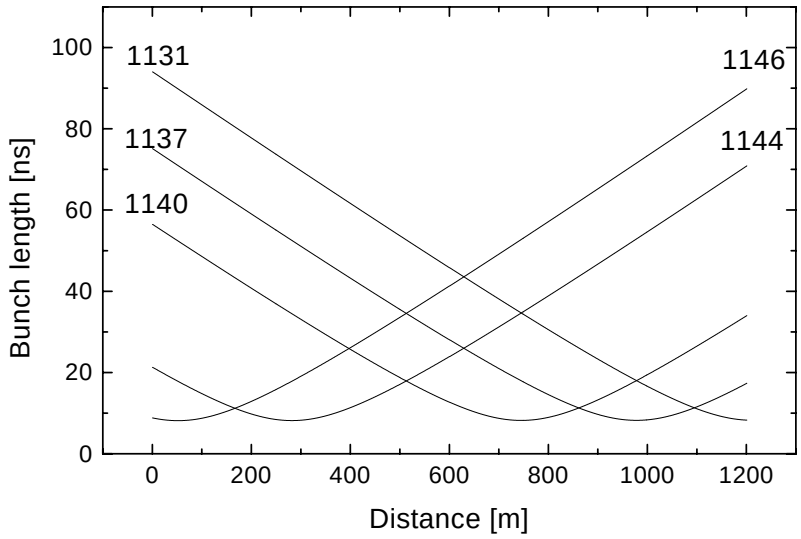

Figure 4.19: Dependence of the bunch length on the distance along the closed orbit during the 141-th turn. Same conditions as in Fig.4.16; the numbers near curves are the values of V_0 in kV.

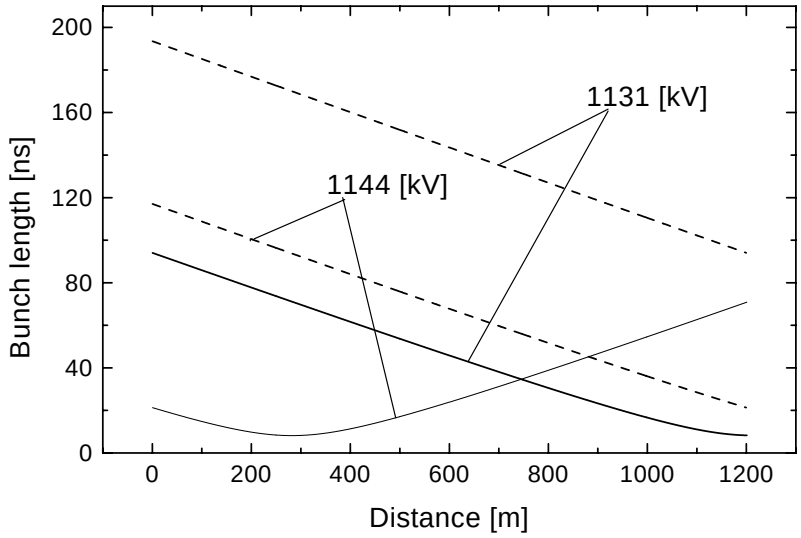

Figure 4.20: Dependence of the bunch length on the distance along the closed orbit during the 141-th (solid lines) and during 140-th (dashed lines) turns of the compression. Same conditions as in Fig.4.16; the numbers near curves are the values of V_0 in kV.

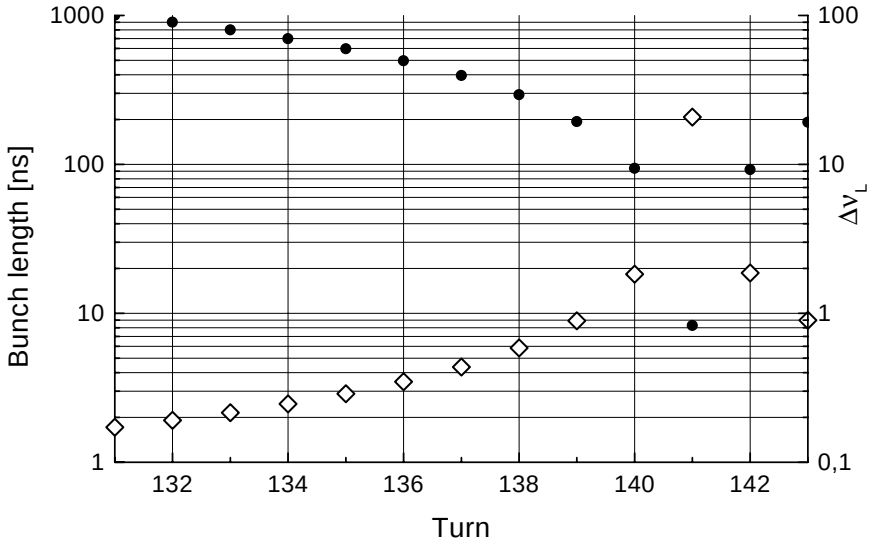

Figure 4.21: Dependence of the bunch length (full circles) and of the Laslett tune shift (open diamonds) on the turn number. $N = 10^{13}$ of U^{4+} ions, W =125 MeV/u, V_0 =1.131 MV, $k = 10$, $\sigma_{in} = 600$ m, $\delta_{in} = 3 \times 10^{-6}$, one RF-station/turn, a drift space between RF-stations is divided by 4800 steps.

Without such variation the minimum value of the bunch length becomes less than 10 ns for higher amplitudes V_0 (see in Fig.4.22).

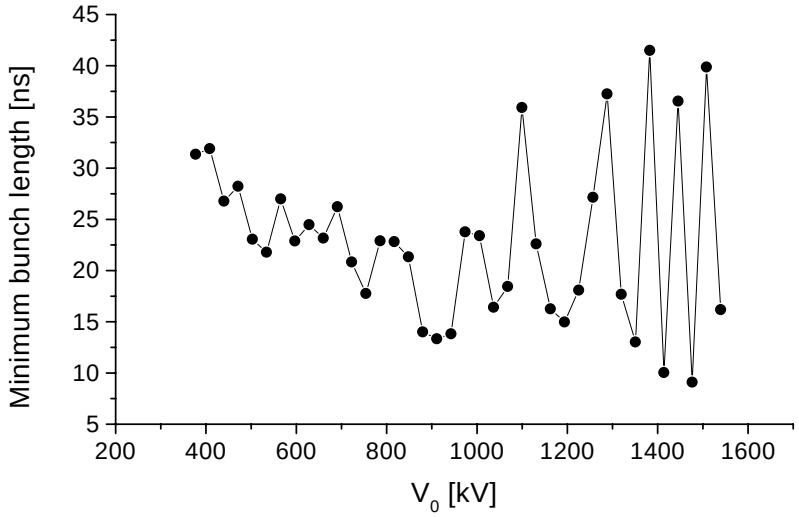

Figure 4.22: Same as in Fig.4.16, but RF-voltage is constant during the bunch compression.

Generally, the minimum value of the bunch length after compression depends on the initial value of the momentum spread in the bunch. As is seen from Fig.4.23, for the beam containing 10^{13} of U^{4+} ions the difference in the minimum bunch length for the bunches having $\delta_{in} = 3 \times 10^{-5}$ and having $\delta_{in} = 3 \times 10^{-6}$ can reach the factor of four, while the maxima in these curves differ only about 30%. This picture also shows that the period in the oscillations of the compressed bunch length is almost independent of the initial value of the momentum spread in the bunch.

These calculations show that, if the single bunch is obtained in the synchrotron without strong blowup of the longitudinal emittance, effects of the bunch space charge fields in the high intensity mode ($N = 10^{13}$) do not limit the possibility of the bunch compression till the length of about 10 ns. Provided that the initial amplitude of RF-voltage linearly varies along the bunch and is high enough, such a compression can be done as a one step in the cycle and without additional energy modulations of the precompressed bunch. However, more complete analysis including the transverse blowup of the compressed bunch is necessary.

4.3.2 Separate energy modulation and bunch compression

During the bunch compression the bunch length decrease approximately 850 times. Correspondingly, the local beam current increase by the same factor approaching the value of 640 A. It means that, if such a bunch will interact with a system having the coupling impedance of about 100 Ohm, it will induce there the voltage of about 64 kV. For example,

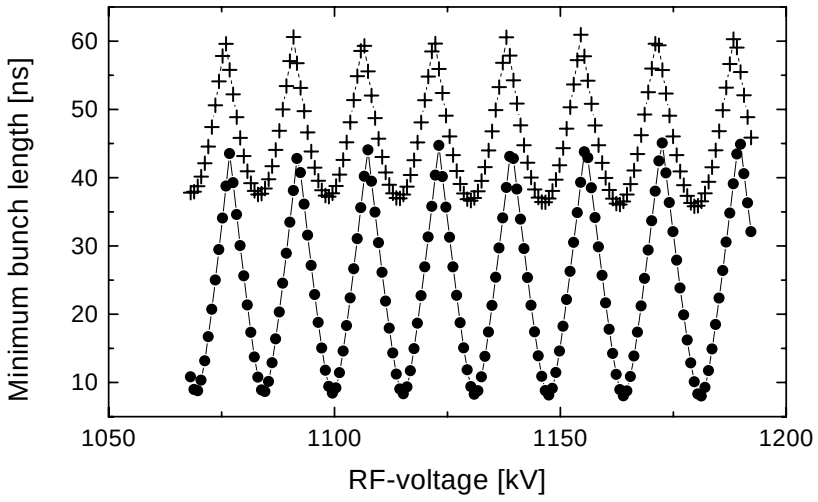

Figure 4.23: Dependence of the minimum bunch length on V_0. Same conditions as in Fig.4.16, but crosses correspond to $\delta_{in} = 3 \times 10^{-5}$, while circles to $\delta_{in} = 3 \times 10^{-6}$.

such an impedance, or higher, may have the RF-system producing the sawtooth compressing voltage. As we saw, even smaller RF-voltage distortions can affect substantially the value of the bunch after compression. On the other hand and as is seen from Fig.4.24 (dashed curve), significant variations of the bunch length start after the period, when the bunch momentum spread increases substantially. This is a specific feature of the compression due to $\pi/2$–rotation in the longitudinal phase space. Using this feature we can avoid additional perturbations of the bunch longitudinal phase space due to undesirable interactions with high impedance devices, if after increasing the bunch momentum spread till necessary value, we move the bunch in the bypass which is free of the RF-systems (the layout of such a synchrotron can look, for example, as is shown in Fig.4.25). The vacuum chamber in this third bypass can be designed to have as low coupling impedance as possible.

The bunch compression using energy modulation and final compression in the separate bypasses was simulated switching off the compressing RF-voltage in the simulation code (Fig.4.26).

Relevant variations of the bunch momentum spread for the cases when the energy modulation occurs during the first 100 and 50 turns are shown in Fig.4.24 (curves 2 and 3, respectively). The turn number, when the final compression occurs in these curves is indicated by dips. According to these data, the bunch compression till the final length of 10 ns can be done using initial RF-amplitude of 1.131 MV, if the bunch is moved to RF free bypass after the first 100 turns. For this RF-voltage, the period of 100 turns is necessary to reach the momentum spread in the bunch ≈ 0.7 %. After this energy modulation the bunch length of 10 ns is reached after passing of 45 turns in the RF-free bypass (inertial compression). During this period the bunch length decreases (while

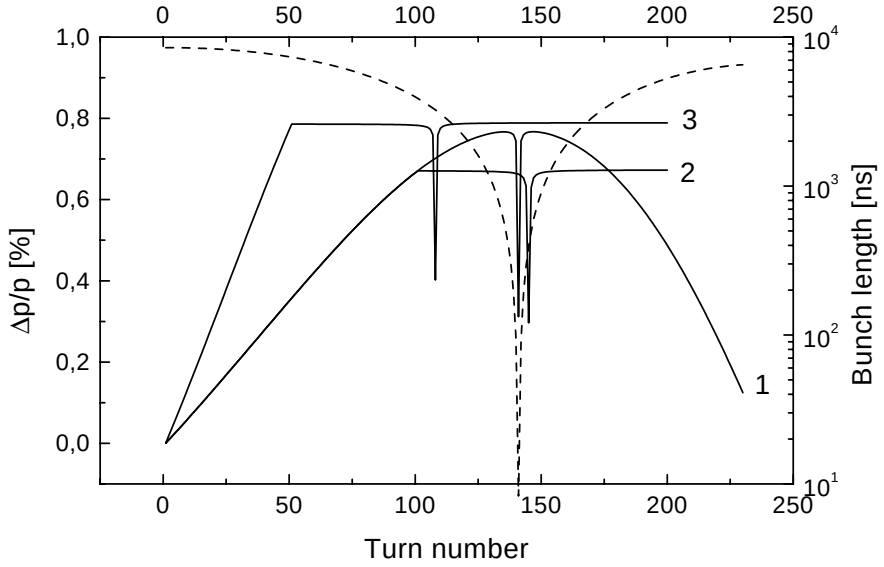

Figure 4.24: Dependence of the bunch momentum spread (left axes) and of the bunch length (right axes; $V_0 = 1.131$ MV) on the turn number. Most conditions are same as in Fig.4.16, but 1– RF-voltage is on during all the compression period, $V_0 = 1.131$ MV, 2– same RF-voltage is on during first 100 turns; 3– RF-voltage is on during first 50 turns, $V_0 = 2.48$ MV.

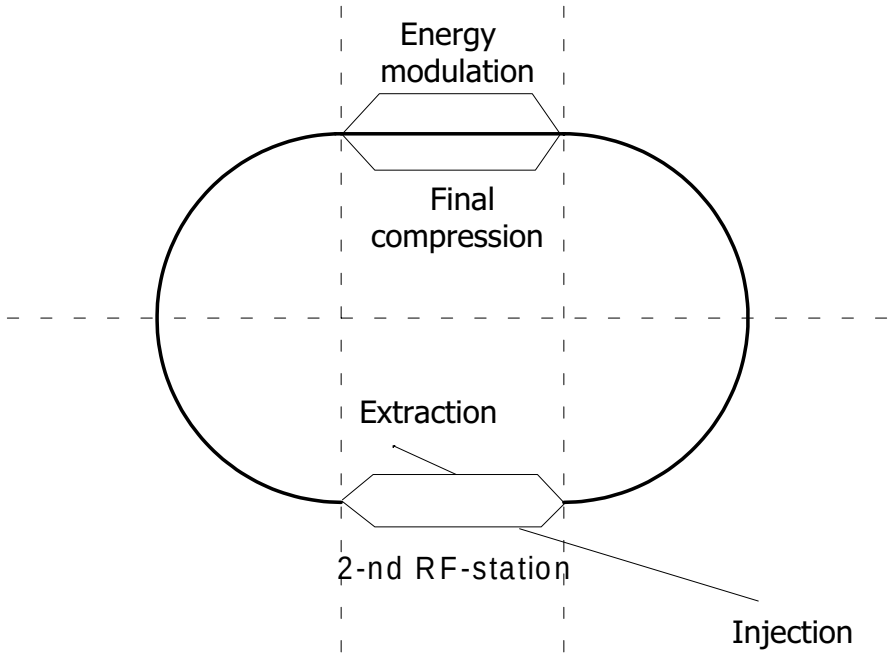

Figure 4.25: Schematic layout of the synchrotron with the separated energy modulation and final bunch compression.

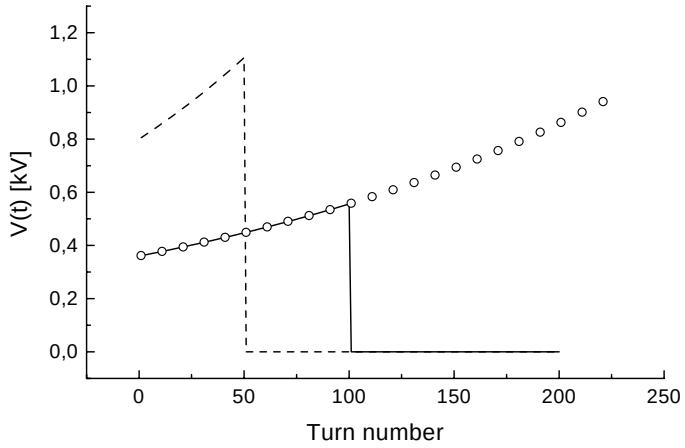

Figure 4.26: Dependence of the RF-voltage on time to simulate bunch compression in two bypasses. Open circles – bunch compression in a single bypass; solid line – bypass switch after 100 turns; dashed line – after 50 turns.

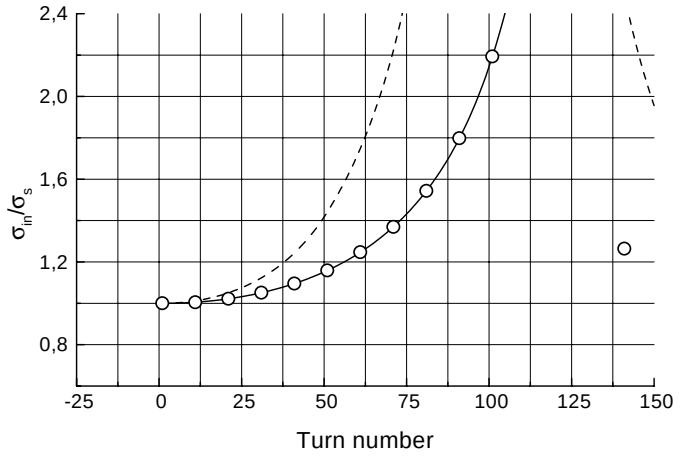

Figure 4.27: Dependence of the bunch length ($\sigma_{in}/\sigma_s(t)$) on the turn number. Most conditions are same as in Fig.4.16. Open circles – continuous compression, V_0 =1.131 MV; solid line same RF-voltage during first 100 turns; dashed line – energy modulation during first 50 turns, V_0 =2.48 MV.

the local bunch current increases) by the factor 2.2. Smaller increase in the local bunch current is possible (by the factor 1.4; Fig.4.27), if the energy modulation occurs during the first 50 turns. However, the final bunch length will reach in this case 10 ns, if the RF-amplitude is increased about twice ($V_0 = 2.48$ MV). This energy modulation mode can be reasonable, if an increase in RF-amplitude can be done with the same amount of the RF-stations.

Chapter 5

Optics of the Synchrotron Ring

The lattice of the synchrotron should enable all functions of the ring in the bunch compression operation mode (U^{4+} ions within the energy range 10–125 MeV/u) as well as two high energy modes providing the possibility to accelerate in the ring the ions of U^{12+} and U^{92+} as it was mentioned in the Introduction.

In the bunch compression mode the ring will operate the beams with heavy space charge conditions both at the injection energy (10 MeV/u) and at the extraction energy during the final stage of the compression (energy 125 MeV/u). In order to suppress the space charge instability the lattice focusing should be strong enough (to enable the final compression as deep as possible). For the same reason, the symmetry of the lattice should be as high as possible to reduce the amount of the lattice resonances and nonlinear resonances due to space charge fields of the beam. The lattice design should also avoid strong modulations of the betatron functions of the ring. In line with these requirements, the lattice should provide enough space for straight sections for injection and extraction of the beam, for RF–stations, for various correctors and for the beam diagnostic tools. It seems that a racetrack scheme with two arcs having very high super-symmetry and connected by two straight sections with the optics matched to the arcs can fit all mentioned requirements.

5.1 Arc lattice

For the arcs of the synchrotron the anti-symmetrical magnetic FODO structure was chosen as a standard cell. The total number of cells in the arcs is 2×50, so that the bending angle of the cell is $\phi_B = 62.83$ mrad. The cell contains two zero-gradient dipoles with the bending angle 31.415 mrad separated by equal spaces from focusing and defocusing quadrupoles (Table 5.1). For the top guiding field $B = 1.4$ T and BR=100 Tm, the bending radius of the closed orbit in a dipole is $R = 71.43$ m. The length of the cell is 10 m, so that the closed orbit perimeter in the arcs is 1 km. Remaining length of the orbit can be divided between long straight sections. The betatron functions for this cell (Fig.5.1) correspond to $\beta_{av} \simeq 16$ m, so that no strong reduction of the lifetime due to charge-changing IBS can be expected, when the ions move inside the arcs.

The betatron phase advance per cell is about 36°, which corresponds to about equal vertical and horizontal betatron tunes of ≃10. The momentum compaction factor of the

Table 5.1: Parameters of the arc cell. The length of the cell is 10 m, BR=100 Tm.

Item	L [m]	B [T]	∇B [T/m]	ϕ_B [mrad]	R [m]
Quad	0.804		8.63	0	
Space	0.6			0	
Dipole	2.245	1.4		31.415	71.43
Space	0.6			0	
Quad	1.525		-9.22	0	
Space	0.6			0	
Dipole	2.245	1.4		31.415	71.43
Space	0.6			0	
Quad	0.804		8.63	0	

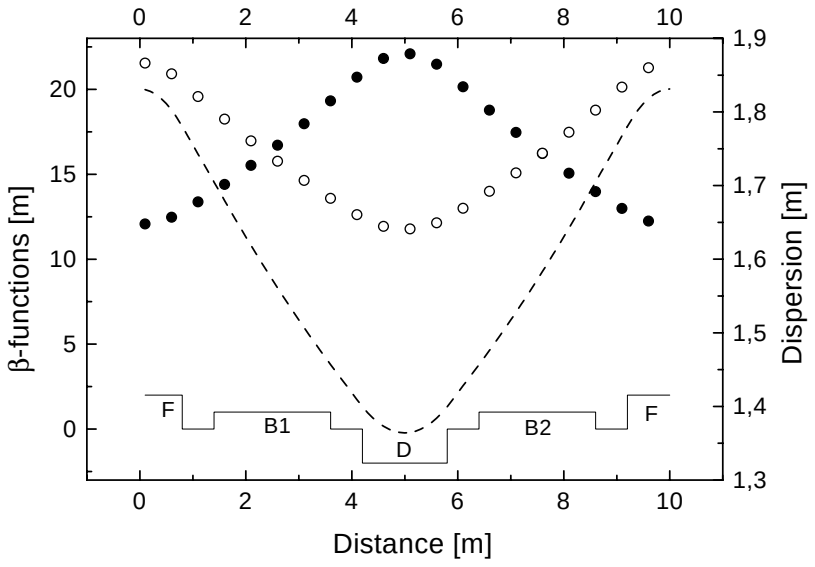

Figure 5.1: Dependences of the betatron functions on the distance inside the arc cell. Full circles – β_y, open circles – β_x, dashed line – dispersion function of the ring.

ring is 0.00827, which corresponds to $\gamma_{tr} = 11$. For the beam with an invariant emittance of $\epsilon_0 = 20$ mmmrad the maximum deviations of the envelope from the closed orbit at injection energy 10 MeV/u are 5.5 cm (Fig.5.2; we remind the reader that the beam emittance $\epsilon = \epsilon_0/[\gamma(v/c)]$ is in this case 138 mmmrad). If the pipe radius exceeds this value about twice, the vacuum chamber diameter should be about 20 cm.

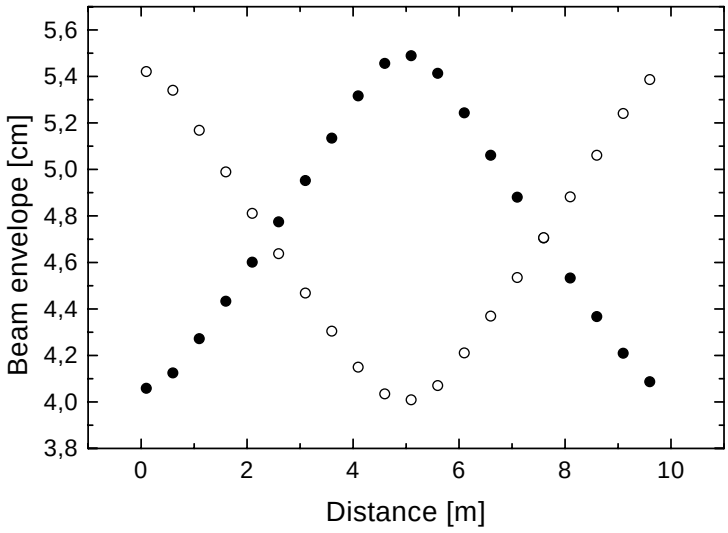

Figure 5.2: Dependences of the betatron envelopes on the distance inside the arc cell. The envelopes were calculated for $W = 10$ MeV/u and for ϵ_0 =20 mmmrad (20-turn injection; corresponding non-invariant emittance $\epsilon \simeq \epsilon_0/(v/c)$ is 138 mmmrad).

5.2 Long straight section lattice

The lattices of the long straight sections should fit the requirements which will enable the operations of the beam injection/extraction system and of the RF-systems of the synchrotron. The optics of these straight sections should be matched to that of the arc cells. In the simplest case, those can be the lattices providing the I-type (or, [-I]-type) transport matrixes for the low intensity beam. For example, such lattice for a single straight section can be constructed using the cells similar to those in the arcs, but with zero bending fields and $\pi/2$ phase advance over a single cell (see in Table 5.1). Four of such cells (of 40 m long) provide the I-type transformation over the straight section. The betatron functions for a single $\pi/2$-cell are shown in Fig.5.3.

All these lattices and parameters of their elements should be considered as examples, which can be specified in more detail during the future design work.

Table 5.2: Parameters of the long straight section cell. The length of the cell is 10 m, BR=100 Tm.

Item	L [m]	∇B [T/m]
Quad	0.8	7.4
Space	3.45	
Quad	1.5	-8.6
Space	3.45	
Quad	0.8	7.4

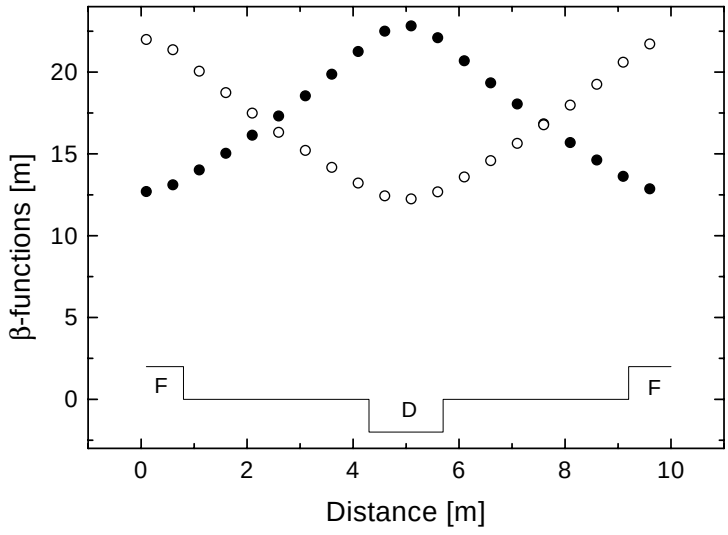

Figure 5.3: Dependences of the betatron functions on the distance inside the cell in the straight section. Full circles – β_y, open circles – β_x.

5.3 Bypass switch

We consider here a possible variant of the switchyard, which enables the single turn passing of the beam from the equilibrium orbit in the synchrotron to the bypass and back. Furthermore, this scheme has two additional beam lines: the first - for injection and acceleration of ions, the second - for energy modulation and initial compression of the beam, and the third - for finally bunch compression. In this report we suppose to use two special insertions (named bypass insertion BI) which are placed in the opposite long straight sections with the relative betatron phase advance close to some integer of 2π. Every one of the BI includes two switching insertions (SI). General schematic layout of the bypass insertion is shown in the Fig. 5.4

Every switching insertion occupies two sells of the lattice (see in Fig.5.5). It includes two full-aperture switching magnets RSM1 and RSM2, and a special two-aperture bending magnet BM (see in Fig. 5.6). The bending magnets inside the bypasses (M) are the standard arc bending magnet in their standard regime.

Every bypass insertion occupies in the straight section four cells of the lattice on two roads and six one - on the third road. All elements are disposed in the horizontal plain. The two-window bending magnet is designed to produce the magnetic fields which have the opposite direction in each of its windows. This provides the beam deflection to opposite directions in the horizontal plain according to a field direction in the RSM1 and RSM2, and respectively, the beam position in the BM aperture. During acceleration the magnetic fields in the magnets BM, RSM1 and RSM2 vary similar to that in the bending magnets of the arc dipoles.

The field directions in every part of BM aperture are fixed. On the contrary, RSM1 and RSM2 have identical field direction but last one must be changed, if we want to keep the beam in the main ring or in the one of the bypass lines. To exchange the field direction it is necessary to apply a high voltage to the switching magnets winding during the field exchanging only. During another time the winding voltage depends on the winding active resistance and field change velocity as in usual magnets. The switching magnets are divided for some section in the longitudinal direction to reduce the winding voltage.

All elements aperture matches to the one of the regular part of the ring equal to 10 cm (diameter). To fit this condition according with a horizontal envelop function behavior, the aperture of the F-lens between RSM1 and RSM2 must be increased since 10 to 12.5 cm. Therefor the one of the D-lens downstream RSM2 must be increased to 14.5 cm. The second insertion presents a mirror image of the one in the longitudinal direction. Main parameters of the bypass insertion are shown in the Table 5.3.

5.4 Transverse dynamics during bunch compression

During the bunch compression the lattice should be tuned in a way which enables suppressions of additional blowups of its longitudinal and transverse emittances. Just after acceleration the beam passes to the RF-free bypass line (Compression and extraction orbit in Fig.5.4) for the debunching into a single bunch. As we saw in Section 4.1, this period takes about 20 ms. During debunching the Laslett tune shift of the beam decreases from

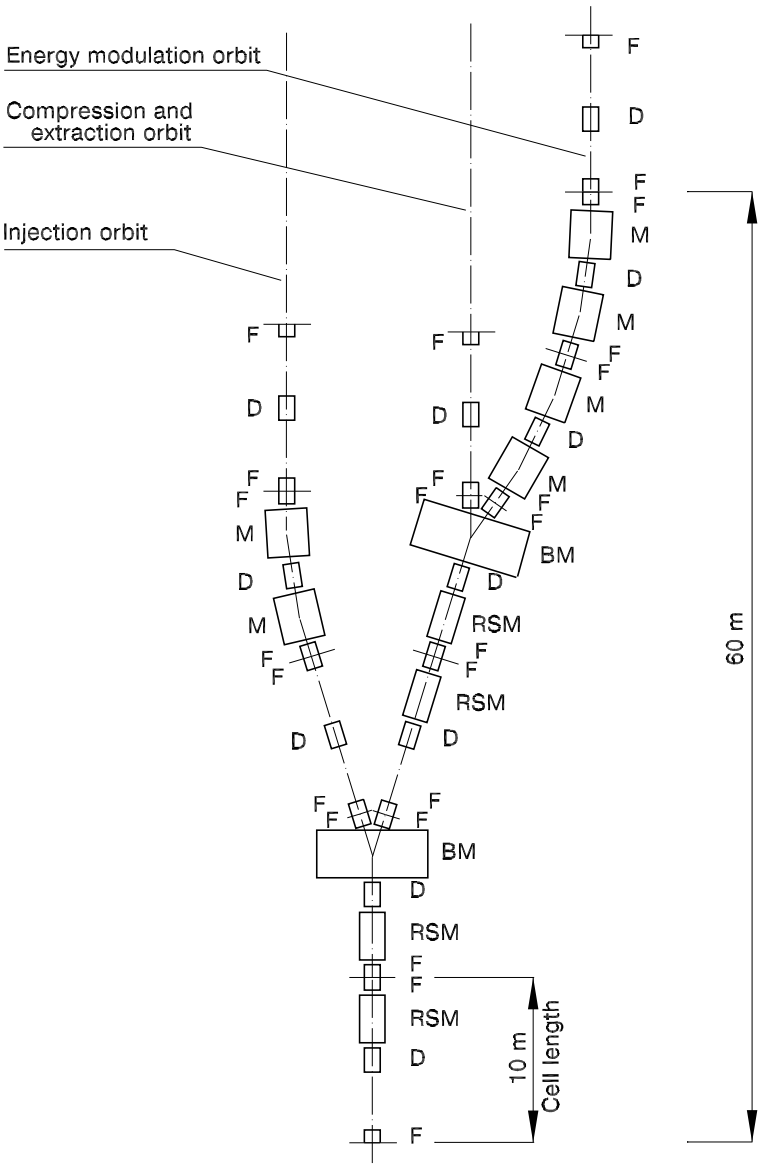

Figure 5.4: General schematic layout of the bypass insertion: F, D - lenses, RSM - switching magnets, BM - two-aperture bending magnets, M - bending magnet (standard for arcs).

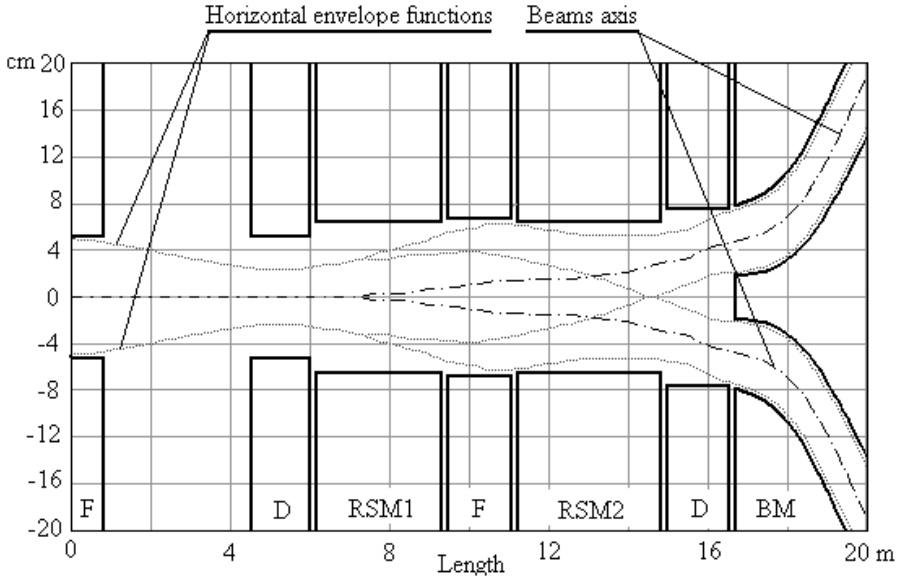

Figure 5.5: Layout of the switching insertion to bypass.

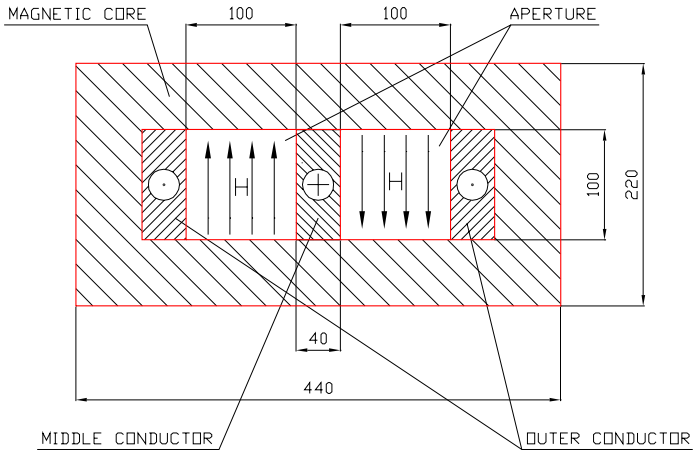

Figure 5.6: Schematic (input) cross section of the two-aperture bending magnet (BM).

Table 5.3: Parameters of the bypass insertion

Parameters	Unit	Value
Beam energy	MeV/u	125
Magnetic rigidity	Tm	100
Particle repetition period	ms	8.511
switching time	ms	0.85
Total horizontal orbit separation at the BM exit	cm	$\pm$ 19.26
Output angle	mrad	$\pm$ 62.83
switching magnets RSM1, RSM2		
Deflection angle	radian	0.005
Horizontal aperture	cm	12
Vertical aperture	cm	10
Total length	m	3.0
Cell number		10
Cell length	m	0.3
Magnetic field	T	0.176
Current	kA	13.33
switching voltage per cell	kV	14
Two-aperture bending magnet BM		
Horizontal aperture (single)	cm	10
Vertical aperture	cm	10
Length	m	3.055
Magnetic field	T	1.5
Bending angle	mrad	45.83
Horizontal thickness of the middle conductor	cm	4.0
Bending magnet M (standard for arcs)		
Length	m	2.245
Magnetic field	T	1.4
Bending angle	mrad	31.415

about 0.04 till 0.02. These values are not very high. So that the betatron tunes may take any convenient positions on the tune diagram.

After debunching, the long bunch is passed to the energy modulation line of the bypass (see in Fig.5.4). During this period and depending on the value of the desired energy modulation gain the bunch length can decrease by the factor of 2, or 1.4. Correspondingly, the Laslett tune shift of the bunch will increase from 0.02 till about 0.04 (or, less for rapid energy modulation). Provided that the working point in the tune diagram is placed below the parametric resonance, this value of the tune shift also should not result in any significant blowup of the transverse bunch sizes.

Most significant blowups of transverse bunch sizes can be expected during the last turns of the compression, when the bunch becomes so short that the betatron tunes approach from the above, or cross the parametric resonance (resonances). For this period, the bunch passes again to the compression and extraction orbit line of the bypass (see in Fig.5.4). Since the tune shift due to repulsion of ions is negative, to that time the working point of the ring in the betatron tune diagram should be tuned as close as possible to the parametric resonance from the below.

Transverse blowup of the compressed bunch was simulated using a simplified code taking into account the bunch compression as was described above and possible variations of the horizontal and vertical beam envelopes due to space charge fields. For the sake of simplicity, we assumed $D\sigma_\delta \ll \sigma_x$, which holds well for our parameter sets. Then, the single turn transport matrix was calculated solving step by step the following equations:

$$\frac{d^2y}{ds^2} + \left[-\frac{\nabla B}{BR} - \frac{C_1}{\sigma_s\sigma_y(\sigma_x+\sigma_y)}\right] y = 0, \quad C_1 = \frac{3}{2}\frac{Z^2 N r_p}{A\gamma^3(v/c)^2}, \tag{5.1}$$

$$\frac{d^2x}{ds^2} + \left[\frac{1}{R^2} + \frac{\nabla B}{BR} - \frac{C_1}{\sigma_s\sigma_x(\sigma_x+\sigma_y)}\right] x = 0, \quad \nabla B = \left.\frac{\partial B_y}{\partial x}\right|_0, \tag{5.2}$$

$$z' = R_0\eta\delta, \quad \delta' = -\frac{ZeV}{A\pi pv} z\delta\,(\theta-\theta_{RF}) + \frac{3}{2}\frac{Z^2 N e^2 \Lambda R_0}{A\gamma^2 pv\sigma_s^3} z. \tag{5.3}$$

As the first approximation, we solved these equations assuming that the bunch sizes [σ_x σ_y and σ_s] are constant within the lattice cell unit [1]. Correspondingly, the transport matrixes for longitudinal motion were calculated as it was described in Subsection 4.3.1, while the transport matrixes for transverse oscillations were obtained using the units:

$$\begin{pmatrix} y \\ y' \end{pmatrix} = \begin{pmatrix} \cos q\theta & \frac{\sin(q\theta)}{q} \\ -q\sin(q\theta) & \cos q\theta \end{pmatrix}, \quad q = R_0\sqrt{\left[-\frac{\nabla B}{BR} - \frac{C_1}{\sigma_s\sigma_y(\sigma_x+\sigma_y)}\right]},$$

$$\begin{pmatrix} y \\ y' \end{pmatrix} = \begin{pmatrix} \cosh q\theta & \frac{\sinh(q\theta)}{q} \\ q\sinh(q\theta) & \cosh q\theta \end{pmatrix}, \quad q = R_0\sqrt{\left[-\frac{\nabla B}{BR} - \frac{C_1}{\sigma_s\sigma_y(\sigma_x+\sigma_y)}\right]},$$

[1] Next approximations can be obtained dividing the cell units by necessary amount of step. Preliminary estimations of the calculation errors for the bunch length show that decreasing the step twice gives the deviation in the bunch length about 0.1 %.

$$\begin{pmatrix} x \\ x' \end{pmatrix} = \begin{pmatrix} \cos q\theta & \frac{\sin(q\theta)}{q} \\ -q\sin(q\theta) & \cos q\theta \end{pmatrix}, \quad q = R_0\sqrt{\left[\frac{1}{R^2} + \frac{\nabla B}{BR} - \frac{C_1}{\sigma_s\sigma_y(\sigma_x+\sigma_y)}\right]},$$

$$\begin{pmatrix} x \\ x' \end{pmatrix} = \begin{pmatrix} \cosh q\theta & \frac{\sinh(q\theta)}{q} \\ q\sinh(q\theta) & \cosh q\theta \end{pmatrix}, \quad q = R_0\sqrt{\left[\frac{1}{R^2} + \frac{\nabla B}{BR} - \frac{C_1}{\sigma_s\sigma_y(\sigma_x+\sigma_y)}\right]}.$$

Calculating the functions $d_{x,y}$, $c_{x,y}$, $b_{x,y}$ and $a_{x,y}$ similar to that described in Subsection 4.3.1, the transverse bunch sizes were calculated using the following equations

$$\sigma_x^2(\theta) = \epsilon\beta_{x0}d_x^2(\theta) + \frac{R_0^2\epsilon}{\beta_{x0}}b_x^2(\theta), \quad \delta_x^2(\theta) = \frac{\epsilon\beta_{x0}}{R_0^2}c_x^2(\theta) + \frac{\epsilon}{\beta_{x0}}a_x^2(\theta), \tag{5.4}$$

and

$$\sigma_y^2(\theta) = \epsilon\beta_{y0}d_y^2(\theta) + \frac{R_0^2\epsilon}{\beta_{y0}}b_y^2(\theta), \quad \delta_y^2(\theta) = \frac{\epsilon\beta_{y0}}{R_0^2}c_y^2(\theta) + \frac{\epsilon}{\beta_{y0}}a_y^2(\theta). \tag{5.5}$$

Here, $(\beta_{x,y})_0$ are initial values of the horizontal and vertical β-functions at the point where the bunch length is observed.

In these calculations we assumed the following lattice of the synchrotron: [10 o-cells, 50 a-cells, 10 o-cells, RF-station, 10 o-cells, 50 a-cells and 10 o-cells], where a-cell means the lattice cell in the arc and o-cell means the lattice cell in the straight section. Smaller transverse blowups occur, if the vertical and horizontal betatron tunes before compression are shifted to the positions below the parametric resonance ($\nu_{x,y} \lesssim 0.5$). Relevant parameters of the cell items are listed in the Tables 5.1 and 5.2. In this lattice, the betatron tunes of the low intensity bunch are $\nu_y = 0.4512$ and $\nu_x = 0.4831$ correspondingly.

With this lattice and during the bunch compression, the transverse bunch sizes are almost constant until the bunch length reaches its minimum and then, blowups dramatically (Fig.5.7). More close inspection of the time dependences of the bunch sizes during the last 10 turns before the compression event (Fig.5.8) show that the transverse bunch sizes increase after the turn when the bunch length passes its minimum value (9.8 ns, turn number is 129).

At the extraction turn and at the extraction point (the turn number 129) the vertical rms beam size is $\sigma_y = 8$ mm, while the horizontal is $\sigma_x \simeq 4$ mm. As is seen from Fig.5.9 (top graph), for this tuning of the lattice increases in transverse bunch sizes start during the next turn. So that this lattice tuning does not limit the possibility of the bunch compression till the length of 10 ns. During the bunch compression and before the bunch length reaches its minimum value the tunes decrease from their initial values down to $\nu_{x,y} = 0$ crossing subsequently the parametric resonances $\nu_{x,y} = -0.5$ and approaching to $\nu_{x,y} = -1$. As is seen from Fig.5.9 (top and bottom graphs), crossing the point $\nu_{x,y} = 0$ does not affect the bunch size. A weak instability of the horizontal betatron oscillations appear when the working point crosses the resonance $\nu_{x,y} = -0.5$ and the vertical oscillations become unstable, when the working point crosses the resonance $\nu_{x,y} = -1$. However, the last instability occurs the next turn after extraction (Fig.5.9).

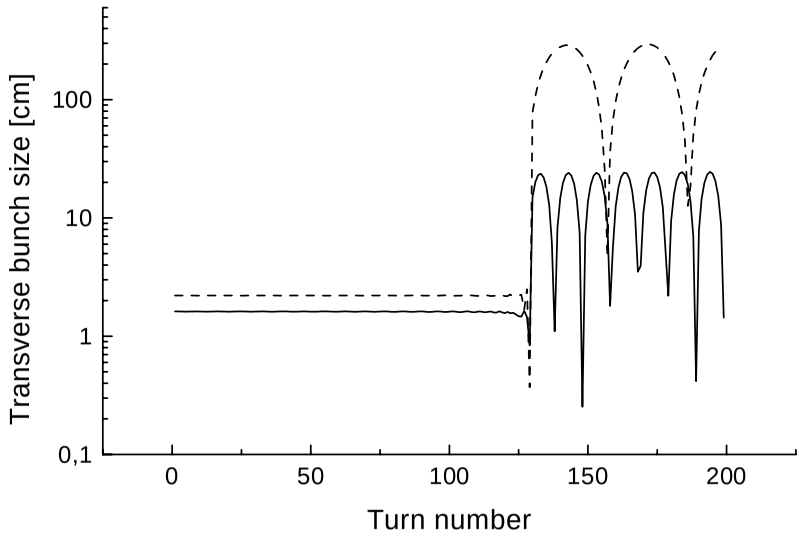

Figure 5.7: Dependences of the vertical (solid line) and horizontal (dashed line) beam sizes on the turn number. Number of particles 10^{13} of U^{4+} ions, $W = 125$ MeV/u, V_0 =1.211 MV during first 100 turns, $\epsilon = 10$ mmmrad, σ_{in} =600 m, $(\sigma_\delta)_{in} = 3 \times 10^{-6}$.

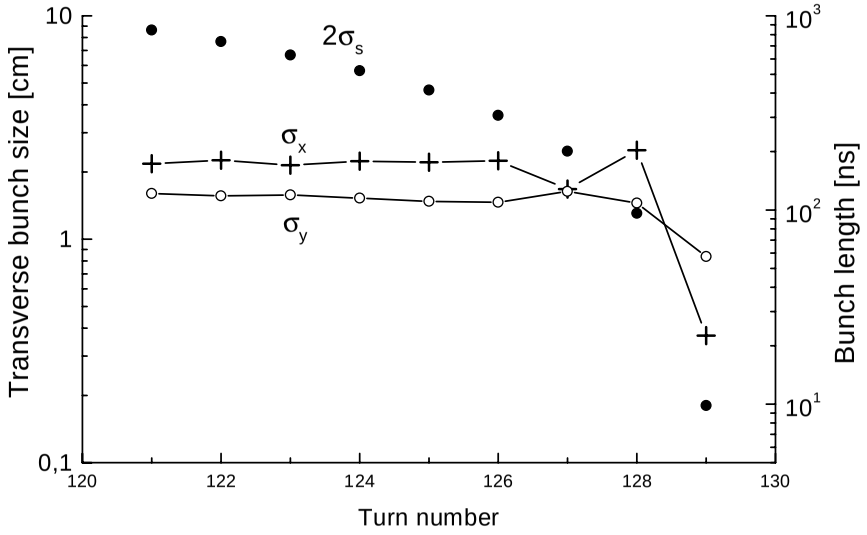

Figure 5.8: The last 10 turns of the bunch compression for parameters same as in Fig.5.7.

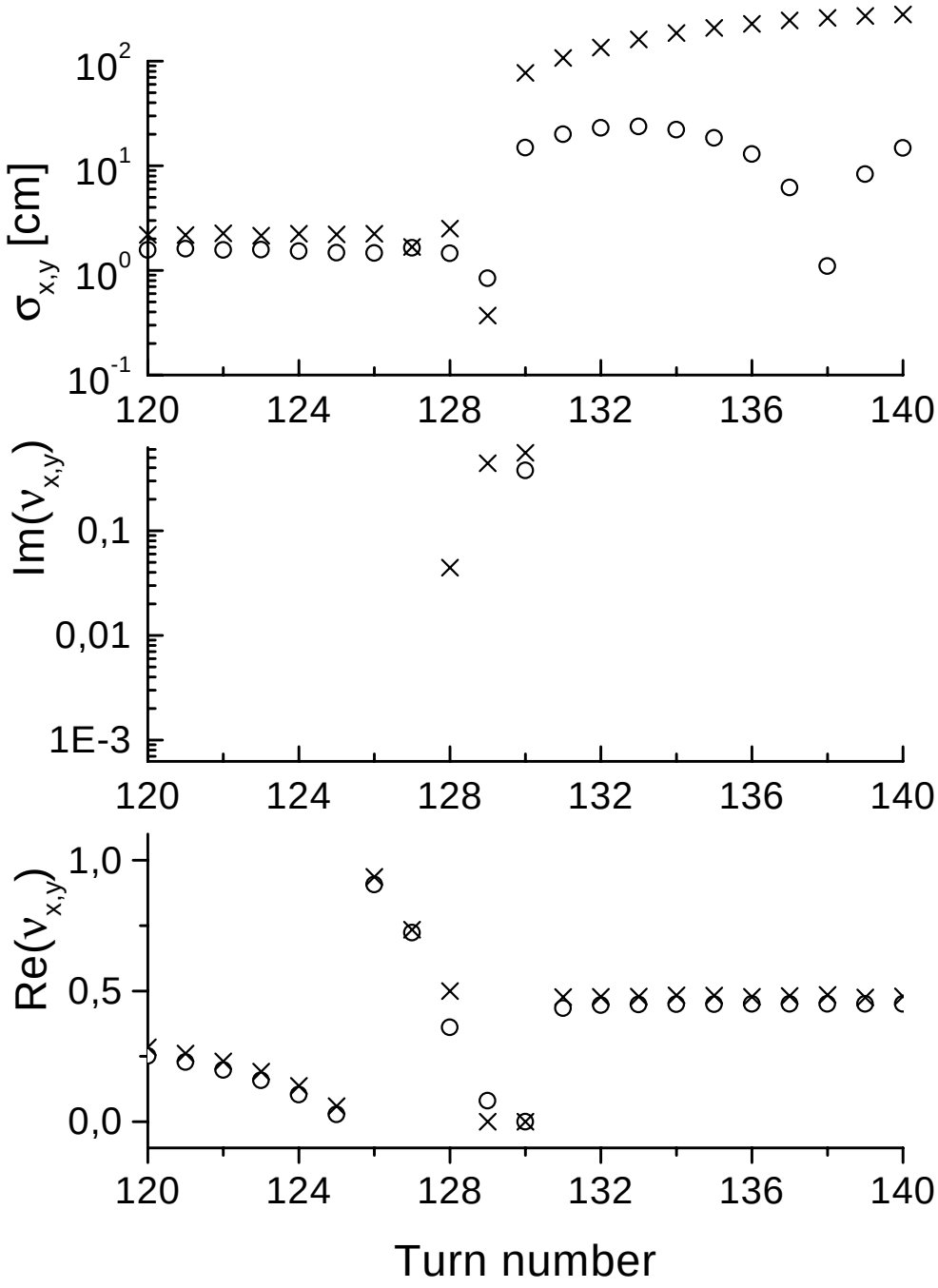

Figure 5.9: Dependences of the transverse bunch sizes (top graph), of the betatron growth rates (middle) and of the betatron tunes (bottom) on the turn number. The parameters same as in Fig.5.7; open circle – vertical and $\times$ – horizontal oscillations.

More detailed study shows that the transverse bunch sizes at the extraction point are very sensitive to the tuning of the ring lattice. As is seen from Fig.5.10, substantial variations in the transverse bunch sizes may occur, when e.g. the strengths of the focusing quadrupoles in (all) arc cells change within $5{\times}10^{-5}$. Similar sensitivity indicate the transverse bunch sizes to the strength of the quadrupoles in o-cells. The reason is that in most cases during the final bunch compression betatron oscillations of particles lose their stability. So that the lattice tuning during the bunch compression mode will be not easy. In particular, that may demand the beam extraction during the turn of the final compression event and transporting of the bunch to the target in a special beam line.

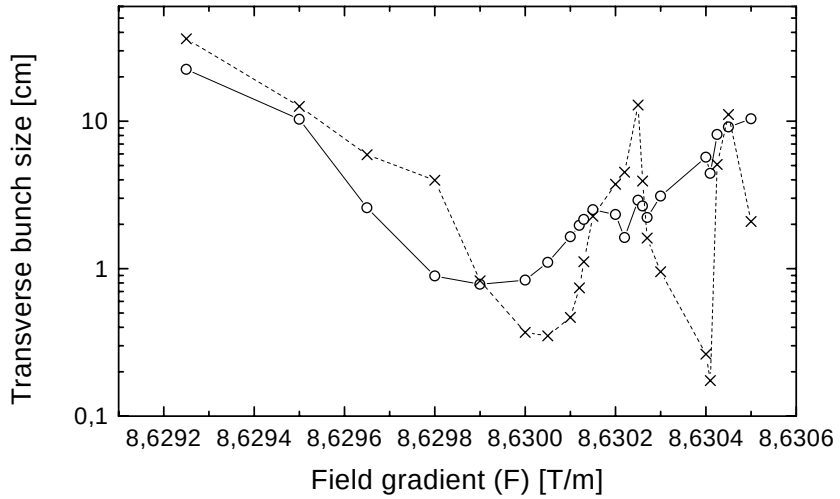

Figure 5.10: Dependences of the transverse bunch sizes on the field gradient ($\partial B_y/\partial x$) in the arc cells. The parameters same as in Fig.5.7; open circle – vertical and $\times$ – horizontal bunch sizes.

5.5 Final focus

The compressed bunch is transported to the target through the final focus system. That was simulated as an inverse problem. We assumed that at the target the bunch must make a spot of the round cross section with the radius $d = 0.1$ cm and that the target is placed at the minimum of the beam transport line β–function. In these simulations we also assumed that the final values of the horizontal and vertical bunch emittances are equal and correspond to the value of the invariant emittance ($\epsilon_0 = \gamma(v/c)\epsilon$) of 10 mmmrad. The bunch transport was simulated using the numerical solution of the bunch

envelope equations:

$$\frac{d^2x}{ds^2} + k_x(s)x = \frac{1}{x^3} + \frac{C}{\sqrt{x(x+y)}}\,,$$
$$\frac{d^2y}{ds^2} + k_y(s)y = \frac{1}{y^3} + \frac{C}{\sqrt{x(x+y)}}\,. \tag{5.6}$$

Here, x and y are the horizontal and vertical bunch envelopes expressed in units of the bunch rms radius on the target

$$x = \frac{\sqrt{\beta_x \epsilon}}{d}, \quad y = \frac{\sqrt{\beta_y \epsilon}}{d}. \tag{5.7}$$

$k_{x,y}(s)$ are the focusing rigidity coefficients. The coefficient C in Eqs.(5.6) describes the strength of the bunch space charge. In our definitions it reads

$$C = \left(\frac{Z^2}{A}\right)\frac{N r_p d^2}{\gamma \epsilon_0^2 \sigma_s}.$$

If the bunch duration is 10 ns, $\sigma_s = 142.3$ cm. Only the simplest triplet focusing segment

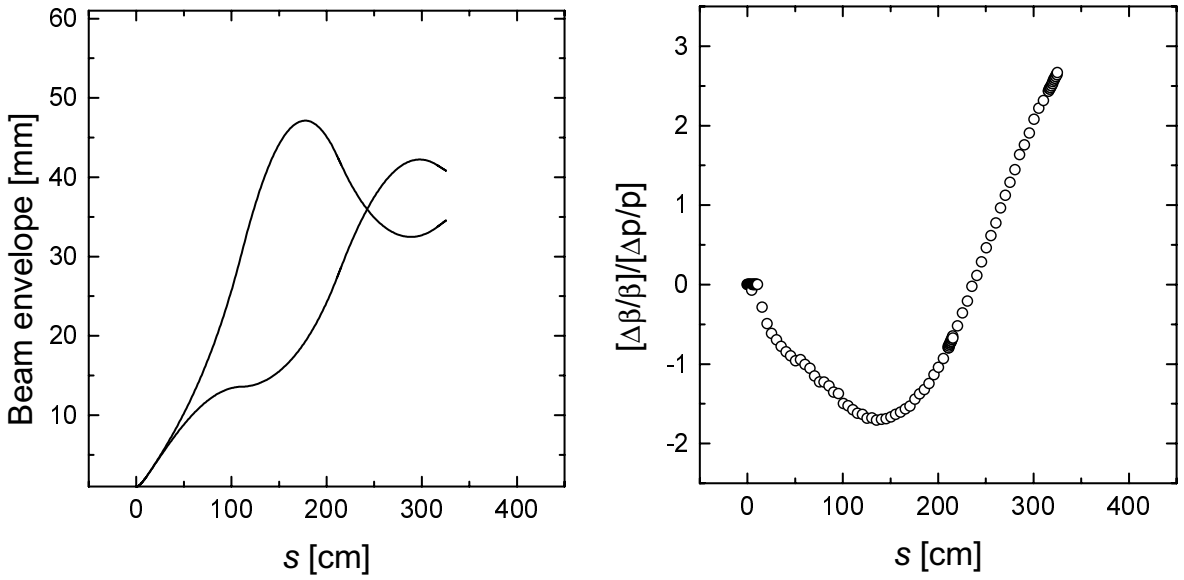

Figure 5.11: The bunch (vertical and horizontal) envelopes (left) and the segment chromaticity distribution (right) from the target through the first triplet. The vertical axes on the left graph starts from 1 mm.

was simulated. The goal for these simulations was to find the parameters of the final focus triplet, which can provide close and not too large values of the bunch radius at the entrance of the final focusing triplet. An example of the variation of the beam envelope

Table 5.4: Parameters of the final focus triplet.

Name	Length, m	Gradient, T/m
Drift	0.1	0
F	1	200
D	1	170
F	1	100

Table 5.5: Parameters of the bump magnets for the multiturn injection.

Parameter		Value	Parameter		Value
Number		2	Pulse shape		Half-sine
Aperture (2X×2Y)	cm×cm	10× 8	Pulse duration	ms	3.3
Length	cm	50	Current	kA	< 1.6
Wind number		50	Voltage	kV	< 2
Maximum field	kGs	<5			

for 10^{13} U^{4+} ions with the energy 125 MeV/u, compressed in the 10 ns bunch, is shown in Fig. 5.11. Parameters of the final focus triplet are given in the Table 5.4

The apertures of the quadrupoles should exceed $2\sigma_{\perp}$. According to data shown in Fig.5.11 is about ±9 cm in the defocusing quadrupole. This estimation shows that the final focus quadrupoles should be the superconducting or pulsed ironless lenses. The final focus system should match the foregoing final compression system lattice.

5.6 Multiturn injection

The multiturn injection scheme of U^{4+} ions at the energy of 10 MeV/u can be done similar to that described in Ref.[14]. The injection occurs in the horizontal plain moving the equilibrium orbit away from a septum magnet using two bump-magnets. During injection the equilibrium orbit displacement decays approximately linearly from an initial value to zero. The septum-magnet is placed before the F-lens entrance. The horizontal beta-function value at the bump-magnet azimuth is equal to 16 m. The beam size (sigma) at this place is approximately equal to 1 cm. The distance between the septum-magnet and the bump magnets corresponds to the phase advance of the betatron oscillations equal to π. Following Ref.[14], we assume the filling factor in the beam betatron phase space approximately equal to 0.3. Taking the vacuum chamber diameter 10 cm, we find that 20 turns could be injected using the bump magnets with parameters listed in the Table 5.5

Chapter 6

RF Systems

Complete R&D study for the RF system of the bunch compression synchrotron is described in Ref.[9]. We shall discuss here only the parts which can be necessary to evaluate relevant limitations on the beam performance, or which are necessary to give the reader better understanding of the synchrotron structure. RF systems of the synchrotron consists of two parts. One is the accelerating system. It is necessary to accelerate the ion beam from the injection energy 10 MeV/u till the final energy 125 MeV/u. This part mainly consists of the Rf cavities loaded with ferrite. The second accelerating system provides the energy modulation which is necessary for the bunch compression. For this purpose the induction type accelerating devices will be employed.

6.1 Accelerating RF system

The accelerating RF system of the synchrotron consists of 250 identical ferrite loaded RF cavities placed in the 'Injection orbit' line of the bypass (Fig.5.4). The ferrite loaded part of the cavity is separated from its high-vacuum part by the ceramic window (Fig.6.1). During acceleration cycle the working frequency of accelerating RF system should vary from f_{in} =36 MHz to f_f=117 MHz. Relevant variation of the frequency of the fundamental mode of the cavity occurs using the biasing solenoidal magnetic field (Fig.6.1). As was shown by the measurement described in Ref.[9], for this frequency range the RF cavities can be loaded using the ferrite of the type 60HH. Designed cavities enable the accelerating rate of 36 kV/m and, correspondingly, the acceleration time of 0.2 s. The cavity is cooled by water which flows in the gaps shown in Fig.6.1. Present cavity design foresees for possibility to bake out the part of vacuum chamber inside the cavity as it is described in Ref.[9].

6.1.1 RF cavity for acceleration system

The magnetic system of the cavity consists of the solenoid and of the yoke. The solenoid creates in the cavity ferrite a periodic magnetic field with the repetition frequency of 0.5 Hz . During the acceleration cycle ($\Delta t = 0.2$ s), the amplitude of this field increases from 1790 to 5870 Gauss. The biasing magnetic fields of adjacent cavities can be set to have

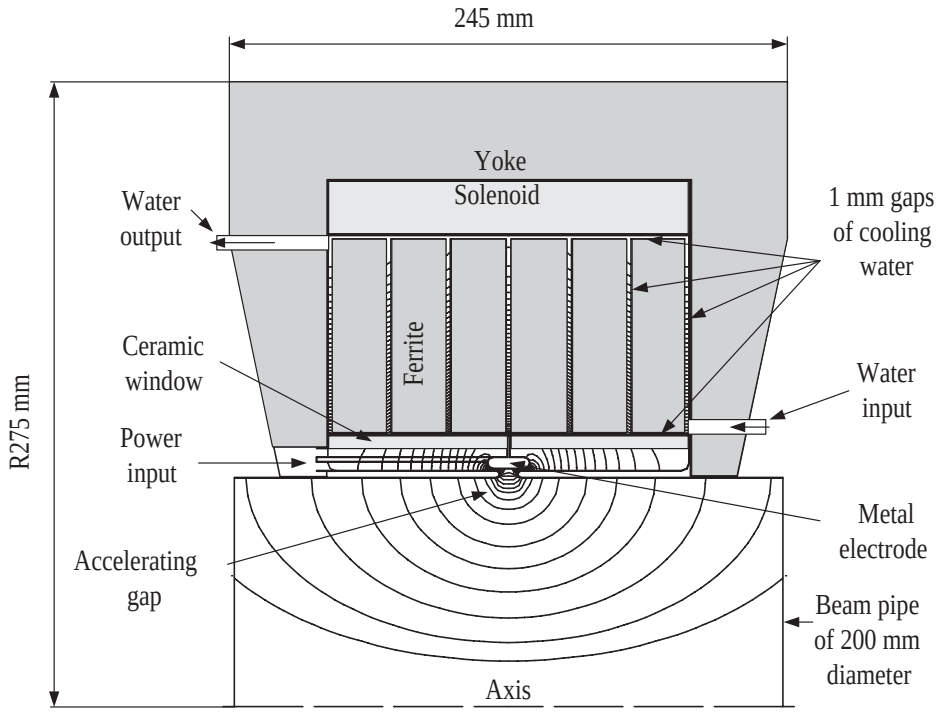

Figure 6.1: Sketch of the acceleration system RF-cavity with RF electrical field lines and outside dimensions.

opposite directions, so that the influence of the magnetic field on the ion trajectories can be reduced.

The ceramic window consists of two parts. Between them a metal (copper) electrode is soldered. The electrode is a part of RF capacitance of the cavity and closes ceramic window from the beam vacuum channel. An RF power feeding of the cavity is made through conducting link to this electrode. Side and cylindrical walls of the cavity body are manufactured from 1 mm sheet of stainless steel. The cavity body is supported by the magnetic system frame.

6.1.2 RF characteristics of the accelerating mode

The properties of the fundamental mode of the cavity were calculated using the program CLANS (see e.g. in Ref.[9]). These calculations used the RF properties of ceramics, cooling water and cavity metals which are listed in Table 6.1 The required for these calculations ferrite properties were measured using RF setup described in Ref.[9]. RF characteristics of the accelerating cavity mode were calculated for five RF frequencies and for 12 kV of RF voltage. RF characteristics of the accelerating cavity mode and properties of ferrite at these frequencies are shown in Table 6.2. The complete length of one cavity with additional units is $\simeq 0.4$ m so that the total length of the accelerating RF system is 100 m.

The calculations showed that the maximum rf magnetic field (B_{max}) differs from its

Table 6.1: The RF property of cavity materials at accelerating frequencies.

Copper resistivity at 60^oC, μOhm·cm	1.89
Stainless steel resistivity, μOhm·cm	73.7
Permeability μ' for the ferrite	11
Ceramic permittivity	12
Dielectric losses in ceramic, tan(δ)	0.001
Permittivity for water	81
Dielectric losses in water, tan(δ)	0.01

Table 6.2: RF properties of the accelerating cavity mode and ferrite properties in accelerating frequency range.

External magnetic field , Gs	1796	2105	2547	3354	5865
Resonance frequency, MHz	35.87	48.002	64.2	85.37	112.8
Quality factor [Q]	88.1	129	192	293	436
Shunt impedance [Z_0], kOhm	7.59	8.36	9.38	10.9	12.6
Total power, kW	9.48	8.61	7.68	6.59	5.71
Specific ferrite losses, W/cm^3	1.57	1.19	1.01	0.81	0.72
Ferrite magnetic permeability	23.82	13.2	7.33	4.07	2.26
Tangent of magnetic losses, tan(δ)	.0104	.0068	.0036	.0025	.0014

minimum value (B_{min}) not more than by a factor of 20%. It is taken into account, that $\tan(\delta)$ is constant for all ferrite volume and corresponds to an average value of a field $B_{av} = (B_{max} + B_{min})/2$.

6.1.3 Higher order modes

Higher order modes (HOM) of the designed cavities were calculated using the program CLANS as it is described in Ref.[9]. The diameter of the vacuum chamber in the beam-line containing the accelerating RF-system is 200 mm. The corresponding critical frequency (namely, for the TM_{01} mode) for a circular waveguide of such a diameter is 1080 MHz. The results of calculations show substantial variations in the HOM-spectra (see in Fig.6.2) during ion acceleration. The cavity impedance $Z(f)$ calculated by the code CLANS was

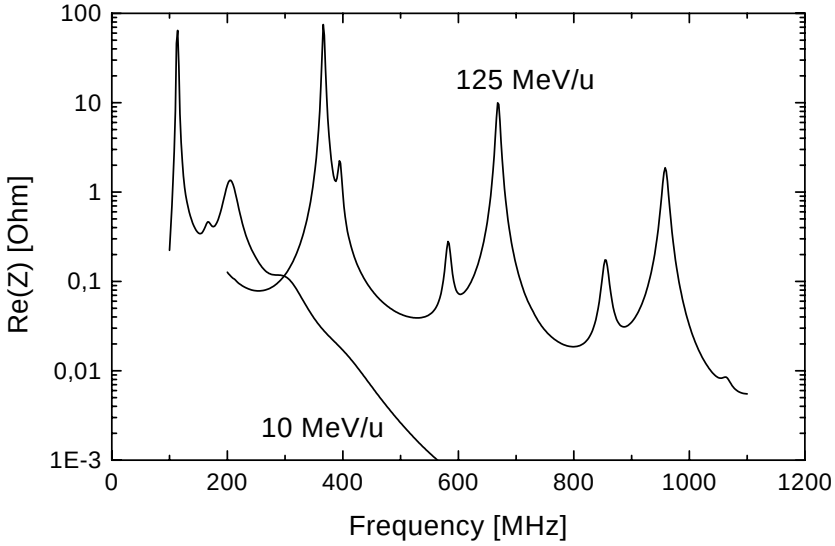

Figure 6.2: HOM spectrum of the cavity at initial (W=10 MeV/u) and at the final (W=125 MeV/u) ion energies.

fitted to that described by the following equation

$$Z(f) = \sum_{k=1}^{n} \frac{Z_{0k}}{1 + iQ_k\left(\frac{f}{f_k} - \frac{f_k}{f}\right)}$$

where Z_{0i}, Q_i, f_i are correspondingly the shunt resistance, quality-factor and the resonance frequency of the i-th mode. For the first modes these values are listed in the Table 6.3. The strength of the interaction of coherent oscillations of the beam with surrounding electrodes is specified by specific coupling impedance, which is

$$\frac{Z(f)}{n} = \frac{f_0}{f} Z(f).$$

Table 6.3: Characteristics of the HOM at (W=10 MeV/u; left part) and at (W=125 MeV/u; right part).

k	f_k, MHz	Z_0, Ohm	Q	f_k, MHz	Z_0, Ohm	Q
1	113.2	77	52	180	0.15	1.9
2	121	3	13	366.6	76.3	80
3	166	0.3	6	394.6	4.28	160
4	205.3	1.36	8	582.5	0.28	40
5	260	0.04	8	669	10.33	90
6	304	0,07	8	855	0.2	65
7				958.2	1.87	90

As is seen from Figs.6.3 and 6.4, for each of designed accelerating cavities these values are negligible small as compared to the coupling impedance of the ideally conductive vacuum chamber of the synchrotron ($(Z/n)_0 \simeq 170$ Ohm)

$$\left(\frac{Z}{n}\right)_0 = \frac{30}{\gamma^2(v/c)}\left[2\ln\left(\frac{l_\perp}{a}\right)+1\right] \simeq 170\,[\text{Ohm}], \quad W = 125[\text{MeV/u}].$$

Here, $l_\perp$ is the radius of the vacuum chamber and a is the beam radius.

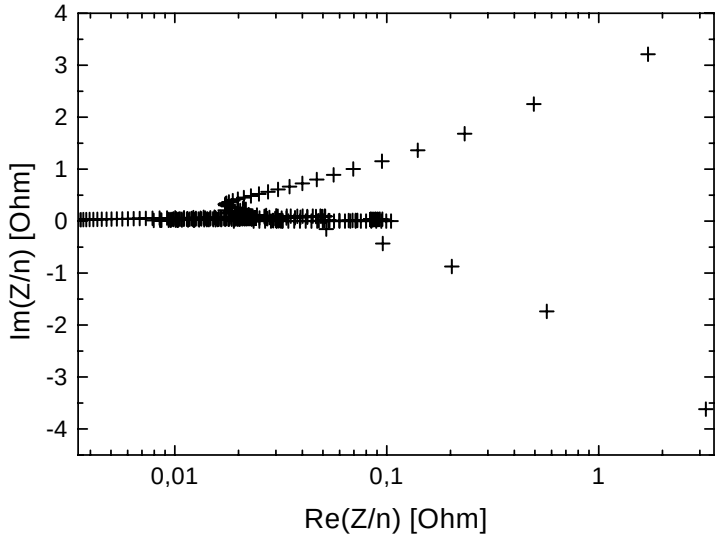

Figure 6.3: HOM spectrum of the cavity in terms of Z/n. Ion energy 10 MeV/u, 250 cavities.

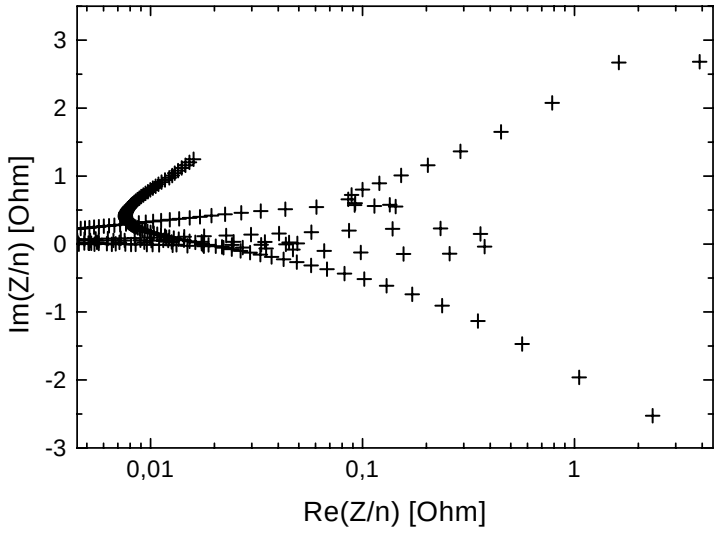

Figure 6.4: HOM spectrum of the cavity in terms of Z/n. Ion energy 125 MeV/u, 250 cavities.

6.2 Sawtooth RF-voltage device

In this Section we estimate a possibility of the generation of the sawtooth-shape RF-voltage which is necessary for the bunch compression. As we already discussed, this acceleration structure will be installed in one of the beam line of the RF containing bypass. Generally, the sawtooth voltage device can be designed using the ferrite loaded cavities with frequencies equal to several first harmonics of the revolution frequency at the compressed energy of the synchrotron. An example of the RF system using the first five harmonics is described in Ref.[9]. One of the strong disadvantages of such a device is that increasing of the useful slope of the RF voltage till, say, 90 % demands a substantial increase in the number of the required harmonics. In this Section we discuss the possibility when the energy modulation system can be designed quite similarly to those which are used in the induction accelerators (see e.g. in Ref.[15]). As is shown on Fig.6.5, such a structure consists of necessary amount of some identical sections .

Each cell of a unit contains the toroid magnetic core located around the equilibrium orbit. The neighbor sections are separated one from another by the gap with a ceramic tube, which is used as the vacuum seal assembly and as the high voltage insulator. Properly, this is quite the accelerating gap. One of a permalloy composition could be used as a magnetic material for the cores. Such kind of the cores were already utilized in induction accelerators [15] with rectangular pulses of the duration about 0.5 μs. In this case, the thickness of the permalloy film was of 10–20 μm. Using an extrapolation of these results to our parameter region, we arrive at the parameter set given in the Table 6.4.

Figure 5.35 shows one period of the specific sawtooth RF-voltage per one meter of the magnetic cores length and the inductance time diagram in the permalloy during one

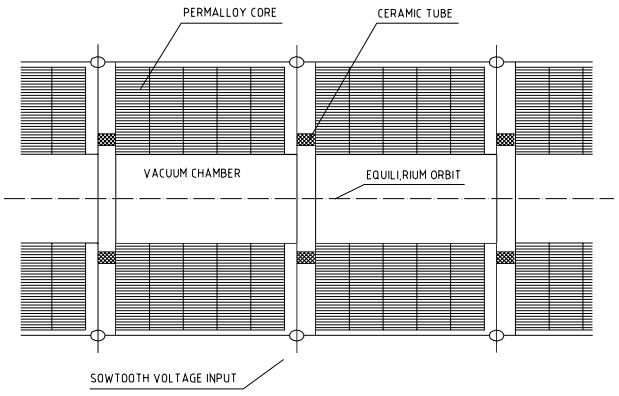

Figure 6.5: Schematic layout of the induction-type RF-structure generating the sawtooth bunch compression voltage.

Table 6.4: Parameter list of the sawtooth voltage device.

Parameter	Unit	Value
Beam energy	MeV/u	125
Revolution period	μs	8.511
Ratio of saw back laps to period		0,1
Core inner diameter	cm	15
Core radial thickness	cm	10
Induction change-over during period in permalloy	T	$\pm$1.0
Specific longitudinal gradient of accelerating voltage	keV/m	$\pm$80
Specific longitudinal gradient on the ceramic tube	keV/cm	<10
Core magnetizing peak current	kA	< 0.5

RF-period.

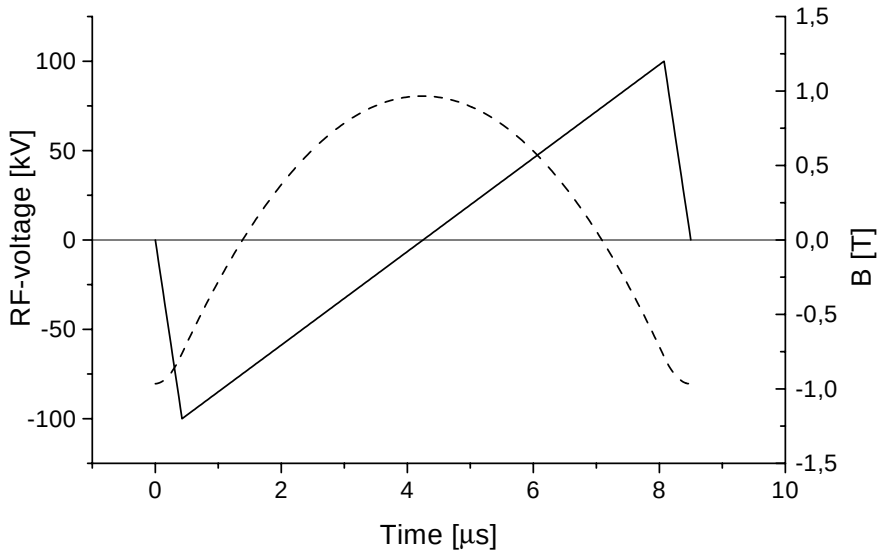

Figure 6.6: The shape of one period of the specific sawtooth RF-voltage per one meter of the magnetic cores length (solid line) and the inductance time diagram in the permalloy during one RF-period (dashed line).

Every section is feed throw some inputs. The sawtooth shape of the RF-voltage is formed using the sawtooth shape of the feeding voltage, which is supplied using coaxial cables.

The single section length could be chosen to fit the desired magnitude of the power supply voltage. As we saw in Subsection 4.3.2, the required energy modulation is reached, if the beam passes the sawtooth RF-voltage of ± 2.48 MV per turn during 50 turns. This energy gain can be provided, if the sawtooth energy modulation device occupies 30 m of the free space in the energy modulation line of the bypass insertion. If every straight section lattice cell contains two free spaces of about 3.5 m length (total length per cell is 7 m), 6 cells could be enough to install the accelerating structure for the required beam energy modulation.

The deviations from the linear dependence of the compression voltage on the synchrotron phase should be smaller than 0.1 %. This poses the requirement for both a nonlinearity of the feeding voltage itself and for effects due to RF-fields, which the bunch induces in the unit. The beam debunching before energy modulation will suppress the high frequency beam loadings. As we saw, during this period an increase in the local bunch current is given by the factor between 1.4 and about 2. Since the average reactive part of the coupling impedance of the vacuum chamber with the perfectly conducting walls $[(Z/n)]$ is about 200 Ohm, the total impedance of the sawtooth voltage unit should not exceed this value. For same reasons, an increasing of the inductive part of the coupling impedance of the unit can be very desirable. Particularly, these problems should be addressed to more detailed engineering designing of this tool (see also in Ref.[9]).

Chapter 7

Coherent Instabilities

In this Chapter we discuss the limitations on the beam intensity which occur due to their collective fields. That can be the fields due to the beam space charge, or the wake fields induced by the beam in the surrounding electrodes. In the last cases we call the instabilities as the conventional ones.

7.1 Collective space charge instabilities during injection

During the multiturn injection the Coulomb interactions of injected bunches can result in instabilities of their dipole betatron coherent oscillations during the periods preceding to their debunching in the betatron phase space. Some properties of these instabilities are very similar to that due to beam-beam interaction in the colliders. In particular, due to conservative nature of the space charge forces those are the resonant instabilities, which occur when the betatron tunes approach the resonant values. The typical values of the oscillation increments divided by the ion revolution frequency are determined by the value of the Laslett tune shift. Like the beam-beam collective instabilities the instabilities in the multiply-injected bunches cannot be suppressed by the Landau damping due to nonlinearities of the space charge fields (see e.g. in Ref.[8]). On the other side, since the bunches in the beam are never separated, the feedback systems suppressing such instabilities should affect the relative motion of the bunches. Due to complexity of the subject we consider here only two simplified model cases, which may have a heuristic worth for the future studies.

7.1.1 Interaction of a new deposit with the stored beam

Just after injection of a new ion deposit in the bunch and prior to its debunching the beam consists of two independent parts each having the dipole momenta d_1 and d_2. Due to space charge forces and in the smoothed focusing approximation the dipole coherent oscillations of these beams obey the following equations

$$d_1'' + \nu_b^2 d_1 = 2\nu_b \Delta\nu_1 [d_1 - d_2], \tag{7.1}$$
$$d_2'' + \nu_b^2 d_2 = -2\nu_b \Delta\nu_2 [d_1 - d_2]. \tag{7.2}$$

Here,

$$\Delta\nu_1 = \frac{Z^2}{A} \frac{N_2 r_p}{2\pi\gamma^2 (v/c)\epsilon_2 B}, \quad \Delta\nu_2 = \frac{Z^2}{A} \frac{N_1 r_p}{2\pi\gamma^2 (v/c)\epsilon_1 B}, \tag{7.3}$$

or, if we take $N_2/\epsilon_2 = N_1/\epsilon_1 = N/\epsilon$,

$$\Delta\nu_1 = \Delta\nu_2 = \Delta\nu_L = \frac{Z^2}{A} \frac{N r_p}{2\pi\gamma^2 (v/c)\epsilon B},$$

$$d_1'' + \nu_b^2 d_1 = 2\nu_b \Delta\nu_L [d_1 - d_2]$$
$$d_2'' + \nu_b^2 d_2 = -2\nu_b \Delta\nu_L [d_1 - d_2]$$

These equations describe free oscillations of the center of gravity ($X = d_1 + d_2$; so-called o-mode) of the beam and the following oscillations for the relative distance between the beams ($b = d_1 - d_2$; so-called π-mode)

$$b'' + \nu_b^2 b = 4\nu_b \Delta\nu_L b. \tag{7.4}$$

The last oscillations will be stable, if

$$\nu_b \geq 2\Delta\nu_L.$$

In the strong focusing machine we have to take into account the modulations of the Coulomb tune shift along the closed orbit

$$(\Delta\nu_L)_{x,y} = \frac{Z^2}{A} \frac{N r_p}{2\pi\gamma^2 (v/c)\epsilon B} \sqrt{\frac{\beta_{x,y}}{\beta_x + \beta_y}}.$$

In a FODO-type lattice the combination $\beta_x + \beta_y$ varies very weakly along the closed orbit, so that the modulations of $(\Delta\nu_L)_{x,y}$ mainly occur due to variations of the functions $\sqrt{\beta_{x,y}(\theta)}$. Assuming for the sake of simplicity

$$\beta(\theta) = \beta_{av} + \Delta\beta \cos(n_c \theta),$$

where n_c is the number of the cells (or, the number of the superperiods) in the ring, and $\Delta\beta \ll \beta_{av}$, we write

$$\sqrt{\beta} \simeq \sqrt{\beta_{av}} \left(1 + \frac{\Delta\beta}{2\beta_{av}} \cos(n_c \theta)\right). \tag{7.5}$$

Then, Eq.(7.4) reads

$$b'' + \nu^2 b = 2\nu_b \Delta\nu_L \frac{\Delta\beta}{\beta_{av}} \cos(n_c\theta) b. \tag{7.6}$$

Here,

$$\nu^2 = \nu_b^2 + 4\nu_b \Delta\nu_L. \tag{7.7}$$

Solutions of Eq.(7.7) describe unstable oscillations when the tune ν approaches to a half-integer

$$\nu = \frac{n_c k}{2}, \quad k = 1, 2, \ldots, \tag{7.8}$$

where the coherent tune shifts can be estimated using (see e.g. in Ref.[8])

$$\Delta\nu_k = \frac{1}{2}\sqrt{\varepsilon^2 - \left[\Delta\nu_L \frac{\Delta\beta}{\beta_{av}}\right]^2}. \tag{7.9}$$

Here,

$$\varepsilon = \frac{n_c k}{2} - \nu_b + \Delta\nu_L$$

is the detuning from the resonance. Correspondingly, the oscillations become unstable within the band

$$\frac{n_c k}{2} + \Delta\nu_L - \Delta\nu_L \frac{\Delta\beta}{\beta_{av}} < \nu_b < \frac{n_c k}{2} + \Delta\nu_L + \Delta\nu_L \frac{\Delta\beta}{\beta_{av}}, \tag{7.10}$$

where the oscillation increments ($\delta_k = \mathrm{Im}(\Delta\nu_k)$) vary according to

$$\delta_k = \frac{1}{2}\sqrt{\left[\Delta\nu_L \frac{\Delta\beta}{\beta_{av}}\right]^2 - \varepsilon^2}. \tag{7.11}$$

We may expect that this instability will be suppressed by the Landau damping due to nonlinear dependencies of the space charge forces on the particle betatron offsets. Relevant (dimensionless) decrement of the Landau damping can be estimated as $0.2\Delta\nu_L$. That yields the following stability condition

$$\left[\Delta\nu_L \frac{\Delta\beta}{\beta_{av}}\right]^2 - \varepsilon^2 < 0.16 \left(\Delta\nu_L\right)^2,$$

or

$$|\varepsilon| > \Delta\nu_L \sqrt{\frac{\Delta\beta^2}{\beta_{av}^2} - 0.16}, \quad \frac{\Delta\beta}{\beta_{av}} > 0.4. \tag{7.12}$$

In a real case, the ratio $\Delta\beta/\beta_{av}$ is not small ($\Delta\beta/\beta_{av} \simeq 0.5$). Substituting this number in the condition in Eq.(7.12) we find that during injection the working point of the ring should not approach the parametric resonance from the above closer than $1.3\times\Delta\nu_L$ and should not exceed it larger than $0.7\times\Delta\nu_L$. We note, that conventional (dipole) feedback systems cannot be used effectively to suppress this instability.

7.1.2 Frequent deposits

Another instability due to Coulomb interactions of injected bunches may occur when new bunches are injected so frequently that their debunching in the betatron phase space during injection is small. For the sake of simplicity we assume that injected bunches are packed so dense that their coherent oscillations can be described in the linear approximation in $|d_k/\sigma_\perp|$, where $k = 1, 2, \ldots n_b$, n_b is the number of injected bunches in the same RF-bucket, $\sigma_\perp$ are transverse radii of injected bunches. Then, coherent oscillations of the beam are described by the following system of equations:

$$d_k'' + \nu_b^2 d_k = 2\nu_b \Delta\nu(\theta) \sum_{m=1}^{n_b} (d_k - d_m). \tag{7.13}$$

Assuming equal vertical and horizontal invariant emittances in injected bunches ($\epsilon_x = \epsilon_y = \epsilon$), we write

$$\Delta\nu(\theta) = \Delta\nu_L \sqrt{\frac{\beta(\theta)}{\beta_{av}}}, \quad \Delta\nu_L = \frac{Z^2}{A} \frac{N_b r_p}{2\pi\gamma^2 (v/c)\epsilon B}, \tag{7.14}$$

and correspondingly,

$$d_k'' + \left[\nu_b^2 - 2\nu_b n_b \Delta\nu(\theta)\right] d_k = -2\nu_b \Delta\nu(\theta) X(\theta), \quad X(\theta) = \sum_{m=1}^{n_b} d_m. \tag{7.15}$$

Since the center of gravity of the beam X obeys a homogeneous equation

$$X'' + \nu_b^2 X = 0,$$

solutions to Eq.(7.14) will describe the stable oscillations unless the betatron tune approaches parametric resonances [1]

$$\nu_b = \frac{n_c k}{2}, \quad k = 1, 2, \ldots$$

However, in contrast to the case, discussed in the previous Subsection, both the tune shifts of the dipole oscillations and the widths of these resonances in the tune diagram is now n_b times larger provided that the ratio N_b/ϵ is constant. For example, the condition in Eq.(7.10) will read now as

$$\frac{n_c k}{2} + n_b \Delta\nu_L \left(1 - \frac{\Delta\beta}{\beta_{av}}\right) < \nu_b < \frac{n_c k}{2} + n_b \Delta\nu_L \left(1 + \frac{\Delta\beta}{\beta_{av}}\right), \tag{7.16}$$

[1] For example, we can define $n_b - 1$ variables

$$b_k = d_k - d_1,$$

which obey the following homogeneous equations

$$b_k'' + \left[\nu_b^2 - 2\nu_b n_b \Delta\nu(\theta)\right] b_k = 0.$$

Solutions to these equations are unstable only near parametric resonances.

while for the oscillation increments we obtain

$$\delta_k = \frac{1}{2}\sqrt{\left[n_b \Delta\nu_L \frac{\Delta\beta}{\beta_{av}}\right]^2 - \varepsilon^2}. \tag{7.17}$$

In order to avoid severe limitations on the injected bunch density in the phase space (N_b/ϵ) the number of the superperiods in the ring should be large. Since only about 20% of the tune shift due to space charge fields contributes to the Landau damping, this instability very unlikely will be suppressed by nonlinearities of the space charge forces. The problem of the suppression of this instability demands a separate study.

7.2 Conventional coherent instabilities

A big value of the Laslett tune shift which is required to assure the possibility of the final focusing in a spot with the desired diameter (1 mm for N_t =10^{13} of U^{4+} ions) practically eliminates possibilities of any long term operations with the beam at the injection energy. On the other hand and for non-relativistic particles, for given values of the beam current and of the impedance of the surrounding electrodes the growth-rates of known coherent instabilities vary proportional to $1/(v/c)^3$. So that an acceleration of the injected beam also reduces the limitations on its current due to interactions with surrounding electrodes in the vacuum chamber. For these reasons, below we assume that just after injection the beam in the synchrotron is quickly accelerated. The operation experience from other similar machines (for example, the synchrotron U-70 in Serpukhov, or FNAL buster) show that fast acceleration significantly suppresses the high current limitations on the beam performance.

In this Section we evaluate conventional coherent effects due to the interaction of the beam with surrounding electrodes. That can be either the accelerating cavity or other devices which can be necessary for various technical purposes (beam diagnostics, possible charge cleaning electrodes etc.). We describe such devices using the model impedance of a cavity with a unit Q-value (see e.g. in Ref. [1]). Due to low particle energies the longitudinal collective effect will be strongly affected by the Coulomb interaction of the beam with a smooth and perfectly conducting vacuum chamber surrounding it. This interaction gives a capacitive contribution to the pipe impedance. For the synchrotron operating below its transition energy, this may pose additional limitations on the resistive part of the coupling impedance. However, for the same reason the threshold currents (of coasting beams) in such synchrotrons can substantially exceed the values, corresponding to the thresholds calculated using the so-called Keil-Schnell criterion (see e.g. in Ref.[8]).

7.2.1 Transverse instabilities during acceleration

If for some reason we ignore the effect of Landau damping on the transverse oscillations of the beam, without ion acceleration the amplitudes of these oscillations (a_c) exponentially increase in time

$$a_c(t) = a_{c0} \exp(t/\tau). \tag{7.18}$$

With given number of particles in the bunch (beam) and provided that the instability occurs due to interaction of the beam with surrounding electrodes due to fields independent on the particle energy, the instability growth-rate $(1/\tau)$ depends on the particle energy according to [2]

$$\frac{1}{\tau(p)} = \frac{Q}{p}, \tag{7.19}$$

where p is the ion momentum. The factor Q in this equation is determined by the number of particles in the beam, by the beam filling pattern, by the geometry of surrounding electrodes but it does not depend on the particle energy. The growth of the amplitudes of transverse coherent oscillations in the accelerated beam can be evaluated using equation similar to Eq.(7.18)

$$a_c(t) = a_{c0} \exp\left(Q \int_0^t \frac{dt'}{p(t')}\right). \tag{7.20}$$

Assuming, for example,

$$p(t) = p_{in} + \dot{p}t, \quad \dot{p} = \frac{p_f - p_{in}}{\Delta t}, \tag{7.21}$$

where Δt is the acceleration time, we obtain

$$a_c(\Delta t) = a_{c0} \exp\left[\frac{\Delta t}{\tau_f} \frac{\ln(p_f/p_{in})}{1 - (p_{in}/p_f)}\right]. \tag{7.22}$$

Here,

$$\frac{1}{\tau_f} = \frac{Q}{p_f} \tag{7.23}$$

is the instability growth-rate of the accelerated bunches. These equations show that effects of the small energy intervals on the amplitude of coherent oscillations of the accelerated beam is described by the factor

$$\chi = \frac{1 - (p_{in}/p_f)}{\ln(p_f/p_{in})}, \quad \tau(\Delta t) = \tau_f \chi. \tag{7.24}$$

For parameters of the discussed synchrotron the factor χ has close values for both injection energies ($\chi \simeq 1/2$). So that the total growth of the oscillation amplitudes during beam acceleration can be estimated as a half of the growth-time at the final energy of acceleration

$$\tau(\Delta t) \simeq \frac{\tau_f}{2}. \tag{7.25}$$

[2] We do not discuss here the so-called resonant instabilities (see, for example, in Ref.[8]) which should be avoided both in the single- and multibunch operation modes anyway.

7.2.2 Transverse multibunch instabilities

After injection and prior debunching the beam consists of $h = 994$ bunches. If the closed orbit perimeter is Π =1200 m, then the bunch-to-bunch distance in the beam is 1.3 m. It means that elements of the vacuum chamber, which remember induced fields during the time intervals in the region of 10–30 ns, will provide the coupling of the coherent oscillations of the bunches in the beam. The interactions of the beam with such surrounding electrodes, generally, produce numerous multibunch instabilities of both longitudinal and transverse coherent oscillations of the beam. The total number of the multibunch modes is equal to number of the bunches in the beam. Although the beam in the synchrotron is assumed to have the bunch filling pattern with a 10% gap, for simplicity we shall calculate increments and stability criteria assuming the uniform filling pattern of the beam. The short gap in the beam will only slightly modify the increments of unstable modes. For the beam with a uniform filling pattern and containing short bunches ($\sigma_s \to 0$) the values of the dipole transverse coherent frequency shifts can be calculated using

$$(\Delta\omega_{m,q})_{mb} = -\frac{Z^2}{A}\frac{Ne^2 m_y}{2p\nu_y}\sum_{k=0}^{\infty}\exp\left(2\pi i k\frac{m_y\nu_y + q}{h}\right) Z^{\perp}(kT_b). \tag{7.26}$$

Here, $T_b = T_0/h$ is the period of bunches in the beam, T_0 is the ion revolution period in the synchrotron, NZe is the bunch charge, $m_y = \pm 1$, $q = 0, 1, \ldots, h-1$ is the multibunch mode number and

$$Z^{\perp}(t) = \int_{-\infty}^{\infty}\frac{d\omega}{2\pi}Z^{\perp}(\omega)e^{-i\omega t} \tag{7.27}$$

is the transverse coupling impedance in the time domain. According to these equations the increments of the multibunch modes ($[1/\tau]$ =Im$(\Delta\omega_{m,q})_{mb}$) depend on the total number of bunches in the beam only in the case where the wakes last longer that the revolution period in the ring.

As an example, we estimate the growth-rates of the resistive wall transverse multibunch instability. Using results from Ref. [7], we obtain

$$\frac{1}{\tau_q} = \frac{Z^2}{A}\frac{\pi Ne^2\beta_{av}}{3pl_{\perp}^3}\sqrt{\frac{f_{RF}}{\sigma_w}}\sum_{a=1}^{\infty}\frac{m}{\sqrt{a}}\sin\left(\frac{2\pi a}{h}[m\nu_y + q]\right). \tag{7.28}$$

Here, $1/\sigma_w$ is the surface resistivity of the pipe material, β_{av} is the average value of the β–function. As is seen from Fig.7.1, even for the high intensity mode ($N = 6.5 \times 10^9$ particles per bunch) the oscillation growth-times exceed 1000 s for the accelerated beam ($W = 125$ MeV/u).

In this case, the contributions of small energies during acceleration in the growth-time of the accelerated beam is described by the factor

$$\chi = \frac{1 + \sqrt{p_{in}/p_f}}{2} \simeq 0.72.$$

Another typical limitation on the beam intensity due to unstable betatron multibunch modes can be described in terms of the interaction of the beam with a Q=1 parasitic

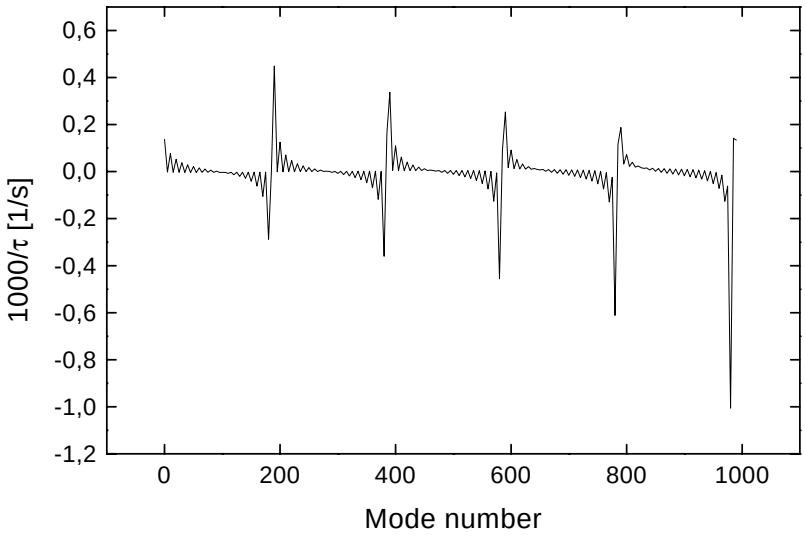

Figure 7.1: Dependences of the resistive wall instability growth-rate on the mode number. Number of bunches 994, $N = 6.5 \times 10^9$, $W = 125$ MeV/u, $\sigma_w = 5.8 \times 10^{17}$ 1/s [copper], β_{av} =15 m.

cavity. In this case, the transverse coupling impedance is described by the following equations

$$Z^{\perp}(\omega) = \frac{v}{l_{\perp}^2}\frac{Z_w(\omega)}{i\omega}, \quad Z_w(\omega) = \frac{Z_0}{1 + i\left(\frac{\omega_r}{\omega} - \frac{\omega}{\omega_r}\right)}, \tag{7.29}$$

where Z_0 is the shunt impedance of the parasitic cavity, ω_r is its resonant frequency, $l_{\perp}$ is the radius of the vacuum chamber. For this case, $Z^{\perp}(t)$ reads

$$Z^{\perp}(t) = -\frac{vZ_0}{l_{\perp}^2}\exp\left(-\frac{\omega_r t}{2}\right)\sin\left(\frac{\omega_k t\sqrt{3}}{2}\right),$$

and hence,

$$\Delta_{m,q} = \Delta_0 \sum_{k=0}^{\infty} \exp\left(2\pi i k\frac{m_y\nu_y + q}{h} - \frac{\pi\nu_r k}{h}\right)\sin\left(\frac{\pi\nu_r k\sqrt{3}}{h}\right), \tag{7.30}$$

where $\Delta_{m,q} = \Delta\omega_{m,q}/\omega_0$ and

$$\Delta_0 = m_y\frac{Z^2}{A}\frac{Ne^2\omega_0 Z_0}{2\pi pv}\frac{\beta_{av}\Pi}{l_{\perp}^2\sqrt{3}}, \quad \nu_r = \frac{\omega_r}{\omega_0}. \tag{7.31}$$

The typical value of ω_r for a single parasitic cavity can be estimated using $\omega_r \simeq \pi c/b$, where b is the radius of the distortion in the vacuum chamber. Then, the value ν_r/h is estimated using

$$\frac{\nu_r}{h} = \frac{\lambda_{RF}}{2b(v/c)} \simeq \frac{\lambda_{RF}}{2l_\perp(v/c)}.$$

For the injection energy W =10 MeV/u, $h = 994$, $l_\perp = 10$ cm and $N_t = 10^{13}$ ions we have $\nu_r/h \simeq 41.6$ and $\Delta_0 = \pm 2.7 \times 10^{-5}$ [1/s]. In this case, no important multibunch instabilities occur.

As is seen from Eq.(7.30), the discussed instability becomes stronger for low resonant frequencies, when $\nu_r \ll h$ so that the interaction couples the oscillations of many bunches in the beam. So low frequencies of the parasitic modes may occur, if several parasitic cavities have close frequencies and are coupled electro-magnetically.

In any case, in the safe region of parameters either the instability growth-time should exceed the cycle period, or the values of Δ_m^μ in Eq.(7.30) should be inside the stability diagram which occur due to Landau damping associated with the nonlinearity of the guiding magnetic field of the ring and with the nonlinearity of the transverse space charge forces of the beam. If I is the action variable of the horizontal (or of the vertical) betatron oscillations, $\Delta\omega_3 = aI$ is the betatron frequency spread due to cubic nonlinearity of the guiding magnetic field of the ring and if $-\Omega(I)$ is the frequency shift of the betatron oscillations due to the beam space charge fields, the dispersion equation for the dipole betatron oscillations in the space charge dominated beam reads (see, for example, in Appendix D.1)

$$\Delta\omega_1 = \Omega_1 + a\frac{Q_2(\Delta\omega_1, I)}{Q_1(\Delta\omega_1, I)}. \tag{7.32}$$

Here, $\Delta\omega_1 = \omega - \omega_y$ is the deviation of the mode frequency ω from the frequency of the (vertical) betatron oscillations ω_y, Ω_1 is the coherent frequency shift of the monochromatic beam, $I = pJ_y/2$ is the action variable of the betatron oscillations,

$$Q_n(\Delta\omega_1, I) = \int_0^\infty dI \frac{I^n \partial f_0/\partial I}{[\Delta\omega_1 - aI + \Omega(I)]}, \quad n = 1, 2. \tag{7.33}$$

Due to repulsion of ions the frequency shift due to space charge fields is negative. Without external octupole fields on the closed orbit ($a = 0$) the space charge forces do not affect the spectrum of the dipole oscillations of the beam

$$\Delta\omega_1 = \Omega_1. \tag{7.34}$$

Due to common effect of the octupole field and of the space charge fields of the beam the tune shift inside the beam varies according to

$$\Delta\omega_y(I) = aI - \Omega(I).$$

That results in the Landau damping of dipole oscillations. The frequency distribution and the frequency spread in the beam depend on the sign of a. Correspondingly, the values of the Landau damping decrements and widths of oscillation stability diagrams also depend on the sign a.

For numerical calculations below we assumed a Gaussian transverse distribution of ions in the beam

$$f(J_x, J_y) = \frac{1}{2\pi\epsilon_x\epsilon_y} \exp\left(-\frac{J_x}{2\epsilon_x} - \frac{J_y}{2\epsilon_y}\right), \quad I_{x,y} = \frac{pJ_{x,y}}{2},$$

and the following model tune distribution in the beam due to its space charge

$$\Omega = \frac{\omega_0 \Delta\nu_L}{1 + J_y/\epsilon_y}.$$

In this case, the total variation of the betatron tune with an increase in the amplitude of betatron oscillations will be a monotonous function of I, if $a \geq 0$, and will have a maximum, if $a < 0$ (Fig.7.2).

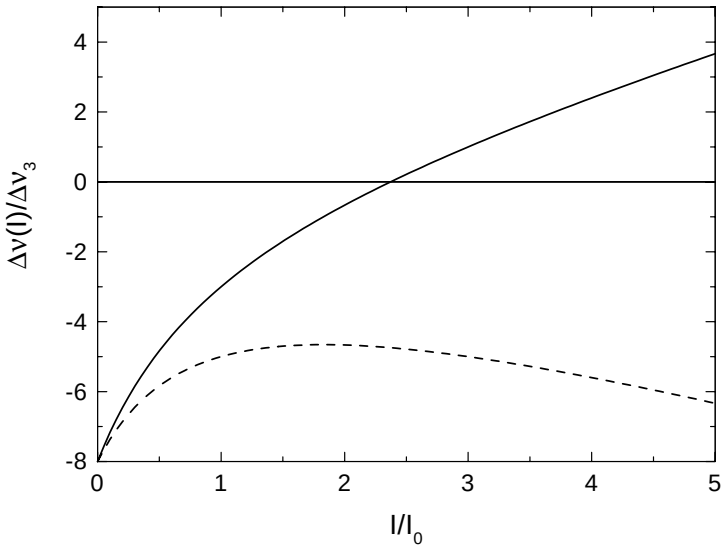

Figure 7.2: Dependence of the tune shift on J/ϵ due to common effect of the octupole and of the space charge fields. Solid line – $a > 0$, dashed line – $a < 0$, $\Delta\nu_L/\Delta\nu_3 = 8$.

In the last case, apart from the single-particle oscillation degeneration ($\Delta\nu(I_1) = \Delta\nu(I_2)$) the width of the tune distribution in the beam substantially shrinks. The (one-dimensional) stability diagrams were calculated for one-dimensional Gaussian distribution functions according to the following equations

$$\zeta_1 = z - \frac{q_2(z)}{q_1(z)}, \quad a > 0, \tag{7.35}$$

where

$$\zeta_1 = \frac{\Omega_1}{\Delta\omega_3}, \quad z = \frac{\Delta\omega_1}{\Delta\omega_3}, \quad \Delta\omega_3 = ap\epsilon = \omega_0\Delta\nu_3$$

and

$$q_n = \int_0^\infty \frac{duu^n e^{-u}}{[z - u + \Phi(u) + i0]}, \quad \Phi(u) = \frac{\Delta\nu_L}{\Delta\nu_3(1+u)}, \quad n = 1, 2. \tag{7.36}$$

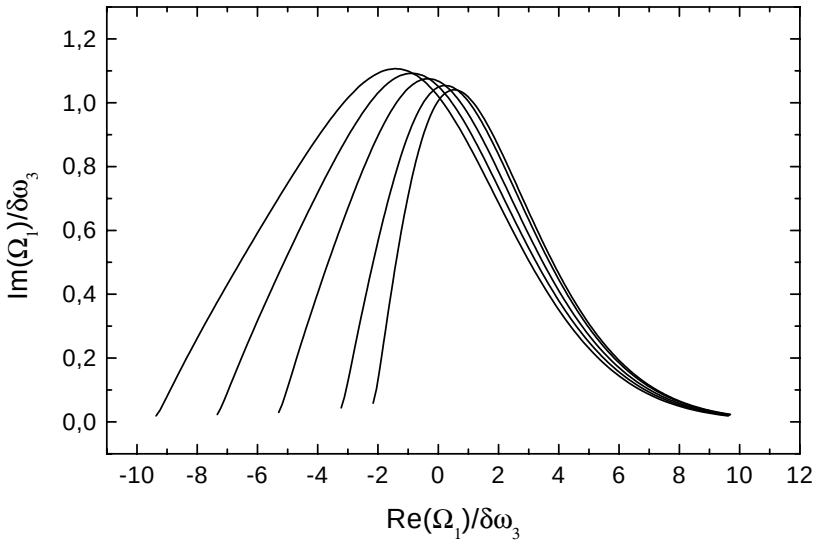

Figure 7.3: Stability diagram for dipole coherent oscillations. Oscillations are stable below the curve; $a > 0$, from left to right $\Delta\nu_L/\Delta\nu_3$ is subsequently equal to 8, 6, 4, 2 and 1.

Inspecting Figs.7.3 and 7.4 we see that in the case, when $a > 0$, the maximal height of the stability diagram is approximately equal to $\Delta\omega_3$ but the horizontal width increases with an increase in the value of the Laslett tune shift. On the contrary, if $a < 0$, an increase in the value of the Laslett tune shift is accompanied by the decrease in the height of the stability diagram. So that for more effective damping of the dipole oscillations the octupole fields should produce the positive shift of the frequencies of betatron oscillations.

These calculations show that for a given value of the beam current the threshold values of the loss factors (real part of the impedances) are determined by the Landau damping due to the cubic nonlinearity of the guiding field. The Landau damping due to nonlinearity of the beam space charge forces is very effective in the suppressing of the conventional instabilities which occur due to strong reactive part of the coupling impedance. The transverse feedback system is not necessary under these conditions.

7.2.3 Longitudinal multibunch instabilities

Among other reasons, these instabilities occur due to interaction of the longitudinal coherent oscillations with the higher order modes of the accelerating system. For the sake of simplicity we assume the uniform filling pattern of the beam. Then, the increments of the multibunch (dipole synchrotron) modes due to interactions of bunches with HOM can be written in the following form (see, for example, in Ref.[1], or [8])

$$\delta_{m,a} = m \sum_{k=1}^{M} \Omega_k \exp\left(-\frac{\pi}{Q_k}\right) F(\nu_k, m\nu_s + a), \quad m = \pm 1, \quad a = 0, 1, \ldots h-1, \qquad (7.37)$$

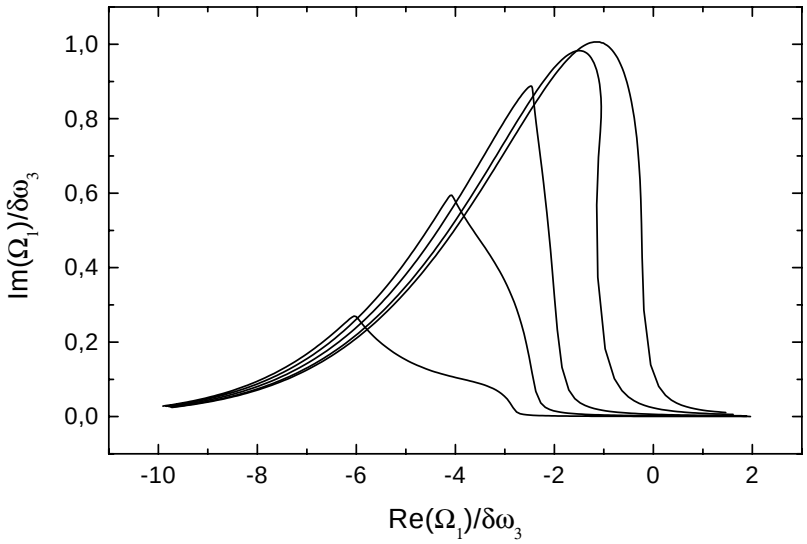

Figure 7.4: Same as in Fig.7.3, but $a < 0$.

$$F(x,y) = \frac{\pi}{n_b}\left\{\frac{\cos(2\pi\alpha_-) - p}{1 - 2p\cos(2\pi\alpha_-) + p^2} - \frac{\cos(2\pi\alpha_+) - p}{1 - 2p\cos(2\pi\alpha_+) + p^2}\right\}, \tag{7.38}$$

$$\alpha_\pm = \frac{x \pm y}{h}, \quad p = \exp\left(-\frac{\pi}{Q_k}\right).$$

Here, k is the number of the HOM, $\nu_k = \omega_k/\omega_0$ (ω_k is the frequency of the k-th cavity mode), and Q_k is the Q-value of the cavity HOM mode. The parameter

$$1/\tau_{mb} = \Omega = N_c \frac{ZeI(Z_k/Q_k)}{T_0 pv}\frac{h^2\eta}{4\nu_s}, \quad h = \omega_{RF}/\omega_0. \tag{7.39}$$

determines the maximum increment of unstable multibunch modes due to their interaction with HOM number k. The modes can be stabilized by the Landau damping of synchrotron coherent oscillations. The cubic nonlinearity of the RF-field produces the synchrotron frequency spread

$$\Delta\omega_s = -\omega_{s0}\left(\frac{\pi B}{4}\right)^2, \quad B = \frac{2\sigma_s}{\lambda_{RF}}. \tag{7.40}$$

Increments of unstable modes should exceed the value $\Delta\omega_s$. Results of calculations of the parameters of the HOM of accelerating cavities [9] are summarized in the Table 6.3. Substituting these data in Eq.(7.39) enables the calculations of the mode increments depicted in Figs.7.5 and 7.6. As is seen from Fig.7.5, the interaction with the HOM of accelerating cavities does not pose any problems. In both cases, all multibunch modes are well damped by the Landau damping due to cubic nonlinearity of the RF field.

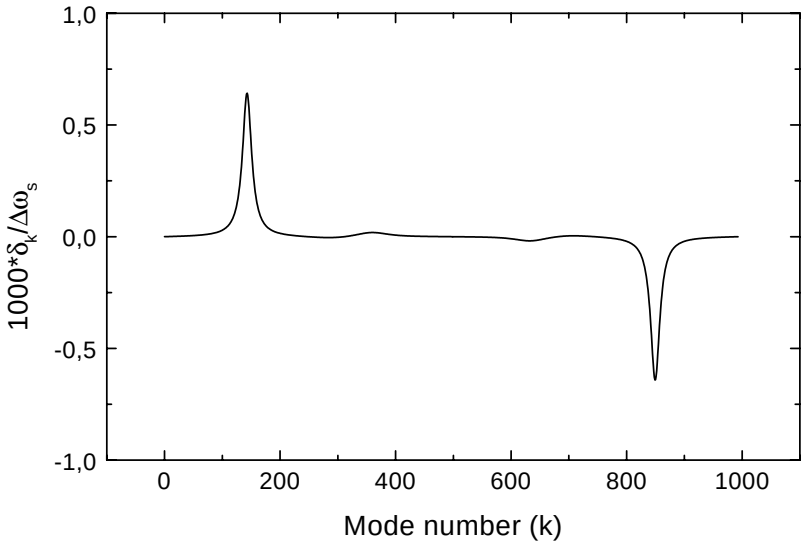

Figure 7.5: Dependence of increments of multibunch modes ($\delta_k/\Delta\omega_s$) on the mode number. Injection energy W=10 MeV/u, bunching factor is 0.7, beam intensity is 10^{13} of U^{4+} ions $h = 994$.

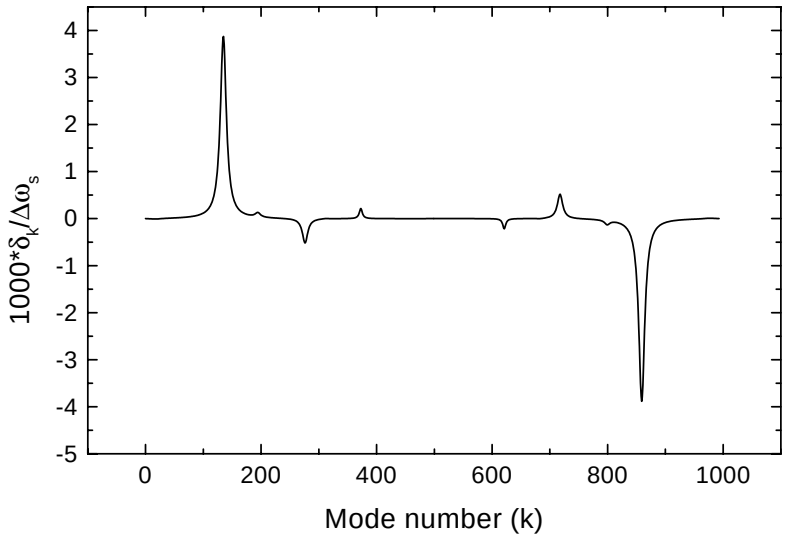

Figure 7.6: Same as in Fig.7.5, but W=125 MeV/u.

7.2.4 Interaction with the fundamental RF-modes of accelerating cavities

In high current machines with long perimeters of the orbit one of the most important source of the multi-bunch longitudinal instability may occur due to the interaction of the beam with the fundamental mode of the accelerating RF-cavity. According to Eqs.(7.37) and (7.38) in the exact resonance, when the ratio ω_r/ω_0 is an integer number proportional to the number of bunches in the beam, the increments of all multibunch modes vanish. However, if for some reason the RF frequency deviates by some amount from the resonant frequency of the fundamental mode of the cavity, the increments of the multibunch modes take finite values. According to Eqs.(7.37) these values are higher the higher are the harmonic number (h), Z_0/Q and the number of the cavities on the orbit. For the discussed synchrotron, the effect of the cavity detuning was evaluated calculating the maximum increments of unstable modes. As is seen from Fig.7.7, the increments of the synchrotron

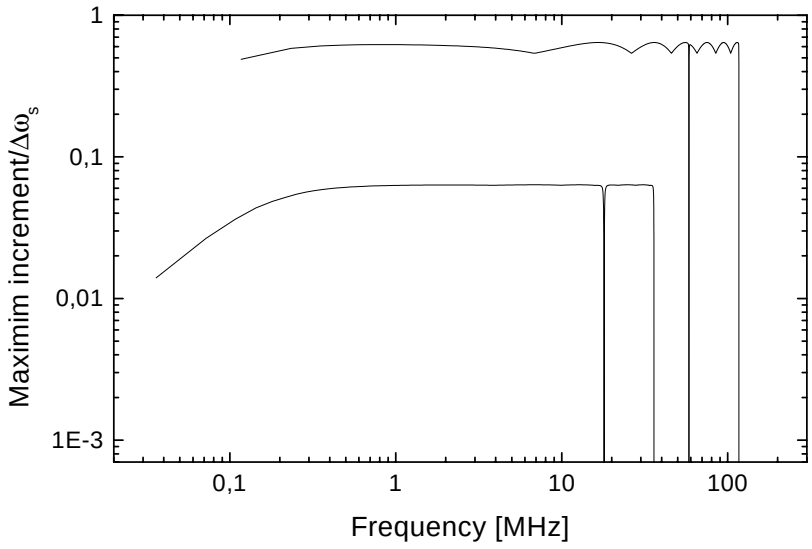

Figure 7.7: Dependence of the maximum increment of dipole synchrotron oscillations (in units of the synchrotron tune spread) on the cavity detuning. Upper line: $W = 125$ MeV/u, lower line: $W = 10$ MeV/u, beam intensity is 10^{13} of U^{4+} ions, $B = 0.7$, $h = 994$.

coherent dipole modes due to their interactions with the fundamental mode of the accelerating RF-system are substantially smaller than their Landau damping decrements. So that these instabilities do not limit the high intensity operations of the synchrotron during the ion acceleration.

7.2.5 Transverse singlebunch instabilities

The threshold current in a bunch due to wideband single bunch instability can be determined by two kind of phenomena. First is the head-tail instability due to chromatic

dependences of betatron tunes on the ion energy. Since the ring should be capable to operate the momentum spread in the beam up to ± 0.7 %, the ring chromaticity must be compensated with sufficient accuracy anyway. That will reduce, or eliminate the conventional head-tail instability. Another possibility occurs, when the wideband interactions of ions inside the bunch results in the so-called synchrobetatron mode coupling instability. The threshold of this instability is evaluated comparing the coherent frequency shift of the dipole betatron mode calculated for the beam of a zero length to a half of the frequency of synchrotron oscillations ($\omega_0 \nu_s$) [11]. Taking for the sake of simplicity that ions in a bunch interact via step-like transverse wakes, we find that the coherent tune shift of the dipole mode can be written in the following form (see, for example, in Ref.[8]):

$$\Delta\nu_\perp = \frac{Z}{A}\frac{eI}{2pv\nu_\perp B}\left(\frac{R_0^2}{l_\perp^2}\right)\left(\frac{Z_w}{n}\right), \tag{7.41}$$

where β_{av} is the averaged value of the β-function of the ring, B is a bunching factor and (Z_w/n) is the coupling impedance of the vacuum chamber due to non-stationary wakes. Comparing the value of $\Delta\nu_\perp$ in Eq.(7.41) and $\nu_s/2$, we obtain an expression for the threshold bunch current (electric)

$$I_{th} = \frac{Bl_\perp^2}{(Z_w/n)\beta_a v R_0}\sqrt{\frac{2eVAW\eta h}{2\pi Z}}. \tag{7.42}$$

For our estimations we take $(Z_w/n) = 25$ Ohm, which substantially exceeds similar typical values in the modern high-current machines and roughly estimates the contributions of the higher order modes of the RF cavities in the accelerating system. Direct calculations yield

$$I_{th} = 51.8 \text{ [A]}, \quad W = 10 \text{ [MeV/u]},$$

and

$$I_{th} = 163.4 \text{ [A]}, \quad W = 125 \text{ [MeV/u]}.$$

These numbers clearly show that single bunch mode-coupling instabilities do not limit the beam performance in the discussed synchrotron.

Chapter 8

Conclusions

Presented calculations show that the compression of the beam of U^{4+} ions in a single bunch having the length of 10 ns and focused on the target in a spot with desired diameter is quite feasible both for the bunch containing 10^{12} of U^{4+} ions and for the bunch containing 10^{13} of U^{4+} ions. Such a possibility is mainly provided due to small longitudinal (ϵ_s =3 [keV/u]·ns) and transverse normalized ($\epsilon_\perp$ = 1 mmmrad) emittances , which are expected from new UNILAC. However, the realization of this possibility in practice still is a very challenging problem in the particle accelerator physics. It demands elimination, or substantial reduction, of at least several effects limiting the synchrotron operational performance. One of the most important limitations occurs due to very low lifetime of the U^{4+} ions caused by their charge changing collisions with atoms of the residual gas. For the gas pressure of $P = 0.01$ nTorr and the gas mixture of 77%H_2+20%N_2+3%Ar, this lifetime is about 2 s at the injection energy (10 MeV/u) and about 5 s for the final ion energy 125 MeV/u. If the acceleration time is taken as 0.3 s and if we want to limit the number of the lost ions during the synchrotron cycle to of 10 % of the beam intensity, then the time available for the post-acceleration beam manipulations reduces to about 50 ms. In the longitudinal compression mode, during this time the bunch has to be debunched and after re-bunching in a single bunch its length has to be reduced down to 10 ns (or, till another desirable value). A decrease in the residual gas pressure increases the discussed lifetime linearly. However, with the same pressure of the residual gas in the vacuum chamber of the synchrotron, a significant increase in the lifetime can be achieved, if the populations of heavy atoms in the gas mixture are reduced. The reason is that contributions to the particle loss rates given by a population of the gas particles of the sort k in the mixture in are determined by the factors $Y^{(k)}(Z_T^2 + Z_T)^{(k)}$, where $Y^{(k)}$ is the partial concentration of the atoms of a sort k in the mixture ($\sum_k Y_k = 1$), and $(Z_T)^{(k)}$ is the atomic number of atoms of the sort k. So that the total ion loss rate is proportional to the value

$$\mathcal{R} = \sum_{k=1} Y^{(k)}(Z_T^2 + Z_T)^{(k)}.$$

For the mixture 77%H_2+20%N_2+3%Ar the value of $\mathcal{R}$ is equal to

$$\mathcal{R} = 3.08 + 22.4 + 10.26 = 35.74.$$

Factor $\mathcal{R}$ has about same value ($\mathcal{R}$ =37.8) for the mixture 90%H_2+10%Ar, but becomes ≈2.5 times smaller ($\mathcal{R}$ =14.8) for the mixture 90%H_2+10%N_2. Correspondingly, with same gas pressure the lifetime in the last case, will be 2.5 times larger (5 s for W= 10 MeV/u and 12.5 s for W = 125 MeV/u) than for the mixture of 77%H_2+20%N_2+3%Ar. Since no experimental data is available concerning the charge changing collisions of U^{4+} ions with the residual gas atoms, the lifetime was evaluated using results of calculations of relevant cross sections from Ref.[3]. The accuracy of these calculations is given by a factor of about 2. For this reason, the measurements of these cross sections would be very desirable prior to future technichal design of such a synchrotron. If the lifetime is in the range of several seconds, the desired lengths of the compressed bunches can be achieved during available short periods only in the case, if the momentum spread in the beam before compression is very small ($\sigma_p = 10^{-5}$, or lower). For realistic parameters of the accelerating RF system this requirement fits the injection conditions and the conditions of the phase space matching of the injected bunches longitudinal emittance to the longitudinal acceptance of the synchrotron. However, the perturbations increasing the bunch momentum spread uncontrollable (e.g. noises in RF system) should be reduced in subsequent synchrotron designs.

In the synchrotron with the closed orbit circumference of 1200 m and using as an injector new UNILAC, the beam with intensity of 10^{12} of U^{4+} ions is obtained using the 2-turn injection, while the beam with intensity of 10^{13} of U^{4+} ions is obtained using the 20-turn injection. The 20-turn injection takes 0.5 ms, which is two times shorter than the length of the bunch train from the UNILAC. In both cases, the longitudinal space charge fields of the beam must be compensated by a sufficiently strong longitudinal electrical field of the accelerating RF system. For a given bunch in the beam, new injected bunches are distributed in the transverse phase space and are injected in the same RF bucket. Correspondingly, the amplitude of RF voltage must be increased linearly during 0.5 ms from about 150 kV till 3 MV. This requirement does not limit the RF system performance. During injection and during the bunch compression operations the beam parameters correspond to the cases, when the perturbations due to space charge fields dominate. During multiturn injection transverse space charge fields can result in the transverse coherent instability of a macrobunch in the beam, if the betatron tunes are within the stopband defined in Eq.(7.16). Since the instability occurs due to relative motions inside a macrobunch, it cannot be suppressed by conventional feedback systems correcting dipole oscillations of the macro bunch. Although fast betatron debunching can reduce the limitations due to this instability, more careful study of this phenomenon could be very desirable. Other limitations due to transverse space charge fields of the beam during the synchrotron operations are reduced to incoherent phenomena and are common for such type of machines. These problems are most important for low energies of ions and can be eliminated by fast acceleration of ions. Since the high intensity beam is obtained using the multiturn injection, these incoherent problems are of the same strength for both low total current and for high total current beams. The bunch compression is performed in three steps using the $\pi/2$ rotation in the longitudinal phase space. After acceleration the beam is debunched using adiabatically slow decrease in the accelerating RF voltage. It takes approximately 20–30 ms. After this period the beam occupying 90% of the closed orbit perimeter is passed in the 'Energy modulation orbit' line of the

bypass (Fig.5.4) for the energy modulation. For the beam with a gap the prebunching step becomes not necessary. The ion energy is modulated along the bunch by increasing the RF voltage linearly in time. To the next turn this dependence is repeated again so that the time dependence of RF voltage has a sawtooth form. This voltage is generated using inductive type accelerating devices. If the amplitude of RF voltage is set to 1.2 MV, required momentum modulation of ± 0.7 % takes 100 turns. For the next 29 turns the bunch is passed into the RF-free 'Compression and extraction orbit' line of the bypass for the final compression. The bunch compression was simulated using the codes which take into account 2-dimensional, or 6-dimensional ion motions in the bunch phase space. The space charge fields of the bunch were accounted in these codes within the framework of the simplified model, when space charge forces depend on the ion coordinates only linearly. In addition, no chromatic effects on the ion motion were taken into account. These simulations enabled us to figure out the main specific features of the longitudinal bunch compression as well as to find a lattice design of the ring, where the compressed bunch does not blowup transversely during its compression until the bunch length reaches its minimum [1]. Due to model used, only parametric resonances could yield such a blowup in the simulations. On the other hand, the number of turns, when the Laslett tune shift takes substantial values (say, $\Delta\nu_L = 0.3$) is only several (6) turns. So that nonlinear resonances have no time to perturb the bunch significantly. Rapid dependences of the final bunch length on the amplitude of RF voltage as well as of the transverse bunch sizes on the values of the quadrupoles in the arcs show that effects of chromatic corrections and of modifications of the dispersion function of the ring on the bunch compression may demand additional studies. Those should be addressed in a future design works on such a synchrotron. The lattice of the ring was chosen to simplify the beam operation in the space charge dominated modes. As we said, these are the injection into the ring and especially the final turns of the bunch compression. The lattice consists of 2×50 identical FODO cells in the arc region connected by two straight sections. One of these straight sections is used for the injection/extraction operations, while the opposite one contains the 3 beam line bypass. Except for the special switching magnets for bypass operations, the lattices of the straight sections are also build up of the FODO cells similar to that in the arcs but with missing bending dipoles. The length of a cell is 10 m both in arcs and straight sections. For better distribution of the accelerating RF stations and of the bypass switching lattice the length of the straight section should be increased to 200 m, so that the total perimeter of the closed orbit of the synchrotron will be 1400 m. This will not change the design parameters significantly. For example, the top RF frequency of the accelerating system will decrease from 117 MHz to 100 MHz, which is inside the design interval of frequencies; the number of injection turns required to inject 10^{13} ions will decrease from 20 to 13. Correspondingly, the maximum beam radius at the injection energy will decrease from about 5.5 cm to 4.4 cm. The RF system of the discussed synchrotron consists of two parts. The first is the accelerating RF system. It provides the accelerating voltage up to 3 MV in the frequency range from 36 MHz to 117 MHz using ferrite loaded RF cavities (stations). The total length which occurs one station along the closed orbit is 0.4 m. The required number of stations is 250, all the system occupies 100 m of the orbit

[1] However, the beam can blowup transversely during the next turn.

in the bypass line 'Injection orbit' Fig.5.4. The second RF system provides the energy modulation for the bunch compression (line 'Energy modulation orbit' in Fig.5.4). This system uses the inductive type acceleration devices, which provide the amplitude of the sawtooth-shape Rf voltage of 2.5 MV using 30 m of the beam line in the bypass. As we already mentioned, the final bunch length strongly depends on the amplitude RF voltage. Due to beam loading this voltage can depend on the beam current. For this reason, the ring operation may demand special feedback systems keeping the acting amplitude of the RF voltage within the required range (typically, about 1 kV).

In the discussed synchrotron, conventional coherent instabilities do not pose any significant limitations on the beam current even for a beam containing 10^{13} of U^{4+} ions. The multibunch instabilities of the synchrotron coherent oscillations due to interactions of bunches with RF-system are well suppressed by the synchrotron frequency spread in the bunches for all ion energies. For dipole betatron oscillations, the Landau damping should be provided by a family of octupoles. In this case, the height of the stability diagram (the maximum damped increment) is determined by the strength of octupole fields, while the width of this diagram (the maximum coherent frequency shift) is determined by the largest of the frequency spreads due to octupole field and due to space charge fields ($\simeq 0.2\omega_0\Delta\nu_L$). However, the longitudinal feedback system can be useful to damp coherent oscillations during the beam debunching.

Additional problems may pose possible microwave radiations of bunches due to low cutoff frequencies in wide vacuum chambers. Traveling along the beam these waves may result in additional multibunch coupling of coherent oscillations in the beam. This problem also should be addressed to future studies. Both elastic and inelastic intrabeam scattering processes do not limit the performance of the discussed synchrotron in the bunch compression mode.

Table 8.1: General parameter set for the U^{4+}-synchrotron operating in the bunch compression mode.

Circumference	m	1400
Injection energy	MeV/u	10
Extraction energy	MeV/u	125
Injected ions/bunch	$1/10^8$	6.51
Injected ions/turn	$1/10^{11}$	7.
BR_{in}	Tm	27.23
BR_f	Tm	100
Acceleration time	s	0.3
Revolution period (injection energy)	μs	32.2
Revolution period (final energy)	μs	10
Harmonic number		1160
Acceleration rate	keV/turn	300
Betatron tune vertical*		0.4512
Betatron tune horizontal*		0.4831
Accepted momentum spread	%	$\pm$1.4
Betatron acceptance	mmmrad	360
$(\Delta\nu_L)_{inj}$		0.215
$(\Delta\nu_L)_f$		0.06
Vacuum	nTorr	below 0.01
Beam lifetime (injection)	s	2.1
Beam lifetime (extraction)	s	5.2
Beam intensity loss factor	%	10

* Fractional part

Table 8.2: Parameter set for the U^{4+}-synchrotron operating in the low and high intensity bunch compression modes.

Number of ions		10^{12}	10^{13}
Number of injections/bunch		2	13
RF-amplitude	MV	0.6	3
Synchronous phase		0.4π	0.46π
Transverse emittance (inv.)	mmmrad	2	13
Transverse emittance (non-inv.)	mmmrad	13.8	90
Bunch length (σ_s; injection)	m	0.25	0.34
Momentum spread (injection)	o/oo	0.01	0.01
Bunching factor ($2\sigma_s/\lambda_{RF}$)		0.5	0.7

Table 8.3: Parameter set for the bunch compression of an intense bunch of U^{4+} ions.

Number of ions		10^{13}
Ion energy	MeV/u	125
Initial bunch length	μs	8.5
Final bunch length	ns	10
Initial momentum spread		$\pm 3 \times 10^{-6}$
Final momentum spread	%	± 0.7
Vertical beam size at extraction point	mm	8
Horizontal beam size at extraction point	mm	4
Energy modulation voltage	MV	1.2
Number of turns for energy modulation		100
Number of turns for final compression		29

Appendix A

Synchrotron Oscillations

In this Appendix we discuss several subjects related to the description of the synchrotron oscillations in the heavy ion synchrotron.

A.1 Acceleration voltage

The voltage required to accelerate the ions with the charge Ze and atomic number A from the energy $E_{in} = m_p c^2 + W_{in}$ till the energy E_f during the time interval Δt can be calculated using the basic acceleration equation (see, for example, in Ref.[13]):

$$\frac{dE}{dt} = \frac{ZeU}{AT_0(E)} = \frac{ZeUc}{A\Pi}\frac{pc}{\sqrt{(pc)^2 + (m_p c^2)^2}}, \tag{A.1}$$

Here, $U = V\cos(\phi_s)$ is the accelerating voltage, ϕ_s is the synchronous RF-phase and $pc = 300ZB(t)R/A$. Using

$$\frac{dE}{vdt} = \frac{dp}{dt},$$

we rewrite Eq.(A.1) in the following form

$$c[p_f - p_{in}] = \frac{Zec}{A\Pi}\int_0^{\Delta t} dtU(t). \tag{A.2}$$

Assume for simplicity that U does not change during acceleration, we find

$$c[p_f - p_{in}] = \frac{ZeUc\Delta t}{A\Pi}, \tag{A.3}$$

or

$$eU = 300\left([BR]_f - [BR]_{in}\right)\frac{\Pi}{c\Delta t}. \tag{A.4}$$

In a low intensity bunch the equations describing synchrotron oscillations of ions read

$$\frac{d\Delta p}{dt} = \frac{ZeV}{A\Pi}\left[\cos(\phi) - \cos(\phi_s)\right],$$
$$\frac{d\phi}{dt} = h\omega_0(p)\eta\frac{\Delta p}{p},$$

or, for small oscillations ($\phi = \phi_s + hz/R_0$, $|z| \ll \lambda_{RF}$, $\lambda_{RF} = \Pi/h$,)

$$\frac{d\Delta p}{dt} = -\frac{ZeV\sin(\phi_s)}{A2\pi R_0^2}hz, \tag{A.5}$$

$$\frac{dz}{dt} = v\eta\frac{\Delta p}{p}. \tag{A.6}$$

These equations are obtained using the Hamiltonian

$$H = \frac{v\eta}{2p}\Delta p^2 + \frac{ZeV\sin(\phi_s)h}{2A2\pi R_0^2}z^2.$$

Defining $\mu = p/(\eta v)$ and

$$\omega_s = \omega_0\nu_s, \quad \nu_s = \sqrt{\frac{ZeV\sin(\phi_s)h\eta}{A2\pi pv}}, \tag{A.7}$$

we arrive at an equation defining the phase space ellipse

$$\frac{\Delta p^2}{2\mu\omega_s J_s} + \frac{\mu\omega_s z^2}{2J_s} = 1, \quad H = \omega_s J_s. \tag{A.8}$$

The area of this ellipse is

$$S_J = 2\pi J_s.$$

The longitudinal bunch emittance is encircled by the ellipse with $S_J = \epsilon_s$, so that $J_s = \epsilon_s/(2\pi)$ and

$$\frac{\pi pv\eta}{\omega_0\nu_s\epsilon_s}\delta^2 + \frac{\pi\omega_0\nu_s pv}{\eta\epsilon_s}\tau^2 = 1, \quad \delta = \frac{\Delta p}{p}, \quad \tau = \frac{z}{v}.$$

The main half-axes of this ellipse read

$$\delta_b = \sqrt{\frac{2\nu_s\epsilon_s}{pv\eta T_0}}, \quad \tau_b = \sqrt{\frac{\eta\epsilon_s T_0}{2\pi^2\nu_s pv}}. \tag{A.9}$$

If both the required accelerating voltage and the RF harmonic number are high, the ion synchrotron oscillations cannot be described in the adiabatic approximation. Assuming a single RF-cavity on the orbit placed at $s = 0$, we obtain relevant transport matrixes for synchrotron oscillations using the following equations

$$x'' + g(s)x = \frac{\delta}{R(s)}, \quad \delta' = -\frac{ZeV\sin(\phi_s)h}{ApvR_0}z\delta\,(s)\,, \tag{A.10}$$

$$z' = -\frac{x}{R} + \frac{\delta}{\gamma^2}. \tag{A.11}$$

Here, $g(s)$ is the rigidity of the horizontal betatron oscillations. Now, we write

$$x = x_b + D(s)\delta, \quad x_b = \sqrt{J_x \beta_x(s)}\cos[\phi_x(s)], \quad \frac{d\phi_x}{ds} = \frac{1}{\beta_x}, \tag{A.12}$$

and $D(s)$ is the dispersion function of the ring. According to the second equation in (A.10) the variation of the ion momentum after passing the cavity is described by the transport matrix

$$M(k) = \begin{bmatrix} 1 & 0 \\ -k & 1 \end{bmatrix}, \quad k = \frac{ZeV\sin(\phi_s)h}{Apv R_0}. \tag{A.13}$$

The variation of z over the closed orbit perimeter depends on the coupling of the horizontal betatron and of the synchrotron oscillations

$$z(\Pi) = z(0) + \eta\Pi\delta - \int_0^{\Pi} ds \frac{x_b}{R(s)}. \tag{A.14}$$

Since

$$\frac{d[x_b D' - x_b' D]}{ds} = \frac{x_b}{R},$$

Eq.(A.14) reads

$$z(\Pi) = z(0) + \eta\Pi\delta - [x_b D' - x_b' D]\Big|_0^{\Pi}. \tag{A.15}$$

If both dispersion function and its derivative vanish at the cavity position, no synchro-betatron coupling occur while the ion phase is transformed using the matrix

$$B = \begin{bmatrix} 1 & \eta\Pi \\ 0 & 1 \end{bmatrix}.$$

The matrix multiplication results in

$$M(k/2)BM(k/2) = \begin{bmatrix} 1 - (k\eta\Pi)/2 & \eta\Pi \\ -k + (k^2\eta\Pi)/4 & 1 - (k\eta\Pi)/2 \end{bmatrix}. \tag{A.16}$$

Using this equation, we find

$$\cos(\mu_s) = 1 - \frac{k\eta\Pi}{2} = 1 - \pi\frac{ZeV\sin(\phi_s)h\eta}{Apv} = 1 - 2\pi^2\nu_s^2, \tag{A.17}$$

and

$$\beta_s = \frac{\eta\Pi}{\sqrt{1 - (1 - 2\pi^2\nu_s^2)^2}} = \frac{\eta R_0}{\nu_s\sqrt{1 - \pi^2\nu_s^2}}. \tag{A.18}$$

The oscillations become unstable, if $\nu_s \geq 1/\pi$. More generally, if ions pass m identical RF-stations uniformly distributed along the orbit circumference, Eq.(A.17) reads

$$\cos\mu_s = 1 - \frac{2\pi^2\nu_s^2}{m}. \tag{A.19}$$

Correspondingly, the synchrotron oscillations are stable in a wider region of the RF-amplitudes in a single RF-station ($\nu_s \leq \sqrt{m}/\pi$)

$$\frac{ZeV\sin(\phi_s)h\eta}{A2\pi pv} \leq \frac{m}{\pi^2}. \tag{A.20}$$

Relevant accelerating voltage (mU) increases proportional to the square of the number of RF-stations.

A.2 Synchrotron oscillations in a space charge dominated bunch

If the accelerated bunch is short, its space charge fields may affect substantially the synchrotron oscillations of particles. In such a case, we have to add in the right-hand side of Eq.(A.5) the contribution due to the longitudinal electric field of the bunch

$$\mathcal{E} = \frac{ZNe\Lambda}{\gamma^2}\frac{d\rho}{dz}, \quad \Lambda = 1 + 2\ln\left(\frac{l_\perp}{a}\right). \tag{A.21}$$

Here, N is the number of particles in the bunch, ρ is its linear density, $l_\perp$ is the pipe radius and a is the bunch cross section radius. For the sake of simplicity we take that ρ is a parabolic distribution

$$\rho(z) = \frac{3}{4\sigma_s}\left(1 - \frac{z^2}{\sigma_s^2}\right). \tag{A.22}$$

Then, the modified Eq.(A.5) reads

$$\frac{d\delta}{dt} = -\frac{ZeV\sin(\phi_s)}{ApR_0\lambda_{RF}}\left[1 - \frac{\sigma_{th}^3}{\sigma_s^3}\right]z, \tag{A.23}$$

where

$$\sigma_{th} = \left(\frac{3}{2}m_pc^2\frac{ZNr_p\Lambda R_0\lambda_{RF}}{\gamma^2 eV\sin(\phi_s)}\right)^{1/3}. \tag{A.24}$$

Equation (A.23) shows that with an increase in the bunch linear density synchrotron oscillations will be stable provided that the bunch length exceeds σ_{th} defined in Eq.(A.24). The phase space trajectories of synchrotron oscillations still are the ellipses. For the ellipse encircling the longitudinal bunch emittance the main half-axes which are determined in Eqs.(A.9), but the synchrotron tune in these equations should be modified according to

$$\nu_s \to \nu_s(N) = \sqrt{\frac{ZeV\sin(\phi_s)h\eta}{A2\pi pv}\left(1 - \frac{\sigma_{th}^3}{\sigma_s^3}\right)} \tag{A.25}$$

So that the modified Eqs.(A.9) will read

$$\sigma_b^2\sqrt{1-\frac{\sigma_{th}^3}{\sigma_s^3}}=\sigma_0^2=\frac{\eta\epsilon_s\Pi}{2\pi^2\nu_s p}, \tag{A.26}$$

$$\delta_b=\sqrt{\frac{2\nu_s\epsilon_s}{p\upsilon\eta T_0}\left(1-\frac{\sigma_{th}^3}{\sigma_s^3}\right)^{1/2}}. \tag{A.27}$$

If the length of the low intensity bunch is small ($\sigma_0 \ll \sigma_{th}$), the root in Eq.(A.26) occurs to be close to σ_{th}:

$$\sigma_b \simeq \sigma_{th}+\frac{\sigma_0^4}{3\sigma_{th}^3}. \tag{A.28}$$

Corresponding value of the bunch momentum spread is small

$$\delta_b \simeq \frac{\epsilon_s}{\pi p\upsilon\sigma_{th}}. \tag{A.29}$$

A.3 Inertial bunch compression

Inertial bunch compression occurs, if we provide a correct modulation of initial ion momenta along the bunch and if the longitudinal space charge fields of the compressed bunch are small. If N is the number of particles in the bunch, while z_a and $\delta_a = \Delta p_a/p$ are positions of the particle (a) $[a = 1, 2, \ldots N]$ in the longitudinal phase space, then after the momentum modulation $\delta_a = \delta_{a0} - \kappa z_{a0}$ and subsequent pass of the drift space of the length L, the particles get the following positions in the bunch

$$z_a = z_{a0} + \eta L\delta_a = z_{a0}(1-\eta L\kappa) + \eta L\delta_{a0}. \tag{A.30}$$

With statistically independent distribution in particle initial conditions, the rms bunch length reads

$$\sigma_s^2=\frac{1}{N}\sum_{a=1}^{N}(z_a- < z >)^2, \quad < z >= \frac{1}{N}\sum_{a=1}^{N} z_a,$$

or

$$\sigma_s^2 = \sigma_{s0}^2(1-\eta\kappa L)^2 + \eta^2 L^2\sigma_\delta^2, \tag{A.31}$$

where

$$\sigma_\delta^2=\frac{1}{N}\sum_{a=1}^{N}(\delta_{a0}-\Delta)^2, \quad \Delta=\frac{1}{N}\sum_{a=1}^{N}\delta_{a0}$$

is the momentum spread in the bunch before modulation. Simple transformations result in

$$\sigma_s^2 = \Sigma^2 \left(\eta L - \frac{\kappa \sigma_{s0}^2}{\Sigma^2} \right)^2 + \sigma_{s0}^2 \frac{\sigma_\delta^2}{\Sigma^2}, \quad \Sigma^2 = \sigma_\delta^2 + \kappa^2 \sigma_{s0}^2. \tag{A.32}$$

Considered as a function of the compression length L, the bunch length reaches its minimum

$$\sigma_{\min}^2 = \sigma_{s0}^2 \frac{\sigma_\delta^2}{\sigma_\delta^2 + \kappa^2 \sigma_{s0}^2}, \tag{A.33}$$

when

$$L = L_{\min} = \frac{1}{\eta \kappa} \times \frac{1}{1 + (\sigma_\delta / \kappa \sigma_{s0})^2}. \tag{A.34}$$

Appendix B

Charge Exchange and Ionization

According to our knowledge, experimental data on charge changing cross sections for U^{4+} ions are not available yet. For this reason, in our estimations of the particle losses from the beam we use results of the calculations, which have been performed in Ref.[5] and [6]. In Ref.[5] the total cross section of the charge changing scatterings have been calculated taking into account the charge transfer (CT)

$$U^{4+} + U^{4+} \rightarrow U^{3+} + U^{5+},$$

and in the ionization reactions

$$U^{4+} + U^{4+} \rightarrow U^{5+} + U^{4+} + e.$$

processes. Results of these calculations are presented in Table B.1 as functions of the so called relative collision energy. If u is the relative velocity of the colliding ions expressed in the atomic units (1 a.u.= 2.2×10^8 [cm/s]), then the relative collision energy reads

$$W_{col}\ [\mathrm{keV/u}] = 25u^2\ [\mathrm{a.u.}]. \tag{B.1}$$

Assuming that the relative velocity in the beam is mainly determined by

$$u_{a.u.} = 10^4 \left(\frac{3}{2.2}\right)^2 \frac{(v/c)\epsilon_0}{\beta_{av}},$$

we obtain

$$W_{col} \simeq 4.62 \times 10^5 \frac{(v/c\epsilon_0)}{\beta_{av}}\ [\mathrm{keV/u}]. \tag{B.2}$$

Here, β_{av} is the average value of the β-function of the ring and ϵ_0 is the invariant transverse beam emittance.

The estimated accuracy of the cross section given in Ref.[5] is a factor of 2. However, if we take as an example $\epsilon_0 = 20$ mmmrad and $\beta_{av} \simeq 16$ m, we shall find $W_{col} \simeq 0.3$ [keV/u]. This value of the collision energy is well below the lowest border of the data given in the Table B.1. The calculations of the charge transfer cross sections in wider collision energy range were made in [6] (Table B.2). As is seen from Fig.B.1, in the common region of the energies the data from Tables B.1 and B.2 mainly differ by a factor of about 3.

Table B.1: Cross sections of the charge exchange and ionization according to Ref.[5].

Collision energies, keV/u.	Cross sections, $\times 10^{-16}$ cm^2		Collision energies, keV/u.	Cross sections, $\times 10^{-16}$ cm^2	
	CT	I		CT	I
1.000	.011		112.5	.856	.722
2.250	.092		134.1	.145	.742
4.000	.198		150.0	.010	.736
6.250	2.06	.012	187.0		.721
10.00	2.61	.054	226.0		.691
18.75	2.76	.243	262.0		.663
37.50	1.83	.384	375.0		.602
75.00	.891	.698	750.0		.403
			1500.		.242

Table B.2: Total cross sections of the charge exchange collisions of U^{4+} ions according to Ref.[6].

W_{col} [keV/u]	$\sigma_{tot} \times 10^{16}$ [cm^2]	W_{col} [keV/u]	$\sigma_{tot} \times 10^{16}$ [cm^2]
0.1	0.0012	20.0	7.1
0.2	0.015	40.0	7.1
0.4	0.12	100.0	5.7
0.8	0.53	200.0	3.4
1.0	0.78	400.0	2.4
2.0	2.0	800	1.1
4.0	3.9	2500	0.088
8.0	5.8	5000	0.010
10	6.2	10000	0.00086

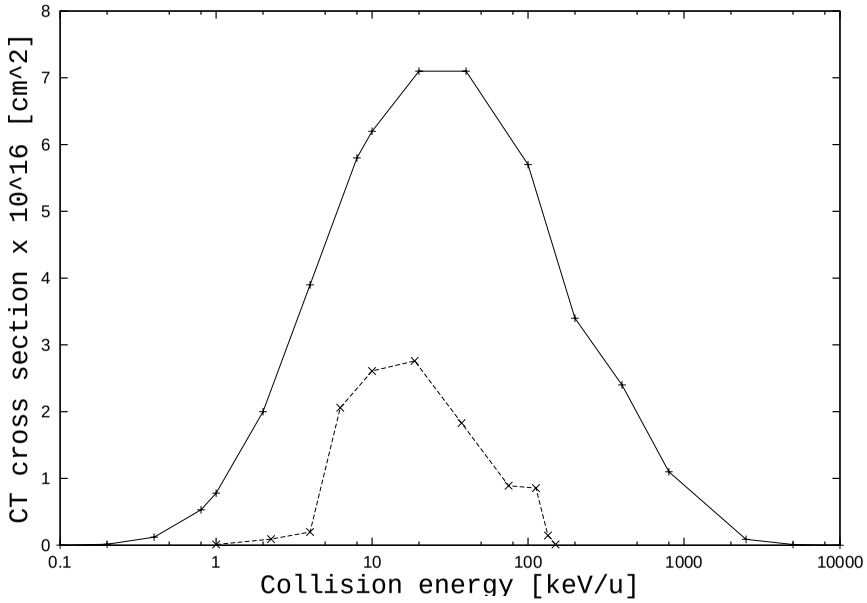

Figure B.1: Dependence of the charge transfer cross section for collisions of the U^{4+} ions on their collision energy. Crosses – data from Table B.2, x – data from the Table B.1.

That is not very dramatic since the accuracy of these calculations is also determined by about same factor. However, the low energy and the high energy behavior of the data in Table B.2 looks smoother. With an accuracy within 70% the data from the Table B.2 can be fitted using the following formula

$$\sigma_{tot} = 7.1 \times 10^{-16} \left(\frac{W}{W_0}\right)^{0.3} \exp\left[-0.08 \left(\left|\ln \frac{W}{W_0}\right|\right)^{2.7}\right] \ [\mathrm{cm}^2], \tag{B.3}$$

where $W_0 = 19.3$ [keV/u]. In the region $W_{col} < 10$ [keV/u] the accuracy of the fitting is better than 20 %.

Appendix C

Intrabeam Scattering Growthrates

Here we follow Ref.[1] and assume the smoothed focusing approximation. then, the vertical emittance blowup rate due to IBS in a non-relativistic bunch reads ($\beta_x \simeq \beta_y = \beta$)

$$\frac{d\ln\epsilon_y}{dt} = \frac{K\beta}{\epsilon_y^2\epsilon_x\sigma_s\delta}\int\frac{d\Omega}{4\pi}\frac{1-3\sin^2\theta\cos^2\phi}{a\sin^2\theta + a_s\cos^2\theta}, \quad K = \frac{N(Z^2/A)^2 r_p^2 c L_{IBS}}{2\pi\gamma^4(v/c)^2}.$$

Here L_{IBS} – Coulomb logarithm, $a = \beta/\epsilon$, $\epsilon_x \simeq \epsilon_y = \epsilon$ and

$$a_s = \gamma^2 a\frac{D^2}{\beta^2} + \frac{\gamma^2}{\delta^2}$$

with D – dispersion and $\delta = \Delta p/p$. Now, we write

$$\begin{aligned}\frac{d\ln\epsilon_y}{dt} &= \frac{K\beta}{\epsilon^3\sigma_s\delta}\int_0^1 dz\int_0^{2\pi}\frac{d\phi}{2\pi}\frac{1-3\cos^2\phi[1-z^2]}{(a_s-a)z^2+a}\\ &= \frac{K\beta}{\epsilon^3\sigma_s\delta}\int_0^1 dz\frac{1-3[1-z^2]/2}{(a_s-a)z^2+a}\\ &= -\frac{K\beta}{2\epsilon^3\sigma_s\delta}\int_0^1 dz\frac{1-3z^2}{(a_s-a)z^2+a}.\end{aligned}$$

Using

$$a_s - a = \frac{\gamma^2}{\delta^2} + a\left(\frac{\gamma^2 D^2}{\beta^2} - 1\right) = a\left(\frac{\gamma^2\epsilon}{\delta^2\beta} + \frac{\gamma^2 D^2}{\beta^2} - 1\right),$$

we obtain

$$\frac{d\ln\epsilon_y}{dt} = -\frac{K\beta\epsilon}{2\epsilon^3\sigma_s\delta\beta}\int_0^1 dz\frac{1-3z^2}{qz^2+1}, \quad q = \frac{\gamma^2\epsilon}{\delta^2\beta} + \frac{\gamma^2 D^2}{\beta^2} - 1.$$

The integral is calculated directly:

$$\int_0^1\frac{1-3z^2}{qz^2+1}dz = \frac{1}{\left(\sqrt{q}\right)^3}\left(-3\sqrt{q} + [3+q]\arctan\sqrt{q}\right). \tag{C.1}$$

That results in

$$\frac{d\ln\epsilon_y}{dt} = -\frac{K}{2\epsilon^2\sigma_s\delta}\left(\frac{[3+q]\arctan\sqrt{q}-3\sqrt{q}}{\left(\sqrt{q}\right)^3}\right)$$

$$= -\frac{N(Z^2/A)^2 r_p^2 c L_{IBS}}{4\pi\gamma^4\epsilon^2(v/c)^2\sigma_s\delta}\left(\frac{[3+q]\arctan\sqrt{q}-3\sqrt{q}}{\left(\sqrt{q}\right)^3}\right).$$

Using that $\gamma(v/c)\epsilon = \epsilon_0$ is an invariant, we can also write

$$\frac{d\ln\epsilon_z}{dt} \simeq -\frac{N(Z^2/A)^2 r_p^2 c L_{IBS}}{4\pi\gamma^2\epsilon_0^2\sigma_s\delta}\left(\frac{[3+q]\arctan\sqrt{q}-3\sqrt{q}}{\left(\sqrt{q}\right)^3}\right).$$

Another possibility occurs, if the value q is negative. Defining $p = -q > 0$ we find

$$\int_0^1 \frac{1-3z^2}{1-pz^2}dz = \frac{3}{p} + \frac{p-3}{p^{3/2}}\frac{1}{2}\ln\left(\frac{\sqrt{p}+1}{1-\sqrt{p}}\right). \tag{C.2}$$

Hence,

$$\frac{1}{\tau_y} = \frac{d\ln\epsilon_y}{dt} \simeq -\frac{N(Z^2/A)^2 r_p^2 c L_{IBS}}{4\pi\gamma^2\epsilon_0^2\sigma_s\delta}\left\{\frac{3}{p} + \frac{p-3}{2p^{3/2}}\ln\left(\frac{\sqrt{p}+1}{1-\sqrt{p}}\right)\right\},$$

$$p = 1 - \frac{\gamma^2\epsilon}{\delta^2\beta} - \frac{\gamma^2 D^2}{\beta^2}.$$

Note, that this growth-rate does not depend on particle kinetic energy until $\delta > \sqrt{(}\epsilon/\beta)$.

Similarly, for the longitudinal motion we write

$$\frac{d\ln(\delta^2)}{dt} = \frac{K\gamma^2}{\epsilon_x\epsilon_y\sigma_s\delta^3}\int_0^\pi \frac{d\theta\sin\theta}{2}\frac{1-3\cos^2\theta}{a\sin^2\theta + a_s\cos^2\theta}$$

$$= \frac{K\gamma^2}{\epsilon^2\sigma_s\delta^3}\frac{\epsilon}{\beta}\int_0^1 dz\frac{1-3z^2}{1+qz^2}. \tag{C.3}$$

Using Eqs.(C.1) and (C.2) we rewrite this expression in the following form

$$\frac{1}{\tau_s} = \frac{d\ln(\delta^2)}{dt} = \frac{N(Z^2/A)^2 r_p^2 c L_{IBS}}{2\pi\gamma(v/c)\epsilon_0\beta\sigma_s\delta^3}\begin{cases}\dfrac{[3+q]\arctan\sqrt{q}-3\sqrt{q}}{\left(\sqrt{q}\right)^3}, & q>0\\ \dfrac{3}{p}+\dfrac{p-3}{2p^{3/2}}\ln\left(\dfrac{\sqrt{p}+1}{1-\sqrt{p}}\right), & p=-q>0.\end{cases} \tag{C.4}$$

The ratio of the transverse to the longitudinal growth rates is estimated by the following expression:

$$\frac{(1/\tau)}{(1/\tau_s)} = \frac{1}{2}\frac{\beta\delta^2}{\gamma^2\epsilon} \tag{C.5}$$

For the horizontal oscillations we write [1]

$$\begin{aligned}\frac{d\ln\epsilon_x}{dt} &= \frac{K\beta}{\epsilon^3\sigma_s\delta}\int\frac{d\Omega}{4\pi}\left[\frac{1-3\sin^2\theta\sin^2\phi}{a\sin^2\theta+a_s\cos^2\theta}+\frac{\gamma^2D^2}{\beta^2}\frac{1-3\cos^2\theta}{a\sin^2\theta+a_s\cos^2\theta}\right]\\ &= \frac{K\beta}{\epsilon^3\sigma_s\delta}\left[\frac{\gamma^2D^2}{\beta^2}-\frac{1}{2}\right]\int_0^1 dz\frac{1-3z^2}{a+[a_s-a]z^2}\\ &= \frac{K}{\epsilon^2\sigma_s\delta}\left[\frac{\gamma^2D^2}{\beta^2}-\frac{1}{2}\right]\int_0^1 dz\frac{1-3z^2}{1+qz^2}.\end{aligned}$$

So that

$$\frac{1}{\tau_x}=\frac{N(Z^2/A)^2r_p^2cL_{IBS}}{2\pi\gamma^2\epsilon_0^2\sigma_s\delta}\left[\frac{\gamma^2D^2}{\beta^2}-\frac{1}{2}\right]\begin{cases}\dfrac{[3+q]\arctan\sqrt{q}-3\sqrt{q}}{\left(\sqrt{q}\right)^3}, & q>0\\ \dfrac{3}{p}+\dfrac{p-3}{2p^{3/2}}\ln\left(\dfrac{\sqrt{p}+1}{1-\sqrt{p}}\right), & p=-q>0.\end{cases}\tag{C.6}$$

The sum of the partial growth-rates reads

$$\Sigma=\frac{1}{\tau_x}+\frac{1}{\tau_y}+\frac{1}{\tau_s}=\frac{Kq}{\epsilon^2\sigma_s\delta}\int_0^1 dz\frac{1-3z^2}{1+qz^2}\tag{C.7}$$

$$=\frac{K}{\epsilon^2\sigma_s\delta}\left[(3+q)\int_0^1\frac{dz}{1+qz^2}-3\right],\tag{C.8}$$

$$q=\frac{\gamma^2\epsilon}{\delta^2\beta}+\frac{\gamma^2D^2}{\beta^2}-1.$$

Appendix D

Collective Phenomena

D.1 Effects of the space charge fields on dipole coherent oscillations

In this Section we obtain dispersion equations for the dipole coherent oscillations of the ion beam which takes into account the space charge repulsion of ions. For the sake of simplicity we assume one-dimensional coherent oscillations and smoothed focusing approximation. In this case, the Vlasov equation reads

$$\frac{\partial f}{\partial t} + v\frac{\partial f}{\partial x} + \left[-M\omega_x^2 x + bx^3 + F(x-d) + F_2(t)\right]\frac{\partial f}{\partial p_x} = 0. \tag{D.1}$$

Here, $f = f(x, p_x, t)$ is the distribution function of the ion beam,

$$d(t) = \int dp_x dx x f \tag{D.2}$$

is the dipole momentum of the beam, $F(x-d)$ is the force describing the space charge repulsion of ions, while $F_2(t)$ is the force describing the interaction of the beam dipole oscillations with surrounding electrodes. The term bx^3 describes effects of the cubic nonlinearity of the guiding magnetic field. In the linear approximation on the amplitude of coherent oscillations we write

$$F(x-d) \simeq F(x) - d(t)\frac{\partial F}{\partial x}, \tag{D.3}$$

and

$$f = f_0(x, p_x) + \delta f(x, p_x, t), \tag{D.4}$$

where f_0 is the beam distribution function without coherent oscillations, while δf describes coherent oscillations. It is more convenient to perform subsequent calculations using the action-phase variables of unperturbed oscillations. We write

$$x = \sqrt{\frac{2I}{M\omega_x}}\cos\psi, \quad p_x = -\sqrt{2IM\omega_x}\sin\psi, \tag{D.5}$$

and assuming that the working point of the ring is far from machine resonances $f_0 = f_0(I)$. For non-resonant oscillations the terms bx^3 and $F(x)$ in the square bracket in Eq.(D.1) give the following frequency shifts of the unperturbed oscillations

$$\Delta\omega_x = -\Omega(I), \quad \Omega(I) = \int_0^{2\pi} \frac{d\psi}{2\pi} \frac{\partial x}{\partial I} F = \frac{1}{\sqrt{2IM\omega_x}} \frac{F_1 + F_{-1}}{2}, \tag{D.6}$$

and

$$\Delta\omega_x^{(a)} = aI, \quad a = -\frac{3b}{4M^2\omega_x^2}, \quad b = \frac{Zev}{6c} \frac{\partial^3 H_z}{\partial x^3}. \tag{D.7}$$

Here,

$$F_{\pm 1} = \int_0^{2\pi} \frac{d\psi}{2\pi} F e^{\mp i\psi}.$$

Since $F(-x) = -F(x)$, we have

$$\int_0^{2\pi} \frac{d\psi}{2\pi} F \sin(\psi) = 0,$$

so that $F_1 = F_{-1}$, while

$$\Omega(I) = \frac{F_1(I)}{\sqrt{2IM\omega_x}}. \tag{D.8}$$

In the action-phase variables the linearized Vlasov equation reads (see, for example, in Ref.[8])

$$\frac{\partial \delta f}{\partial t} + [\omega_x + aI - \Omega(I)] \frac{\partial \delta f}{\partial \psi} + \left[F_2(t) \frac{\partial x}{\partial \psi} - d(t) \frac{\partial F}{\partial \psi} \right] \frac{\partial f_0}{\partial I} = 0. \tag{D.9}$$

Using Fourier transform in time and phase variable

$$\delta f = e^{-i\omega t} \left[f_1(I) e^{i\psi} + f_{-1}(I) e^{-i\psi} \right] \tag{D.10}$$

and assuming no coupling between modes $f_{\pm 1}$, we obtain

$$f_m = \frac{m \partial f_0 / \partial I \sqrt{2IM\omega_x}}{[\Delta\omega_m - maI + m\Omega(I)]} \left[\frac{F_2(\omega)}{2M\omega_x} + d_m(\omega)\Omega(I) \right], \quad m = \pm 1 \tag{D.11}$$

and

$$d_m(\omega) = \int_0^\infty dI \sqrt{\frac{I}{2M\omega_x}} f_m \tag{D.12}$$

Substituting in Eq.(D.11)

$$\frac{mF_2(\omega)}{2M\omega_x} \to -\Omega_m d_m(\omega), \tag{D.13}$$

where Ω_m is the coherent frequency shift calculated for the beam without frequency spread, and using Eq.(D.12) we find the dispersion equation of the problem in the following form ($m = 1$)

$$1 - \int_0^\infty dI \frac{I\Omega(I)\partial f_0/\partial I}{[\Delta\omega_1 - aI + \Omega(I)]} = -\Omega_1 \int_0^\infty dI \frac{I\partial f_0/\partial I}{[\Delta\omega_1 - aI + \Omega(I)]}. \tag{D.14}$$

Now, using

$$\frac{\Omega(I)}{[\Delta\omega_1 - aI + \Omega(I)]} = \frac{\Delta\omega_1 - aI}{[\Delta\omega_1 - aI + \Omega(I)]} - 1$$

and

$$\int_0^\infty dI I \frac{\partial f_0}{\partial I} = -1,$$

we obtain

$$\Delta\omega_1 = \Omega_1 + a\frac{Q_2(\Delta\omega_1, I)}{Q_1(\Delta\omega_1, I)}, \tag{D.15}$$

where

$$Q_n(\Delta\omega_1, I) = \int_0^\infty dI \frac{I^n \partial f_0/\partial I}{[\Delta\omega_1 - aI + \Omega(I)]}, \quad n = 1, 2. \tag{D.16}$$

In particular, from Eq.(D.15) we see that without external (cubic) nonlinearity the frequency spread due to space charge fields produces no Landau damping and no additional frequency shift of the dipole coherent oscillations:[1]

$$\Delta\omega_1 = \Omega_1, \quad a = 0.$$

[1]This fact should be expected beforehand. Without nonlinearity of the guiding field Eq.(D.1) splits onto the following uncoupled equations

$$\ddot{d} + \omega_x d = \frac{F_2}{M}, \quad \frac{\partial\Phi}{\partial t} + \frac{P}{M}\frac{\partial\Phi}{\partial y} + F(y)\frac{\partial\Phi}{\partial P} = 0,$$

where, $y = x - d(t)$, $P = p_x - M\dot{d}(t)$, and $f = \Phi(y, P, t)$.

Appendix E

Bunching

E.1 Orthogonal transformations of the longitudinal phase space

In this Section we shall collect some general formulae describing transformations of the bunch length and its momentum spread due to orthogonal transformations of initial conditions of particles into their instantaneous values. For the sake of simplicity, we neglect the space charge effects on the bunch length. We take that initial distribution of ion in the bunch is described by a Gaussian function

$$f_0(q,p) = \frac{1}{2\pi\sigma\delta}\exp\left(-\frac{q^2}{2\sigma^2} - \frac{p^2}{2\delta^2}\right). \tag{E.1}$$

Here, $q = z_0$ and $p = z_0'$ are initial values of the ion longitudinal coordinates in the phase space, while σ and δ are their rms widths. If azimuth θ is used as an independent variable, the instantaneous value of the distribution function reads

$$f(z,z',\theta) = f_0(q[z,z',\theta], p[z,z',\theta]). \tag{E.2}$$

We take that an initial point (q,p) is obtained from the point (z,z') using the following transformation

$$q = az + bz', \quad p = cz + dz', \quad ad - bc = 1, \tag{E.3}$$

where a, b, c and d are functions of the independent variable θ. Substituting q and p from Eq.(E.3) in Eq.(E.1), we find

$$\frac{p^2}{\delta^2} + \frac{q^2}{\sigma^2} = z^2\left(\frac{c^2}{\delta^2} + \frac{a^2}{\sigma^2}\right) + \left(\frac{cd}{\delta^2} + \frac{ab}{\sigma^2}\right)2zz' + \left(\frac{d^2}{\delta^2} + \frac{b^2}{\sigma^2}\right)(z')^2. \tag{E.4}$$

Note that the determinant of the quadratic form in the right-hand side of this equation is exactly equal to inverse of the longitudinal phase space volume of the bunch $(1/[\sigma\delta])$. The instantaneous linear density of the bunch is calculated using

$$\lambda(z,\theta) = \int_{-\infty}^{\infty} d(z')f(z,z',\theta). \tag{E.5}$$

Simple transformations in Eq.(E.4) result in

$$\frac{p^2}{\delta^2}+\frac{q^2}{\sigma^2}=\left(\frac{d^2}{\delta^2}+\frac{b^2}{\sigma^2}\right)\left[z'+z\frac{\left(\frac{cd}{\delta^2}+\frac{ab}{\sigma^2}\right)}{\left(\frac{d^2}{\delta^2}+\frac{b^2}{\sigma^2}\right)}\right]^2+\frac{z^2}{\sigma^2d^2+\delta^2b^2}.$$

Calculating Gaussian integrals, we find

$$\lambda(z,\theta)=\frac{1}{\sqrt{2\pi}\sigma(\theta)}\exp\left(-\frac{z^2}{2\sigma^2(\theta)}\right),\quad \sigma^2(\theta)=\sigma^2d^2+\delta^2b^2. \tag{E.6}$$

Similarly, for the momentum distribution we obtain

$$\rho(z',\theta)=\frac{1}{\sqrt{2\pi}\delta(\theta)}\exp\left(-\frac{(z')^2}{2\delta^2(\theta)}\right),\quad \delta^2(\theta)=\delta^2a^2+\sigma^2c^2. \tag{E.7}$$

The rms widths in Eqs.(E.6) and (E.7) define the lengths of the projections of the main half-axes of the instantaneous phase space ellipse on axes z and z'. For this reason, the product $\sigma(\theta)\delta(\theta)$, generally, exceeds the longitudinal phase space volume of the bunch $[\sigma(\theta)\delta(\theta)\geq\sigma\delta]$. Indeed, the rotation

$$z=Z\cos(\phi)+Z'\sin(\phi),\quad z'=-Z\sin(\phi)+Z'\cos(\phi), \tag{E.8}$$

transforms the quadratic form in Eq.(E.4) to the main axes

$$z^2\left(\frac{c^2}{\delta^2}+\frac{a^2}{\sigma^2}\right)+\left(\frac{cd}{\delta^2}+\frac{ab}{\sigma^2}\right)2zz'+\left(\frac{d^2}{\delta^2}+\frac{b^2}{\sigma^2}\right)(z')^2=\frac{Z'^2}{\Delta^2}+\frac{Z^2}{\Sigma^2}, \tag{E.9}$$

provided that

$$\sin(2\phi)=\frac{2(\delta^2ab+\sigma^2cd)}{\sqrt{\left[\delta^2b^2+\sigma^2c^2+\sigma^2d^2+\delta^2a^2\right]^2-4\sigma^2\delta^2}}. \tag{E.10}$$

The values Σ and Δ read

$$\Sigma^2=\frac{\delta^2b^2+\sigma^2d^2+\sigma^2c^2+\delta^2a^2+\sqrt{\left[\delta^2b^2+\sigma^2c^2+\sigma^2d^2+\delta^2a^2\right]^2-4\sigma^2\delta^2}}{2}, \tag{E.11}$$

$$\Delta^2=\frac{\delta^2b^2+\sigma^2d^2+\sigma^2c^2+\delta^2a^2-\sqrt{\left[\delta^2b^2+\sigma^2c^2+\sigma^2d^2+\delta^2a^2\right]^2-4\sigma^2\delta^2}}{2}, \tag{E.12}$$

so that their product does not depend on time:

$$\Sigma\Delta=\delta\sigma. \tag{E.13}$$

In the simplest case, the transformation in Eq.(E.3) can describe the bunch rotation with a constant tune of the synchrotron oscillations, so that

$$q = z\cos(\psi) - z'\frac{\sin(\psi)}{\nu_s}, \quad p = z\nu_s\sin(\psi) + z'\cos(\psi), \quad \psi = \nu_s\theta + \psi_0.$$

Using these equations, we find

$$\begin{aligned}\sigma^2(\theta) &= \sigma^2\cos^2(\psi) + \delta^2\left(\frac{\sin(\psi)}{\nu_s}\right)^2 = \sigma^2 - \left[\sigma^2 - \frac{\delta^2}{\nu_s^2}\right]\sin^2\psi,\\ \delta^2(\theta) &= \delta^2 + \left[\nu_s^2\sigma^2 - \delta^2\right]\sin^2\psi.\end{aligned} \tag{E.14}$$

These equations show that no bunch compression occurs, if the bunch emittance is matched to the longitudinal phase space acceptance ($\nu_s^2\sigma^2 = \delta^2$). On the contrary, if $\nu_s\sigma \gg \delta$, the bunch length is reduced very strongly after a $\pi/2$–rotation. The momentum spread after such a rotation strongly increases ($\delta_{\pi/2} = \nu_s\sigma$).

E.2 Synchrotron oscillations with variable tunes

In this Section we remind the reader several cases, when equations for small synchrotron oscillations of a particle can be solved directly even in the case, when the oscillation tune varies with the time. Taking as an independent variable the ion azimuth θ, we write

$$z'' + \nu_s^2 e^{\theta/\theta_0} z = 0. \tag{E.15}$$

In this example the synchrotron tune varies with time according to

$$\nu_s(\theta) = \nu_s\exp\left(\frac{\theta}{2\theta_0}\right). \tag{E.16}$$

If $\theta_0 > 0$, this case may correspond to the bunching due to, for example, an exponential increase in the RF–voltage. If $\theta_0 < 0$, this Eq.(E.15) may describe small oscillations during debunching.

As we said, Eq.(E.15) can be solved directly. Taking as a new independent variable the function

$$u = \exp\left(\frac{\theta}{2\theta_0}\right), \quad \frac{d}{d\theta} = \frac{u}{2\theta_0}\frac{d}{du},$$

we transform Eq.(E.15) into the Bessel equation

$$\frac{1}{u}\frac{d}{du}\left[u\frac{dz}{du}\right] + k^2 z = 0, \quad k = 2\nu_s\theta_0. \tag{E.17}$$

which solution reads

$$\begin{pmatrix} z \\ z' \end{pmatrix} = \begin{pmatrix} J_0(ku) & N_0(ku) \\ -\nu_s u J_1(ku) & -\nu_s u N_1(ku) \end{pmatrix}\begin{pmatrix} A \\ B \end{pmatrix}. \tag{E.18}$$

Here, $J_p(x)$ and $N_p(x)$ are the Bessel and Neumann function respectively. Using

$$J_p(x)N_{p+1}(x) - J_{p+1}(x)N_p(x) = -\frac{2}{\pi x},$$

and solving Eq.(E.18) relative to A and B, we obtain

$$\begin{pmatrix} A \\ B \end{pmatrix} = \pi\theta_0 \begin{pmatrix} -\nu_s u N_1(ku) & -N_0(ku) \\ \nu_s u J_1(ku) & J_0(ku) \end{pmatrix} \begin{pmatrix} z \\ z' \end{pmatrix}. \tag{E.19}$$

Assuming that initial conditions are given at the point $\theta = 0$, we write

$$\begin{pmatrix} z \\ z' \end{pmatrix}_0 = \pi\theta_0 \begin{pmatrix} J_0(k) & N_0(k) \\ -\nu_s J_1(k) & -\nu_s N_1(k) \end{pmatrix} \begin{pmatrix} -\nu_s u N_1(ku) & -N_0(ku) \\ \nu_s u J_1(ku) & J_0(ku) \end{pmatrix} \begin{pmatrix} z \\ z' \end{pmatrix} \tag{E.20}$$

Using Eq.(E.19), we find the functions a, b, c and d from Eq.(E.3):

$$a = \pi\nu_s\theta_0 u \left\{J_1(ku)N_0(k) - N_1(ku)J_0(k)\right\}, \tag{E.21}$$
$$b = \pi\theta_0 \left\{J_0(ku)N_0(k) - N_0(ku)J_0(k)\right\}, \tag{E.22}$$
$$c = -\pi\nu_s^2\theta_0 u \left\{J_1(ku)N_1(k) - N_1(ku)J_1(k)\right\}, \tag{E.23}$$
$$d = \pi\nu_s\theta_0 \left\{N_1(k)J_0(ku) - N_0(ku)J_1(k)\right\}. \tag{E.24}$$

Direct calculations result in

$$ad - bc = 1, \tag{E.25}$$

so that using Eqs.(E.6) and (E.7) we obtain for the instantaneous rms length and momentum spread of the bunch

$$\sigma^2(\theta) = \sigma^2 d^2 + \delta^2 b^2, \quad \delta^2(\theta) = \delta^2 a^2 + \sigma^2 c^2. \tag{E.26}$$

Since the functions d and b exponentially decay, while the functions a and c exponentially increase, when $ku \gg 1$

$$d \propto \sqrt{\pi\nu_s\theta_0}\, e^{-\theta/[4\theta_0]}, \quad b \propto \sqrt{\frac{\pi\theta_0}{\nu_s}}\, e^{-\theta/[4\theta_0]},$$

the bunch length decreases $\sigma(\theta) \propto e^{-\theta/[4\theta_0]}$, while the bunch momentum spread increases $\delta(\theta) \propto e^{\theta/[4\theta_0]}$ during these variations of the synchrotron tune. All these equations hold until $\pi\nu_s(\theta) \ll 1$. It means that such a bunching should be not longer than during

$$\Delta\theta < \theta_0 \ln\left(\frac{1}{\pi\nu_s}\right). \tag{E.27}$$

Correspondingly, the asymptotic regions $ku = 2\theta_0\nu_s(\theta) \gg 1$ are available, if the bunching occurs slowly, so that θ_0 is large enough.

Bibliography

[1] Conceptual Design Study of the Electron–Nucleon Collider. Budker INP 97-51, Novosibirsk,1997; GSI Report 97-07, GSI, Darmstadt, 1997.

[2] W. Chou. Proton Driver Study at Fermilab. ICFA Beam Dynamics Newsletter, **20**, p. 51, 1999.

[3] V.P.Shevelko, D.Böhne, B.Franzke, Th.Stöhlker: Projectile ionization and capture reactions in ion-atom collisions, in: Atomic Physics with Heavy Atoms, ed. by H.F.Beyer and V.P.Shevelko, Springer, Berlin 1999, pp. 305-322.

[4] V.P. Shevelko, D. Böhne, Th. Stöhlker, NIM **A-415**, 609, 1998.

[5] L.P. Presnyakov. Private communication, 1997.

[6] V.P. Shevelko. GSI Annual Report 1999. GSI, Darmstadt, 2000.

[7] N.S. Dikansky, A.N. Skrinsky. Atomnaya Energiya, **21**, p. 176, 1966.

[8] N.S. Dikansky, D.V. Pestrikov. Physics of Intense Beams and Storage Rings. AIP Press, New York, 1994.

[9] N. Fomin, E. Gorniker, et al. RF Systems for a high-intensity heavy ion synchrotron with strong bunch compression (Part II). BINP, Novosibirsk, 2000.

[10] I.S. Gradshteyn, I.M. Ryzhik. Tables of Integrals, Sums and Products. Academic Press, New York, 1965.

[11] R.D. Kohaupt. DESY Report 80/22, 1980.

[12] E. Keil, W. Schnell. CERN-ISR-TH-RF-69-48, CERN 1969.

[13] A.A. Kolomensky, A.N. Lebedev. Theory of Cyclic Particle Accelerators. Willey, New York, 1962.

[14] R. Billinge, E.L. Hubbard, R. Juhala and R.W. Oram. IEEE Trans. Nucl. Sci. **NS-18** No. 3, 979 (1971).

[15] Yu.P. Wakhrushin, A.I. Anackii. Linear Induction Accelerators. Moscow, Atomizdat, 1978 (in Russian).